CRANFIELD UNIVERSITY

JANTHANEE DUMRONGSAK

NUMERICAL STUDY OF HELICOPTER COMBUSTOR AND EXHAUST EMISSIONS USING LARGE EDDY SIMULATION

SCHOOL OF ENGINEERING
Department of Power and Propulsion

DOCTOR OF PHILOSOPHY THESIS
Academic Year: 2011 - 2014

Supervisor: Professor Mark Savill
February 2014

CRANFIELD UNIVERSITY

SCHOOL OF ENGINEERING
Department of Power and Propulsion

DOCTOR OF PHILOSOPHY THESIS

Academic Year 2011 - 2014

JANTHANEE DUMRONGSAK

Numerical Study of Helicopter Combustor and Exhaust Emissions Using Large Eddy Simulation

Supervisor: Professor Mark Savill

February 2014

This thesis is submitted in partial fulfilment of the requirements for the degree of Doctor of Philosophy

ABSTRACT

Although Large Eddy Simulation (LES) has demonstrated its potential for modelling the reaction in simple academic combustors, it is more computationally expensive than Reynolds Averaged Navier-Stokes (RANS) which has been used widely for industrial cases. The aim of this research is to employ LES at minimal grid resolution and computational resource requirements to capture the main characteristics of the reacting flows in a helicopter combustor and exhaust plume with the focus on NO_x emissions.

Test cases have been carried out to validate the current LES code for non-reacting jet, non-premixed combustion and unstructured grids. Despite the moderate grid refinement and simple chemistry models employed, the findings from these test cases have demonstrated good capabilities of the current LES to capture the mixing, flame and flow characteristics. In a farther test case, a key gas-phase chemical reaction selected for the helicopter exhaust plume modelling has also been tested.

The validated LES code is then employed in the numerical study of the reaction in the helicopter combustor. The LES predictions in terms of the temperature and $EINO_x$ agree generally well with the combustor design, analytical solutions, previous LES and test measurements. Subsequently, the potential application of LES for the calibration of simpler models has been assessed for the generic and helicopter combustors. The results obtained from LES are compared with those from a one-dimensional combustor performance and emissions code, HEPHAESTUS, developed within the Cranfield University Power and Propulsion Department. The discrepancies between the results are found to be primarily due to specific simplification and assumptions established in the HEPHAESTUS model which can be addressed.

Finally, LES has been employed to model the transformation of NO to NO_2 in the helicopter exhaust plume. The findings from this research have demonstrated that, even without the implementation of highly dense mesh or advanced reaction model, LES is able to provide results with an acceptable level of fidelity at relatively low computational costs. These advantages make it a powerful predictive tool for future design and emissions optimisation investigations, and calibration of other simpler modelling approaches.

Keywords:

Atmospheric reaction, Jet-A, non-premixed combustion, NO_x, turbulence

DEDICATION

This thesis is lovingly dedicated to my parents and aunts.

My mother, Ms. Panida Atchariyasil, has made a lot of sacrifices to ensure I receive the best education and opportunities. Her unconditional love and encouragement have sustained me throughout my life. I owe everything to her.

I am very blessed to have my kind aunts, Ms. Jintana, Ms. Phanthira and Ms. Sumon Atchariyasil, in my life. Without their love, support and generosity, I could not have come this far.

I would also like to dedicate this thesis to the memory of my late father, Mr. Bunjurd Nakchaleaw, who always believed in me. Although I can never share my happiness with him, I know he is now smiling down at me from heaven.

ACKNOWLEDGEMENTS

This thesis would not have been possible without the help and support of my supervisor, Professor Mark Savill, who has provided me with invaluable advice, responded to all my queries promptly, and guided me in the right direction throughout this endeavour. His immense intelligence, dedication, and integrity have inspired me to do my best every day. Life away from home is not easy but Professor Mark Savill has never made me feel alone. In time of crisis with no one to turn to, he has always been the only person who would go the extra mile to lend me a hand. For that, I am forever grateful to him. I feel extremely fortunate to have a supervisor who cares so much not only about my work but also my well-being. I could not wish for a better and kinder mentor.

I would like to express my sincere gratitude to my examiners, Professor Xi Jiang and Professor David Mba, for reviewing this thesis. I greatly appreciate their constructive feedback and insightful comments. I am very grateful to Dr. Bobby Sethi for his generous support and sharing his extensive knowledge of gas turbine combustion.

I would like to gratefully acknowledge the European Clean Sky programme and Funds for Women Graduates for the partial research funding.

Special thanks to my colleagues: Mr. John Oliver for his IT assistance, Mr. Gilberto Materano Blanco for the interesting combustion discussions, Dr. Nurul Mazlan for the HEPHAESTUS generic combustor results, Dr. Salwan Saddawi for the generic combustor mesh, and Mr. Fakhre Ali for the HEPHAESTUS helicopter combustor results.

I am indebted to the IT staff, especially Mr. Andy Gittings, for patiently solving all my technical and high performance computing problems. I would also like to thank Ms. Alison Waters and Ms. Deborah Hiscock for their help with the thesis template.

My heartfelt appreciation goes to all my friends for their encouragement and moral support. I would like to particularly thank Mr. Arthit Jaroenchaichana, Mr. Baoying Yang, Mr. Glenn and Mrs. Susan Jarrett, Ms. Hafizah Hasan, Ms. Jing Shi, Mr. Kritkaew Somton, Ms. Nurhana Rouyan, Ms. Oratai Chokjutha, Mr. Pongpun Othaganont, Mr. Shiwei Fan, Dr. Supunnika Somjaipeng, Mr. Teng Lei, Mr. Terdsak Suphatharophatphong, and Mr. Xiaojian Huang for always motivating and cheering me up.

Most of all, I would like to thank my beloved mother, Ms. Panida Atchariyasil, for her sacrifices, patience and unconditional love which has always been the source of my strength and courage. I am also deeply grateful to my aunts, Ms. Jintana, Ms. Phanthira and Ms. Sumon Atchariyasil, my cousin, Mr. Chanvit Atchariyasil, my grandfather, Phar Suwan Tonsuwan, my uncle, Mr. Preecha Pornchaijareon, and my sister, Ms. Sutheera Dumrongsak, for their love, support and always being there for me through all my ups and downs.

TABLE OF CONTENTS

LIST OF FIGURES

LIST OF TABLES

NOMENCLATURE

Uppercase

A	Pre-exponential factor
A	Magnussen constant for reactants
B	Magnussen constant for products
C	Constant
C	Molar concentration
C_s	Smagorinsky coefficient
C_ξ	Volume fraction constant
$C\tau$	Time scale constant
D	Scalar diffusivity
D	Characteristic diameter
E_a	Activation energy
G	Low pass filter function
J	Species mass flux
K_r	Equilibrium constant
L_s	Subgrid length scale
M	Subgrid species mass flux
R	Universal gas constant
S	Strain rate tensor
Sc	Schmidt number
T	Temperature
U	Velocity
W	Molecular weight
Y	Species mass fraction
Z	Mixture fraction

Lowercase

a	Oxygen reaction order
d	Diameter
f	Correction factor
k	Turbulent kinetic energy
k	Reaction rate constant
p	Pressure
r	Reaction
t	Time
u	Velocity component in the x-direction
x	Cartesian coordinate
y	Cartesian coordinate
z	Cartesian coordinate

Symbols

α	Chemical species
β	Temperature exponent
γ	Chemical species in the reaction
Γ	Effect of third bodies
ξ	Length fraction
χ	Scalar dissipation
Φ	Equivalence ratio
ε	Turbulent kinetic energy dissipation rate
μ	Dynamic viscosity
ν	Kinematic viscosity
ν'	Stoichiometric coefficient for a reactant
ν''	Stoichiometric coefficient for a product
η'	Forward rate exponent
η''	Backward rate exponent
σ	Stress tensor due to molecular viscosity
σ_t	Constant
ρ	Density
τ	Stress tensor
τ	Time scale
ω	Chemical reaction term
$\hat{\omega}$	Molar rate of creation/destruction
χ	Scalar dissipation rate
Δ	Filter width

Subscripts

F	Fuel
O	Oxidizer
P	Product
R	Reactant
Z	Mixture fraction
b	Backward reaction
f	Forward reaction
i	Unit vector in the x-direction
j	Unit vector in the y-direction
k	Unit vector in the z-direction
st	Stoichiometry
r	Reaction
r	Reverse reaction
t	Turbulent

Superscripts

e	Equilibrium
fl	Flamelet
SGS	Subgrid
*	Fine-scale quantity

ABBREVIATION

ACARE	Advisory Council for Aeronautics Research in Europe
AESO	Aircraft Environmental Support Office
CFD	Computational Fluid Dynamics
DCB	Double Cone Burner
DSM	Dynamic Smagorinsky Model
EDC	Eddy Dissipation Concept
$EINO_x$	Oxides of Nitrogen Emission Index
EPA	Environmental Protection Agency
FAR	Fuel to Air Ratio
FDF	Filtered Density Function
FLITES	Fibre-Laser Imaging of Gas Turbine Exhaust Species
FOCA	Federal Office of Civil Aviation
IATA	International Air Transport Association
ICAO	International Civil Aviation Organisation
JTI	Joint Technology Initiative
LES	Large Eddy Simulation
LFM	Laminar Flamelet Method
NASA	National Aeronautics and Space Administration
NLES	Numerical Large Eddy Simulation
PAH	Polycyclic Aromatic Hydrocarbon
PDF	Probability Density Function
RANS	Reynolds Averaged Navier-Stokes
RMS	Root Mean Square
SGS	Subgrid Scale
SM	Smagorinsky Model
SST	Shear Stress Transport
UDF	User Defined Function
URANS	Unsteady Reynolds Averaged Navier-Stokes

1 INTRODUCTION

This chapter provides an introduction to the current research. It includes the research motivations, problem statement, aim, objectives, and thesis structure.

1.1 Motivations and Problem Statement

Due to the continuous growth of air travel over the past few decades, there have been increasing environmental concerns over the impacts of aviation emissions on the climate and air quality. These have led to the development of more stringent policies and significant world-wide efforts to reduce aviation emissions, and given rise to the European Clean Sky programme, in which Cranfield University has been actively taking part. The Clean Sky Joint Technology Initiative (JTI) began in 2008 and represents a partnership between the European Commission and the aeronautical industry. It has the mission to develop breakthrough technologies to design more environmental-friendly, highly efficient aircraft which will meet the goals set by Advisory Council for Aeronautics Research in Europe (ACARE) in 2020. These targets are to reduce 50% of carbon dioxide (CO_2) emissions through the reduction of fuel consumption, reduce 80% of nitrogen oxides (NO_x) emissions, reduce 50% of external noise, and design a green product life cycle.

Meeting the Clean Sky JTI goals by reducing aircraft harmful emissions will be beneficial to the human health and environment, and reduce the airline operational costs. To achieve these targets, improving combustion technologies seems to be the most promising approach since the combustion process controls the amount of aircraft emissions generated. Predominant pollutants emitted from modern aircraft engines are NO_x (Bahr, 1992). NO_x enhance the formation of ozone (O_3) in the troposphere which results in the climate warming (Penner *et al*., 1999; Sausen *et al*., 2005). Furthermore, at ground level, they contribute to the production of photochemical smog and acid rain.

The NO_x production, which is directly influenced by the quality of the combustion process, can be reduced by lowering the reaction temperature, decreasing the residence time, and eliminating the hot spots from the reaction zone. However, the decrease in NO_x production is normally achieved at the expense of the combustor performance, and carbon monoxide (CO) reduction. Therefore, one of the main challenges in designing gas turbine combustors is the optimisation of harmful emissions, performance, and stability of the combustion process.

Combustion involves many complex processes, such as turbulence, mixing, thermodynamics, chemistry, heat and mass transfer, which often interact and are interdependent. The chemical reaction takes place in a highly turbulent environment where the unsteady fluid motions of a wide range of length and time scales are present. The mixing process is crucial for the engine performance and pollutant emissions. For the combustion process, the rate of reaction depends on the mixing and entrainment rates. The mixing between the aircraft jet exhaust and ambient air is also important because it controls the reaction and dispersion of pollutants in the environment.

Since the aircraft emissions are dictated by the combustion process, the combustion flow characteristics, as well as the parameters affecting the pollutant formation, have to be well understood. Successful improvement of the combustion process with high efficiency and reduced pollutant emissions requires accurate predictions of important flow-field quantities. Although experimental studies have been undertaken to understand the characteristics of reacting turbulent flows, they may not be able to provide adequate information for the combustor design process. This is due to the limitations in the measurement technology, and high setup costs associated with comprehensive parametric studies.

Advances in the numerical simulation, combustion modelling and parallel computing made over the years have significantly enhanced the application of computational fluid dynamics (CFD) in the design and optimisation processes for the development of more environmental-friendly, energy efficient and reliable combustors. It increases the understanding of the complex flow phenomena, and reduces the amount of the experimental trial and error.

The combustion process in CFD is described by the governing transport equations for fluid flow and heat transfer, along with models for combustion chemistry. Reynolds Averaged Navier-Stokes (RANS) CFD, a classical turbulence modelling approach used widely in the industry, models all scales of motions and describes flows in a statistical sense. Another turbulence model which has recently been the focal point of combustion modelling is Large Eddy Simulation (LES). In this approach, the larger-scale eddies are resolved directly while the smaller eddies and their interactions with the large-scale motions are represented by the mathematical models.

In LES, the combustion process has to be modelled since the chemical reaction and heat release occur primarily at the smallest scales. However, by solving for the large, energy-containing scales of motions which dictate the behaviours of turbulent flows and the mixing rate, the LES approach is expected to be superior to RANS in capturing turbulent combustion characteristics. LES has also been demonstrated to provide excellent evaluations of reacting flow fields for simple academic combustors.

Despite its promising performance, LES of turbulent combustion is nonetheless a challenge. The difficulty of applying the LES approach in reacting flows involves treating the unclosed terms related to combustion processes and incorporating chemistry into LES. Therefore, its application as an analytical production tool to real aeronautical gas turbine combustors still requires further development and validation.

Of particular interest is the study of helicopter combustor and emissions, which has only been considered by a limited number of researchers. This is partly due to the fact that there are no emission certification requirements imposed by International Civil Aviation Organization (ICAO) for helicopter engines at present (ICAO, 1993). In addition, the helicopter emissions are very difficult to evaluate because their engine emission data are not usually publicly accessible and there is limited information available for conducting emissions inventories. While there are currently not any helicopter NO_x emission standards, the pollutants emitted from the helicopter engines should not be disregarded. This is because their adverse impacts on the environment and human beings can be significant due to the large number of helicopters in service, the high-performance and relatively low-altitude nature of the helicopter operations.

Notable amount of research carried out on aircraft exhaust has been primarily concerned with the jet development, spreading, mixing and entrainment. Although the knowledge of these processes is crucial for the study of aircraft jet noise, exhaust plume dilution and pollutant dispersion, the investigation of atmospheric effects of aviation requires further information on the chemical processes which occur while the hot exhaust gases cool and mix with the ambient air.

However, important exhaust species are presently inaccessible to quantitative measurements. Furthermore, there are only few studies focused especially on the aviation plume chemistry. Therefore, it is important to reproduce the reactive jet flow in order to provide a better understanding of the interaction between the exhaust and environment, and aid the design and development of aircraft engine with reduced emissions. This has triggered the interest to investigate the reaction in helicopter exhaust plume in the context of NO_x emissions.

Despite the level of detail and fidelity it provides, LES is computationally expensive. Therefore, it is generally more practical to employ simpler performance and emissions modelling codes for the design optimisation processes which only require the predictions of bulk flow properties. However, since these basic codes have been significantly simplified, they need to be validated and calibrated in order to become powerful modelling tools for practitioners. In cases where the experimental data are unavailable to be used for validation, a higher-fidelity approach, such as LES, has the potential to be applied in the calibration of these performance and emissions models.

Therefore, to apply LES to gain more insights into areas which lack understanding and available data such as the helicopter NO_x emissions and reaction in the helicopter jet exhaust will be greatly beneficial to the development of more environmentally-friendly helicopter engines. The validated LES at minimal grid can be employed in the design optimisation processes with high fidelity at reasonably low computational cost. Furthermore, it can also be used to calibrate or enhance other simpler combustion performance and emissions models. Hence, the reliance on the experimental studies diminishes.

1.2 Aim and Objectives

This research aims to employ LES at minimal grid resolution and computational resource requirements, in terms of the number of processors utilised and execution time, to capture the main characteristics of the reacting flows in a helicopter combustor and reactive exhaust plume with the focus on NO_x emissions. This will be significantly beneficial to the future design optimisation processes and calibration of other simpler performance and emissions modelling codes which will lead to the development of more environmentally-friendly, highly-efficient helicopter engines.

The objectives of this research are as follows:

- To develop a framework for LES of helicopter combustor by selecting, from the literature survey, appropriate combustion and chemistry models with the consideration of the level of fidelity, computational cost, and its potential application in the future design optimisation studies.
- To test and validate the LES code against the measurements from well-established experiments for a non-reacting jet and non-premixed combustion to assess the performance of the code in capturing mixing and flame characteristics, and predicting important flow quantities.
- To carry out the sensitivity analysis for the LES code to investigate the effects of chemistry models, grid types and resolution on the simulation results.
- To select a reference helicopter combustor, create the geometry, perform LES to provide an insight into the flow phenomena in a helicopter combustor, predict temperature and NO_x emissions.
- To assess the potential application of the validated LES code as a calibration tool, and investigate the limitation of a one-dimensional (1-D) in-house emissions modelling code, HEPHAESTUS, by comparing the temperature and NO_x predictions obtained from the LES code with those from HEPHAESTUS.
- To select, from the literature review, a key chemical reaction and kinetic parameters in the context of the reaction between NO_x emissions in the exhaust plume and the atmosphere.
- To test and validate the selected chemical reaction mechanism against the classic experimental data prior to its application for the helicopter exhaust plume study.

- To employ LES to investigate the chemical reaction of NO_x in the helicopter exhaust plume with the ambient air, and the effects of exhaust temperature on the reaction.

1.3 Thesis Structure

This thesis consists of eight chapters:

Chapter 1 provides a general introduction to this thesis. It includes the research motivations, problem statement, aim, objectives and thesis structure.

Chapter 2 discusses the introduction and background to the current research. A review of literature on non-reacting and reacting jet flows, combustion, environmental emissions with the focus on NO_x and exhaust modelling has been conducted. The information on jet flows, combustion characteristics, NO_x formation and aircraft exhaust obtained from the literature survey provides the preliminary grounds for the current research.

Chapter 3 provides a summary of the numerical methods employed in this study. This starts with the governing equations for LES, followed by the reaction and NO_x models.

Chapter 4 presents the results of four test cases. The first test case is LES of a non-reacting round jet with a co-flow carried out to evaluate the performance of the LES code in capturing passive scalar mixing. The significance of this test case is that this jet configuration resembles that of a simplified combustor and engine exhaust. An understanding of the mixing characteristics is important since the mixing rate controls the rate of reaction. The second test case is LES of a coaxial jet combustor. This test case is conducted to validate the LES code for non-premixed combustion studies and investigate the sensitivity of the LES results to the grid resolution and chemistry models employed. Moreover, a comparison between the performances of LES and RANS in modelling combustion is made. The third test case is carried out to compare the results of

combustion LES on structured and unstructured grids. Finally, the last case, which is a reacting jet, is performed to test the NO_x chemical reaction and kinetic parameters which will be employed in the modelling of the helicopter exhaust plume reaction in Chapter 7.

Chapter 5 details the results from LES of a helicopter combustor. It includes the description of the helicopter combustor configuration, operating conditions and computational setup employed in this research. Thenceforth, the LES results in terms of temperature and NO_x emission index ($EINO_x$) are compared with those obtained from the combustor design, analytical solutions, previous LES and test measurements.

Chapter 6 serves to assess the potential of the current LES code to be used as a calibration tool for other simpler performance and emissions modelling codes. The modelling assumptions made in LES and HEPHAESTUS are first discussed. The temperature and $EINO_x$ predictions obtained from both methods are then compared for the reaction in the generic and helicopter combustors.

Chapter 7 presents the LES results of the reaction between NO in the helicopter exhaust plume and ambient air. The flow conditions, computational domain and setup are described. In addition, the effects of exhaust temperature on the NO chemical process are investigated in this chapter.

Chapter 8 concludes the findings from the current research. Furthermore, the recommendations for the future research are discussed in this chapter.

2 BACKGROUND TO THE CURRENT RESEARCH

This chapter consists of four main sections which are non-reacting jets, reacting flows and combustion, NO_x emissions, and engine exhaust modelling. The information obtained from this literature survey provides the preliminary grounds for the current research.

2.1 Non-Reacting Jets

The study of jet flow is vital for the current research since the jet configuration manifests flow phenomena which resemble those in jet engine combustors and exhaust. Understanding the characteristics of these flow features will help shed light on their influences on the rate of mixing and reaction. Therefore, studies have been conducted to investigate the jet flow structures and characteristics. The physical nature of the large-scale structures in the mixing layer of a round jet was experimentally investigated by Yule (1978). He found that the large eddies were three-dimensional and contained irregular small-scale turbulent structures. These small-scale eddies contributed significantly to the local velocity fluctuations and the statistical correlations (Yule, 1978).

Gazzah *et al*. (2010) numerically investigated the effects of a co-flowing jet on the spreading and entrainment rates of a turbulent round jet employing the RANS k- epsilon (k-ε) and Reynolds Stress Model (RSM). When compared with the free jet case, the results showed that the main effect of the co-flowing jet was the reduction of the jet decay rate. Therefore, the co-flowing jet tended to mix more slowly with the ambient air than the jet without a co-flow. The results suggested that the co-flowing jet introduced a considerable restriction on the spreading rate and the turbulent mixing.

Doolan and Mi (2007) employed the Unsteady RANS (URANS) Spalart-Allmaras turbulence model to numerically study the passive scalar mixing in the wake of a slightly heated cylinder. The URANS approach was able to capture the key features of the flow fields, the unsteady flow structures in the separation shear layers and the passive scalar fluctuations in the near-wake regions. However, excessive dissipation produced by the turbulence model affected the near-wake flow. The URANS method under-predicted the size of the recirculation bubble behind the cylinder and over-predicted the drag. These limitations had to be taken into account when employing the URANS model in solving for the scalar mixing behind bluff bodies.

The RANS approach is employed to compute the flow fields of most turbulent jet flows (Wilcox, 1993). However, it is not accurate for jet applications because it only provides a statistical representation of the turbulent flow (Georgiadis *et al*., 2006). This leads to a growing interest in employing the LES approach to reproduce such flows, owing to the higher degree of flow detail which can be obtained.

2.1.1 LES for Non-Reacting Jets

Recently, the LES approach has been employed extensively for turbulent round jets due to its superior accuracy over the RANS approach and the detailed physical insights it provides. As shown in the study of a round jet by Zhang and Stanescu (2010), the LES approach was able to capture instantaneous and statistical turbulent structures very well. The instantaneous, less-organized coherent structures in the study were resulted from Kelvin-Helmholtz instabilities. The axial velocity component decelerated downstream due to the conical vortex breakdown of the laminar high-speed fluid sheet into small-scale turbulent structures. In addition, the total turbulent fluctuation energy also decreased with increasing downstream distance. Zhang and Stanescu (2010) also found that the fine grid was able to capture more turbulent fluctuation energy than the coarse grid.

Suto (2004) employed the LES model with a higher-order differencing scheme in a developing round jet. The flow domain consisted of initial, transitional and established stages of the jet. In this study, two subgrid-scale (SGS) models tested were the Smagorinsky model (SM) and dynamic Smagorinsky model (DSM) (Smagorinsky, 1963). The simulation results from LES with both SGS models agreed well with the experimental data except at the transitional stage of the flow fields, where DSM provided more accurate predictions than SM.

Since LES directly solves for the large-scale turbulent structures which are responsible for the mixing process, it is able to provide high-fidelity predictions of the mixing characteristics. This leads to a growing interest in applying LES of non-reacting jet flows particularly in the study of the environmental emissions and noise. Poll *et al*. (2009) employed LES of a turbulent co-flowing jet to study the flow fields and passive scalar mixing in the initial jet development region to provide an insight into the effects of the interaction between the engine exhaust and aircraft trailing vortices on the air quality. The simulation results from the study showed that the LES approach was able to accurately capture the key flow features, mixing and jet development, especially in the near-field region.

Ranga-Dinesh *et al.* (2010a) carried out LES of a turbulent jet, with and without a bluff body, at a high Reynolds number. The study aimed to analyse the turbulence intermittency of the velocity, the scalar fields and their variation corresponding to different inlet conditions. In addition, Ranga-Dinesh *et al.* (2010b) carried out a numerical study employing LES to investigate the mixing and intermittency of a turbulent high-velocity coaxial jet with a core jet. The simulation was able to capture the inner potential core, outer potential core and intense fluctuations in the mixing regions.

Due to the stringent requirements to reduce aircraft engine noise, the design and development of noise reduction devices for the jet exhaust systems have been a vital research area. Some of the noise reduction concepts aim at increasing the exhaust streams mixing and modifying the jet turbulent characteristics (Janardan *et al.*, 2000). Accurate CFD simulations are, thus, required to enhance the analysis of these noise reduction concepts by providing an insight into the jet aerodynamics and complex turbulent flows characteristics.

The major issue of the RANS calculation is its time-averaging approach which removes all the spectral information necessary for noise prediction. The LES approach, on the other hand, solves for the spectral information of the large-scale motions. As most downstream noise in a turbulent jet is produced by the large-scale structures at the potential core tip, LES is a promising method which is able to provide the detailed descriptions of the turbulent structures and capture major noise sources.

De Bonis and Scott (2002) carried out LES of a turbulent compressible round jet using a computational grid which included the entire nozzle geometry. The simulation results showed that LES was able to accurately capture the turbulent flow physics. The influence of the nozzle modelling in LES of turbulent free jets for a low-speed condition and a high-speed condition was investigated by Wu *et al.* (2005). Despite the superior performance of the LES approach demonstrated in these studies, the inclusion of the nozzle geometry in the computational domain does not always produce more accurate flow predictions due to the high near-wall grid requirements of LES. This was demonstrated by Eastwood *et al.* (2010), who carried out Numerical LES (NLES) of a co-flowing jet on a computational grid which included the short-cowl nozzle geometry. In this study, the NLES approach over-predicted the mean axial velocity at the jet centreline because the near-wall mesh resolution at the nozzle rear was inadequate for LES to accurately capture the flow behaviours in this region. This caused rapid mixing behind the nozzle and non-physical flow separation from the nozzle wall.

2.2 Reacting Flows and Combustion

When assessing the impact of aircraft emissions on the climate and air quality, it is necessary to consider reacting flows since the combustion process inside gas turbine engines determines the amount of emissions being discharged into the environment. In addition, after being emitted from the engines, some of the exhaust species continue to react with the ambient air, and are transformed into other chemical species. In this section, the survey on different types of flames is first carried out to provide the information on the flame characteristics. The flame types presented are the non-premixed, premixed and partially-premixed flames.

Subsequently, a review on the experimental and numerical studies of other researchers on reacting jet flows and gas turbine combustors is carried out to provide the information on expected flow features. For the numerical studies, the review focuses on LES which is the main turbulence modelling approach employed in this research. Furthermore, requirements, advantages and limitations of various numerical techniques for reacting flows employed by these researchers are discussed so that appropriate models for the current research can be selected.

2.2.1 Non-Premixed Flame

In non-premixed combustion, the fuel and oxidiser are introduced through different inlets, and mixed at the molecular level by turbulence. The product formation and heat release from the chemical reaction occur in the regions along the interface. The streamwise fluid shear initiated by the difference between the inlet velocities of the fuel and the oxidiser enhances the turbulence in the mixing layer.

Experimental studies on non-premixed jet flames have been conducted to provide a better understanding of the structures of such flows. Seitzman *et al.* (1990) carried out an experiment of a highly turbulent non-premixed hydrogen (H_2) jet flame burning in the air and observed that the large-scale motions carried the thin conical region generated near the nozzle exit into the jet downstream. This finding agreed with the finding of Schefer *et al.* (1994) who showed the locations of the flame sheets in a lifted methane flame.

The Roquemore group at Wright Laboratory carried out experiments and illustrated that the large-scale motions were present within several fuel flames (Chen *et al.*, 1991). Similar conclusions about the structures of reacting jet flows were made by Kim and Shin (1994) who carried out an experimental study of a slow co-flowing jet of propane (C_3H_8), methane (CH_4), and N_2-CH_4 mixture burning in the air.

Besides the experiments, numerical studies have been carried out to reproduce non-premixed combustion. Colucci *et al.* (1998) developed and implemented a Filtered Density Function (FDF) method for LES of a developing mixing layer and planar jet. Broadwell and Lutz (1998) showed in their studies that downstream of the jet exit, the large-scale motions carried the flame sheet into the central regions. This agreed with the findings in the experiments described previously.

Kurose (2001) carried out an LES of non-premixed reacting mixing layer to study the effects of heat release on the reaction process. Tkatchenko *et al.* (2007) carried out a numerical study to compare the performances of the LES and RANS approaches in modelling the reaction in a coaxial jet mixer. The comparison revealed that LES was able to capture oscillating movements of the recirculation vortex while the URANS approach failed to predict the unsteady flow characteristics.

2.2.2 Premixed and Partially-Premixed Flame

In premixed combustion, the flame is generally stabilised by a recirculation zone formed behind the stabiliser and spreads obliquely across, consuming the reactants in the unburned stream. The reaction zone is highly convoluted and consists of many isolated hot and cold gas pockets (Spalding, 1971). According to Bray *et al.* (1985) the turbulent combustion zone in a premixed flame comprises either a single thin wrinkled flame or pockets of reactants and products separated by thin flames.

Calculation procedures and numerical models have been developed by researchers to describe the premixed flame. One of the earlier numerical methods was proposed by Spalding (1971) to solve the partial parabolic differential equation of turbulent premixed flame. Bray *et al.* (1985) developed a general formula for premixed turbulent flames. The model was subsequently revised for the mean product creation rate based on an extension of the Bray-Moss thermochemistry description to include the influence of the strain rate (Bray *et al.,* 1989). Bray *et al*. (2005) later used a mixture fraction and a progress variable to describe the partially-premixed combustion.

Derksen *et al*. (2003) proposed a combustion model based on the transport of reaction progress variables, mixture fraction, and enthalpy. The proposed model was able to describe premixed, non-premixed, adiabatic and non-adiabatic combustion with heat loss through radiation. Weller *et al.* (1998) proposed a new flame-wrinkling combustion model for LES, derived using conditional filtering, in which flame-wrinkle density function was used to represent flame distribution. The model was employed in the simulations of non-reacting and reacting flows over a backward-facing step with a lean propane-air mixture. Hawkes and Cant (2000) employed the flame surface density concept for the LES modelling of premixed turbulent combustion.

Research has been carried out to assess the fidelity of LES for premixed combustion. Möller *et al.* (1996) employed LES to study the premixed combustion of flow passing a triangular-shaped flame stabiliser with propane as the fuel. The simulation results showed that the LES approach was able to capture the flame front movement and predict flow properties well.

Chakravarthy and Menon (2000) performed LES of a jet impinging on an adiabatic wall to simulate premixed flames in turbulent stagnation zones. The simulation results revealed that LES with the subgrid flamelet method was able to accurately capture the characteristics of the flame propagation and their effects on the fluid dynamics. Duchamp de Lageneste and Pitsch (2001) performed LES of a premixed methane-air Bunsen flame. Duwig and Fureby (2007) employed the LES approach in the simulations of perfectly premixed and stratified premixed reacting flows.

2.2.3 LES of Gas Turbine Combustors

Some of the main numerical approaches developed for modelling turbulent combustion are the flamelet model (Peters, 1984), probability density function (Pope, 1985), linear eddy modelling (Kerstein, 1992), and conditional moment closure (Klimenko and Bilger, 1999). Although these concepts were first proposed in the context of RANS, they have been extended for LES. A significant amount of research has been carried out to demonstrate the potential of LES for modelling the reaction in simple academic combustors. For such configurations, LES provides accurate predictions of mean and root mean square (RMS) of velocity, scalar mixing, temperature and species concentrations (Pitsch, 2006).

LES with the steady flamelet model was successfully implemented in non-premixed combustion by Cook *et al.* (1997). The unsteady flamelet model employed in LES of a piloted jet diffusion flame performed by Pitsch and Steiner (2000) was able to predict CO quantities which matched the experimental data very well. In LES of a turbulent jet diffusion flame carried out by Forkel and Janicka (2000), a mixture of H_2 and N_2 (nitrogen) was discharged from a round jet into co-flowing air in a cylindrical computational domain. Mahesh *et al.* (2001, 2004) studied the reacting flow in a simple coaxial jet combustor with swirling annular air employing LES.

Pierce and Moin (1998) employed a dynamic procedure to model the sub-grid scale variance and the dissipation rate of a conserved scalar in LES of turbulent reacting flows. They then developed a progress variable approach for LES of non-premixed combustion (Pierce and Moin, 2004). The model was tested in a methane-fuelled coaxial jet combustor with non-swirl air co-flow. The LES approach employed in the study was able to capture realistic flame behaviours such as the unsteady, lifted flame dynamics which agreed well with the experimental data. However, this approach was unable to provide the details of combustion process such as pollution formation.

Pitsch and Ihme (2005) proposed an unsteady flamelet progress variable model for LES, which was an extension of the LES model developed by Pierce and Moin (2004), and implemented in the numerical study of a confined swirl coaxial jet combustor. Mehesh *et al.* (2006) applied the LES model developed by Pierce and Moin (2004) to gain an insight into the combustion process in a complex gas turbine combustor. Wang *et al.* (2007) successfully incorporated the relaxation method into LES of non-premixed combustion for a coaxial jet combustor.

Albouze *et al*. (2009) coupled chemical kinetics modelling with turbulent combustion models for LES of a lean premixed swirled combustor. They found that the prediction of CO mass fractions within the flame depended on the model employed. Duchamp de Lageneste and Pitsch (2001) carried out an LES investigation of a partially-premixed dump combustor with two channel flows carrying a propane-air mixture of different equivalence ratios. The comparison between the results of non-reacting and reacting cases revealed that the recirculation zones behind the steps were shorter in the reacting case due to the strong acceleration behind the flame.

Di Mare *et al.* (2004) employed LES with the non-premixed combustion model to predict temperature and species concentrations in a can-type gas turbine combustor. LES was able to capture, in great detail, complex flow patterns developed from the strong interaction between the swirling flow in the primary zone and the impinging jets.

Selle *et al.* (2004) performed LES of a square combustor with an industrial gas turbine burner using unstructured grid. The simulation results demonstrated the potential of LES for predicting reacting and non-reacting mean flow fields as well as the main combustion instability modes. Roux *et al.* (2005) studied reacting and non-reacting flows in the combustor with the configuration similar to that in the study of Selle *et al.* (2004). The LES results of the mean flow fields closely matched the experimental data. This combustor configuration was also considered in the LES instability analysis of an industrial swirled burner carried out by Selle *et al.* (2006).

2.2.4 LES of Helicopter Combustors

Although a notable amount of work on LES of simple academic flames has been carried out and communicated to the open public, hitherto LES of a helicopter combustor has only been considered by a limited number of researchers.

Boudier *et al.* (2007) compared LES and RANS of a helicopter combustor designed by Turbomeca (Safran group). The simulation results revealed that LES out-performed the RANS approach. Compared to RANS, LES predicted higher temperature values in the reaction region and less pronounced jet penetrations. For LES, the peak temperature was essentially encompassed in the combustor primary zone while RANS predicted longer flame front which spread beyond the primary zone. The discrepancies between the results were mainly due to the smearing effects of the RANS model.

Boudier *et al.* (2008) later studied the influences of grid resolution on LES of the helicopter combustor employing their specialised higher order scheme LES code on meshes consisting of 1.2 to 44 million tetrahedral elements.

Other work on the same helicopter combustor geometry included the LES study of combustion instabilities carried out on meshes composing of 38 to 336 million tetrahedral elements (Staffelbach *et al.*, 2009; Wolf *et al*., 2009, 2012) and the incorporation of the detailed chemistry in the LES code to study the effects of the fuel stream equivalence ratio on high temperature regions (Auzillon *et al.*, 2013). Boileau *et al.* (2008) employed 700 processors to compute LES of an ignition sequence in the helicopter combustor. All of these studies either employed very dense meshes, high-order numerical schemes or both. Massively parallel computing was, therefore, necessary to perform such calculations.

High computational resource requirements for performing these LES calculations have provided the motivation for the current research to employ LES at minimal grid resolution to capture the core flow and flame front development in a helicopter combustor in lieu of detailed unsteadiness and fine-scale near-wall motions since important aspects of the combustion process, such as the main reactions and pollution formation, usually take place far away from the wall.

2.3 NO_x Emissions

This section details a review of environmental emissions with the focus on NO_x. To appreciate the need to reduce aviation emissions, the impacts of these emissions on the climate and air quality have to be first understood. Moreover, a review on NO_x formation characteristics is vital for the current research as it provides insights into different NO_x mechanisms and important parameters controlling the NO_x generation which are necessary for the NO_x emission studies. Since aviation NO_x are produced mainly from the combustion process, previous experimental and numerical investigations on gas turbine combustor NO_x emissions are surveyed. Furthermore, the information on how different numerical techniques are employed in the NO_x emission predictions provides NO_x modelling guidelines for the current research.

2.3.1 Aviation Emissions

As the air traffic worldwide is expected to grow by 3%-5% per year (Penner *et al.*, 1999), it is crucial to understand the characteristics of harmful aviation emissions, their impacts on the human health and environment in order to appreciate the urgency to develop suitable measures to reduce these emissions. Aircraft engine exhaust consists mainly of N_2, O_2 (oxygen), NO_x, CO_2, H_2O (water vapour), CO, UHC (unburnt hydrocarbons), soot, and SO_x (oxides of sulphur). NO_x are combustion by-products while CO_2 and H_2O are the final products of the combustion process. CO, UHC, soot, and SO_x result from incomplete combustion. SO_x are of little concern, since aviation fuels have very low sulphur contents (Wulff and Hourmouziadis, 1997).

Aviation emissions are increasingly recognised as the main contributors to global warming (Penner *et al*., 1999). CO_2 is a greenhouse gas which causes global warming. It absorbs infrared radiation emitted by the atmosphere and earth surface, preventing it from being radiated into the outer space (IPCC, 2007). CO and NO_x are toxic. NO_x contribute to the formation of acid rain and

chemical smog in the atmosphere. These are harmful to human, plants, aquatic animals and structural infrastructure (Brasseur *et al*., 1998). NO_x from aviation emissions also enhance the O_3 concentration in the troposphere (Janic, 1999). An increase in the tropospheric O_3 influences radiative forcing (IPCC, 1990), and affects human health, vegetation and materials (Tilton, 1989). Prolonged exposure to high O_3 concentration of about 100 ppb leads to respiratory illnesses, allergies, headaches and impaired vision. In the stratosphere where supersonic aircraft typically fly, emitted NO_x deplete the O_3 layer, allowing more harmful ultraviolet rays to reach the earth surface (Penner *et al*., 1999).

Pison and Menut (2004) analysed the impacts of air traffic emissions on the O_3 concentration in the troposphere and found that the effects of commercial aircraft emissions in large urban areas were significant. The results also showed that the NO_x emissions affected the O_3 concentration more than the volatile organic compounds (VOCs), especially during the night.

Gardner *et al*. (1997) presented a global inventory of NO_x emissions from civil and military aviation. The vertical distribution of the NO_x emissions showed that for civil aircraft, 60% of NO_x were emitted at cruise altitudes of 10-12 km while the bulk of the military emissions were associated with low level activities.

Pham *et al.* (2010) presented an aviation emission inventory for Australian Airspace. The emission data indicated that by weight, CO_2 was the largest contributor to aviation emissions followed by CO, UHC, NO_x and SO_x accordingly. The findings also suggested that NO_x emissions from aviation might have a considerable impact on the O_3 layer in the upper troposphere but not within the stratosphere.

2.3.2 NO_x Formation Characteristics

Nitric oxide (NO) formed in combustion processes is subsequently oxidised to nitrogen dioxide (NO_2). Therefore, it is customary to combine NO and NO_2 in terms of NO_x. There are four mechanisms responsible for the NO formation: the thermal NO (Zeldovich), prompt NO (Fenimore), nitrous oxide (N_2O) intermediate, and fuel NO (Lee *et al*., 2004). In non-premixed hydrocarbon combustion, the first two mechanisms contribute to most of NO formed (Bowman, 1992). In non-hydrocarbon flames, only the thermal mechanism is responsible for the NO formation. The N_2O intermediate mechanism becomes important as the pressure increases (Bowman, 1992). The fuel NO mechanism only occurs in fuel with bound nitrogen.

The production of NO depends on parameters such as the local temperature, O atom concentration, local mixing rates, flame residence time, radiative heat loss, NO formation mechanisms, flame strain, and, for hydrocarbon flames, the fuel-rich chemistry (Frank *et al.*, 2000, Drake and Blint, 1989; Chen and Kollmann, 1992; Buriko and Kuznetzov, 1978; Turns and Lovett, 1989; Turns and Myhr, 1991). A decrease in the residence time and temperature increases the strain at the flame front which, in turn, reduces the NO formation (Drake and Blint, 1989, 1991).

Experimental and numerical studies have been carried out to investigate the effects of various parameters on the NO emission characteristics. Broadwell and Lutz (1998) computed NO_x emissions from CH_4, CO-H_2, and H_2 flames at various conditions. Their model included the assumption that the scalar mixing fluctuations had an insignificant effect on the average concentration of the products leaving the flame. This assumption was based on the experimental studies of Brown and Roshko (1974), and Dimotakis *et al.* (1983), which suggested that the entrainment of fluid into the turbulent jets and the subsequent mixing were dictated by the unsteady large-scale motions. The computations of Broadwell and Lutz (1998) revealed that buoyant forces increased the entrainment rates, shortened the flame length, increased the gas

velocity, and thus reduced the gas residence time in the flame while the radiation lowered the flame temperature. For the CH_4 flame, the NO_x formation occurred primarily in the regions near the flame tip, where the high temperature, O and CH radical concentrations promoted the thermal and prompt mechanisms respectively.

Ouimette and Seers (2009) measured the $EINO_x$ of partially-premixed laminar flames for five different synthetic gas mixtures over a range of equivalence ratios. They found that the thermal mechanism was a dominant mechanism responsible for the NO_x formation in the H_2-CO-CO_2 flames and the NO_x emissions were mostly a function of the flame temperature. Compared to hydrocarbon combustion, synthetic fuels produce less NO_x due to their lower flame temperatures and the absence of the prompt NO_x mechanism associated with hydrocarbon combustion chemistry (Turns, 2000).

Turns (1995) studied the influences of nozzle exit diameter, initial jet velocity and fuel type on the $EINO_x$ in non-premixed jet flames. For all the fuels studied, the characteristic temperatures fell with increasing global residence time. The results also showed that the N_2 dilution reduced the flame lengths, global residence times, adiabatic flame temperatures and radiant fractions. For the C_2H_4 and C_3H_8 flames, the $EINO_x$ increased with the N_2 dilution as a result of the higher characteristic non-adiabatic flame temperatures.

2.3.3 Gas Turbine Combustor NO_x Emissions

The NO_x emission characteristics of gas turbine combustors were investigated by Saito and Sato (1994). In their experiment, the combined effects of the inlet air temperature, combustor pressure, and combustion air-fuel ratio on the NO_x emissions were investigated for a premixed gas fuel with methane as the main composition. The experiment results revealed that the NO_x emissions increased with the inlet air temperature and combustor pressure. A larger increasing rate of the NO_x emissions with an increasing inlet air temperature was resulted when

the air-fuel ratio in the combustion zone was decreased. The findings suggested that the air-fuel ratio had a significant influence on the NO_x emission rates.

The need to lower the NO_x emission level has led to an increasing use of CFD to provide an insight into emission processes. Benim and Syed (1998) employed the standard RANS k-ε turbulence model in conjunction with the Laminar Flamelet Method (LFM) to predict the NO production in a lean premixed recirculating flame. The simulation was carried out on a two-dimensional (2-D) grid. The results revealed that the LFM constantly under-predicted the NO level since it only considered the thermal NO mechanism, while in the highly lean premixed combustion, the N_2O intermediate mechanisms dominated the total NO formation. Benim and Syed (1998) also suggested that the k-ε turbulence model, which performed poorly in highly swirling flows, contributed to the inaccuracy of the simulation results.

Hamer and Roby (1997) performed a 2-D RANS k-ε analysis of an axisymmetric, swirl-stabilised stationary gas turbine combustor. The results demonstrated that the trend in NO emissions was well predicted. However, the limitation of the k-ε model was that it under-predicted the mixing associated with the swirling flows due to its isentropic turbulence assumption.

For the industrial gas turbines, the use of lean premixed combustion has effectively led to the reduction of NO_x emissions through lowered flame temperature (Saito and Sato, 1994; Benim and Syed, 1998). This is because, at a stoichiometric condition, the regions of high fuel-air ratio burn at high temperatures, thus promoting the NO_x formation. An example of the lean premixed combustion application is the vortex-breakdown stabilized, lean-premixed, double cone burner (DCB) developed at ABB (Sattelmayer *et al*., 1992) which has successfully reduced the NO_x emissions and achieved high efficiency. However, the benefits of reducing the NO_x emissions by employing the lean premixed flame concept may be offset by rising combustion instabilities. Therefore, this concept does not apply to aircraft engines due to the stability requirement for a wide range of operating conditions.

The formation of NO_x in a staged diffusion flame combustor was investigated numerically by Barths *et al.* (1998) employing the RANS k-ε model. The results were validated against the experimental data of the kerosene-fuelled combustor at BR715 engine take-off conditions. The analysis of the reaction paths revealed that the thermal NO was the major contributor to the total NO production in the combustor. Furthermore, the RANS k-ε approach was employed by Shakariyants (2006) to cross-check the NO_x emission solutions obtained from the multi-reactor combustor models for an aero-engine combustor at the design operating point.

2.4 Exhaust Modelling

This section presents the literature review on exhaust modelling. Firstly, the studies of reactive vehicle exhaust have been surveyed to provide an insight into the important atmospheric reaction and numerical techniques which can be employed to model this reaction. This information is significant for the current research because helicopters typically operate at low-altitude close to the ground. Therefore, the chemical reactions between the pollutants in the vehicle exhaust and ambient air should be similar to those in the helicopter exhaust plume.

In addition, a review on aircraft exhaust modelling is carried out to provide the information on chemical species concentrations, flow conditions, reaction mechanisms, computational setup, and flow characteristics. Finally, helicopter exhaust studies are surveyed in order to gain an understanding of the exhaust flow characteristics, and identify the research gap which can be filled by the current research.

2.4.1 Reactive Vehicle Exhaust

Chan *et al.* (2001) employed the 2-D RANS k-ε model to evaluate the effects of exhaust velocity, wind speed and chemistry on the initial dispersion of NO and NO_2 from a vehicle exhaust. Baik *et al.* (2007) modelled reactive pollutant dispersion in an urban street canyon employing RANS in conjunction with a photochemistry. The pollutants considered, which were emitted from the vehicles into the background O_3 in the street canyon, were NO and NO_2. Similar reaction was considered in LES of reactive pollutant dispersion in and above street canyons carried out by Baker *et al.* (2004).

Furthermore, Kikumoto and Ooka (2012) employed LES to study reactive pollutant dispersion in urban street canyons. In this study, they only considered the conversion of NO to NO_2, $NO + O_3 \rightarrow NO_2 + O_2$, which was an important photochemical reaction in the atmosphere (Wayne, 1991).

2.4.2 Reactive Aircraft Exhaust

Prior to the popularity of CFD, 1-D and 2-D computational models have been developed to study the chemical evolution of aircraft exhaust species. Karcher *et al*. (1996) carried out 2-D simulations to investigate the chemical transformation of exhaust species in a plume within the first few kilometres behind a B747 airliner engine. The results, however, were representative for other aircraft types and flight levels. The potential effects of the turbulent mixing and chemical processes in a near-field high speed aircraft plume on the lower stratosphere ambient air have been studied employing several numerical models (Miake-Lye *et al*., 1993; Wang and Chen, 1997; Menon and Wu, 1998).

CFD modelling of aircraft exhaust was carried out by Garmory *et al.* (2008) who employed RANS to investigate the chemistry in the early part of hot exhaust plume. One of the key chemical processes studied was the transformation of NO to NO_2. The flow conditions considered represented those of a turbofan at idle thrust setting. The results revealed that much of the reaction took place inside the jet core before mixing occurred and NO_2 was produced within the plume in the first few meters. However, the corresponding reduction in NO was much less pronounced because of the considerably higher concentration of this species in the plume. Compared to the mixing time scale, the reaction of NO with the ambient O_3 was slow. Garmory *et al.* (2010) later performed another chemical transformation analysis of a turbofan engine exhaust plume in the first 1000 m at take-off and idle conditions employing the RANS k-ε model with the incorporation of the turbulence effects on the reaction rate.

2.4.3 Helicopter Exhaust

A significant amount of research has been carried out to study the aerodynamic interaction between the main rotor and helicopter fuselage. Nam *et al*. (2006) employed an unstructured adaptive mesh to study unsteady rotor-fuselage interaction. Steijl and Barakos (2008) introduced the concept of sliding meshes to account for the relative motion between the main rotor and the fuselage, and further employed this methodology to study the rotor-fuselage interactional aerodynamics. CFD simulations of the flow around a complete helicopter configuration excluding the engine were also carried out by Steijl and Barakos (2012), and Biava *et al*. (2012) employing the URANS model to capture the complex flow phenomena around the helicopter.

Although a substantial amount of work has been communicated to the open public in terms of helicopter flow investigations, hitherto the effects of the engine on the flow fields have only been considered by a limited number of researchers. This stems from the fact that capturing the rotor-fuselage interaction alone is already a challenging problem without an additional level of complication. Furthermore, wind tunnel experimental data for helicopter flows which are available for CFD simulation validations are limited in number, and commonly exclude the engine. However, modelling the engine exhaust is necessary for the study of helicopter emissions. In addition, accurate predictions of the helicopter exhaust quantities are required for the evaluation of the overall engine performance, determining the potential impacts of hot flow impingement on the airframe, and the design of infra-red signature suppressor.

The flow fields and mixing characteristics of a helicopter exhaust plume, as well as its interaction with downwash, were numerically investigated by Gatland *et al.* (2002) employing the RANS k-ε approach. The validation of simulation results against the experimental measurements revealed that the fine grid was able to capture exhaust flow features such as the jet core and flow recirculation better than the coarse grid. Furthermore, free-stream flow was important as it influenced the effects of the downwash on the exhaust flow, especially in the regions near the nozzle exit.

In another research carried out by Xie (2011), the aerodynamic interaction between the helicopter fuselage, rotor and engine, and their impacts on the turboshaft engine performance were studied. The flight modes considered in this particular study were the hover, near-ground hover and vertical climb modes. The RANS approach was employed to simulate the flow fields around a helicopter model with intake and exhaust systems. In addition, Xie (email, 10 February, 2011) performed RANS on the same helicopter configuration during the forward flight mode. The results revealed that the helicopter exhaust plume was almost straight in the free-stream direction. This suggested that it was reasonable to assume that the flow characteristics of helicopter exhaust in forward flight were similar to those of the fixed wing aircraft exhaust.

O'Brien *et al.* (2008) investigated the engine exhaust effects on helicopter aeromechanics using the RANS approach. The helicopter geometry used in the study was the ROBIN model developed within NASA (Freeman and Mineck, 1987; Mineck and Gorton, 2000). Two exhaust configurations considered in this study were the baseline engine with a square aft exhaust face, and an upward exhaust configuration. Simulations were carried out at three flight conditions representing the low, intermediate and high flight speed cases. The results revealed that at the low forward flight speed, the exhaust plume was strongly influenced by the rotor wake. However, at the high flight speed, the effects of rotor wake on the exhaust flow diminished, especially for the baseline engine which produced a nearly straight plume. These findings agreed with the study of Xie (2011). The study of O'Brien *et al*. (2008) also demonstrated that the exhaust configuration might affect the flow characteristics, helicopter loads, lift and drag forces. By modifying the angle of the exhaust face, the interaction between the exhaust jet and local flow changed accordingly and became that of a jet in crossflow.

Gursoy (2009) performed RANS flow analysis of a medium-lift utility helicopter exhaust during a forward flight mode at four advance ratios. The flow streamlines obtained from the all computations exhibited an almost straight exhaust path except for the low speed case with the advance ratio of 0.07 where the path of the exhaust plume was deflected slightly due to the rotor downwash.

The mixing characteristics of an isolated helicopter exhaust system were investigated by Ozel and Edis (2006). In this study, the flow physics associated with a multi-stream turboshaft engine were simulated using RANS. Among the various RANS-based turbulence models, the Shear Stress Transport (SST) model was identified as the most suitable model for high temperature jet flows.

Although the findings from these studies provide a better understanding of helicopter exhaust flow characteristics, they neither consider the application of LES nor the chemical interaction between the species in the hot exhaust plume and ambient air. This has triggered the interest to investigate the NO_x reaction in the helicopter exhaust plume employing LES.

3 NUMERICAL METHODS

The present CFD computations have been performed on the high performance computing facility within Cranfield University employing 16, 32 and 48 processors. The CFD solver employed is the commercial code, FLUENT, which offers good parallel computing efficiency. It is thus possible to take advantage of a linear speed-up scaling in moving from 16 to 32 processors, such that the execution time is halved. Utilising 48 processors results in a further reduction of 34% in execution time. The user-defined functions (UDFs) for the inlet profiles and data averaging have been written in C^{++} and loaded into FLUENT. The results are post-processed in Tecplot. This chapter summarises the LES concept, governing equations, and closure modelling approaches. Furthermore, the reaction and NO_x models employed in the current research are described.

3.1 Large Eddy Simulation

In LES, the motion of the large energy-containing eddies, which influence the main flow characteristics, are computed directly while the smaller-scale eddies and their interaction with the large-scale turbulent structures are represented by mathematical models. Figure 3-1 summarises the concept of LES in Kolmogorov energy spectrum. The x-axis represents the eddy size from large to small, and is plotted against the y-axis which indicates the energy level contained in these eddies. In the current research, the ratio of resolved kinetic energy to subgrid kinetic energy of LES computations ranges from 7.4×10^3 to 8.2×10^4.

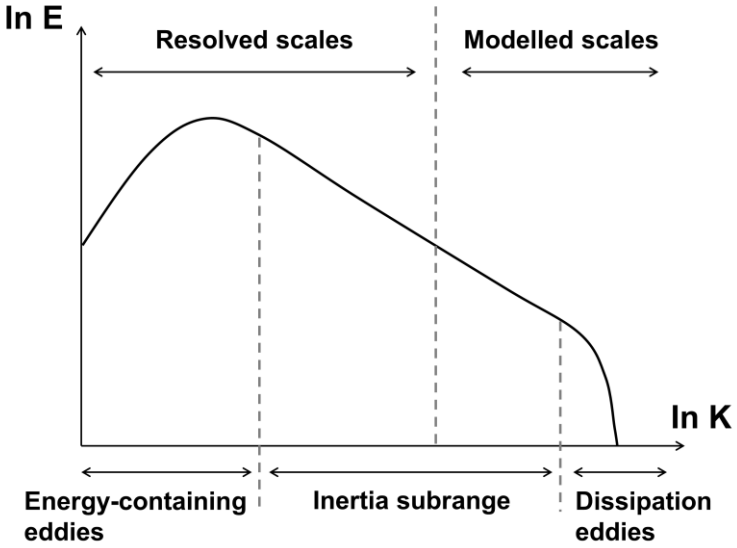

Figure 3-1 LES in the Kolmogorov energy spectrum, energy, E, plotted against wave number, K.

3.1.1 Governing Equations

LES involves a filtering operation which separates the resolved components of the flow-field variables from the SGS components (Leonard, 1974). Applying the filtering operation to the flow transport equations with chemical reaction yields the LES equations (Branley and Jones, 2001),

$$\frac{\partial \bar{\rho}}{\partial \mathrm{t}} + \frac{\partial(\bar{\rho}\bar{u}_i)}{\partial x_i} = 0, \tag{3-1}$$

$$\frac{\partial \bar{\rho}\bar{u}_i}{\partial t} + \frac{\partial\left(\bar{\rho}\bar{u}_i\bar{u}_j\right)}{\partial x_j} = -\frac{\partial \bar{p}}{\partial x_i} + \frac{\partial \bar{\sigma}_{ij}}{\partial x_j} - \frac{\partial \tau_{ij}^{sgs}}{\partial x_j}, \tag{3-2}$$

$$\frac{\partial \bar{\rho}\bar{Y}_\alpha}{\partial t} + \frac{\partial(\bar{\rho}\bar{u}_i\bar{Y}_\alpha)}{\partial x_i} = -\frac{\partial \bar{J}_i^\alpha}{\partial x_i} - \frac{\partial M_i^\alpha}{\partial x_i} + \bar{\omega}_\alpha, \tag{3-3}$$

where u_i and u_j are the velocity vectors, p, Y_α and ω_α represent the pressure, species mass fractions and chemical reaction terms for species α (α = 1, 2,..., n) respectively.

The filtered stress tensor due to molecular viscosity, $\bar{\sigma}_{ij}$, is given by,

$$\bar{\sigma}_{ij} = 2\mu\bar{S}_{ij}. \tag{3-4}$$

The filtered strain rate tensor, $\bar{S}_{ij}$, can be expressed as,

$$\bar{S}_{ij} = \frac{1}{2}\left(\frac{\partial\bar{u}_i}{\partial x_j} + \frac{\partial\bar{u}_j}{\partial x_i}\right) - \frac{1}{3}\delta_{ij}\bar{S}_{kk}. \tag{3-5}$$

The filtered species mass flux, $\bar{J}_i^\alpha$, is defined by,

$$\bar{J}_i^\alpha = -\frac{\mu}{Sc}\left(\frac{\partial\bar{Y}_\alpha}{\partial x_i}\right), \tag{3-6}$$

where μ is the dynamic viscosity, and Sc denotes the Schmidt number. The unclosed terms in the transport equations which require closure modelling are the subgrid stress,τ_{ij}^{sgs}, subgrid species mass flux, M_i^α, and filtered chemical reaction term, $\bar{\omega}_\alpha$.

3.1.2 Subgrid Scale Modelling

The unresolved subgrid stress,$\tau_{ij}^{sgs} = \bar{\rho}\left(\overline{u_i u_j} - \bar{u}_i\bar{u}_j\right)$, which results from the filtering operation can be modelled applying the Boussinesq turbulent viscosity assumption (Pope, 2000),

$$\tau_{ij}^{sgs} = -2\mu_t\bar{S}_{ij} + \frac{1}{3}\delta_{ij}\tau_{kk}. \tag{3-7}$$

The turbulent viscosity, μ_t, is defined by the standard Smagorinsky model as (Smagorinsky, 1963),

$$\mu_t = \bar{\rho}(C_s\Delta)^2|\bar{S}|. \quad \textbf{(3-8)}$$

The Smagorinsky coefficient, C_s, which is an empirical constant is set to be 0.1 in the current research. The filter width, Δ, can be approximated by the cube root of the cell volume. The characteristic filtered strain rate is defined by,

$$|\bar{S}| \equiv \left(2\bar{S}_{ij}\bar{S}_{ij}\right)^{1/2}. \quad \textbf{(3-9)}$$

As similar to the species mass flux, the subgrid species mass flux, $M_i^\alpha = \bar{\rho}(\overline{u_i Y_\alpha} - \bar{u}_i\bar{Y}_\alpha)$, is expressed as (Eidson, 1985),

$$M_i^\alpha = -\frac{\mu_t}{Sc_t}\left(\frac{\partial \bar{Y}_\alpha}{\partial x_i}\right). \quad \textbf{(3-10)}$$

3.2 Reaction Models

In FLUENT, the chemical reactions are modelled as source terms in the species transport equations. The reaction rates, which appear as source terms, can be computed by three approaches: the laminar finite-rate, eddy-dissipation and eddy-dissipation-concept (EDC) models. For the current research, turbulent flames in the combustor are modelled employing the non-premixed combustion model which is based on the mixture fraction approach.

3.2.1 Laminar Finite-Rate Model

The laminar finite-rate model neglects the effect of turbulent fluctuations. Instead, the reaction rates are calculated by Arrhenius expressions. The net source of chemical species α is defined as the sum of sources over the N_R reactions which the species α participates in,

$$\omega_\alpha = W_\alpha \sum_{r=1}^{N_R} \widehat{\omega}_{\alpha,r}, \tag{3-11}$$

where W_α is the molecular weight of species α and $\widehat{\omega}_{\alpha,r}$ denotes the Arrhenius molar rate of creation/destruction of this species in reaction r, which can be expressed as,

$$\widehat{\omega}_{\alpha,r} = \Gamma\left(\nu''_{\alpha,r} - \nu'_{\alpha,r}\right)\left(k_{f,r}\prod_{\gamma=1}^{N_r}\left[C_{\gamma,r}\right]^{\eta'_{\gamma,r}} - k_{b,r}\prod_{\gamma=1}^{N_r}\left[C_{\gamma,r}\right]^{\eta''_{\gamma,r}}\right), \tag{3-12}$$

where Γ represents the effect of third bodies, $\nu'_{\alpha,r}$ is the stoichiometric coefficient for a reactant, $\nu''_{\alpha,r}$ is the stoichiometric coefficient for a product, N_r denotes the number of species, $C_{\gamma,r}$ is the molar concentration, $\eta'_{\gamma,r}$ represents the forward rate exponent and $\eta''_{\gamma,r}$ represents the backward rate exponent for each reactant and product in reaction r. The forward rate constant is calculated by the Arrhenius expression,

$$k_{f,r} = AT^{\beta}e^{-E_a/RT}, \tag{3-13}$$

where A is the pre-exponential factor, β denotes the temperature exponent, E_a represents the activation energy and R is the universal gas constant. If applicable, the backward rate constant can be computed from the relationship, $k_{b,r} = k_{f,r}/K_r$, where K_r represents the equilibrium constant.

3.2.2 Eddy-Dissipation Model

The eddy-dissipation model is based on the work of Magnussen and Hjertager (1977). Chemical reactions in this model are assumed to take place much faster than turbulence mixes the reactants. Hence, the reaction rates are mixing limited and the calculations of Arrhenius chemical kinetics can be excluded. The net production rate of chemical species α as a result of reaction r is computed by the smaller of the two following equations:

$$\omega_{\alpha,r} = \nu'_{\alpha,r} W_\alpha A \rho \frac{\varepsilon}{k} \min_R \left(\frac{Y_R}{\nu'_{R,r} W_R} \right), \quad \textbf{(3-14)}$$

$$\omega_{\alpha,r} = \nu'_{\alpha,r} W_\alpha A B \rho \frac{\varepsilon}{k} \frac{\sum_P Y_P}{\sum_\gamma^N \nu''_{\gamma,r} W_\gamma}, \quad \textbf{(3-15)}$$

where k is the turbulent kinetic energy, ε is the turbulent dissipation rate, Y_R represents the mass fraction of a particular reactant, Y_P denotes the mass fraction of any product species, A and B are Magnussen constants for reactants and products respectively. For LES, the turbulent mixing rate, k/ε, is replaced by SGS mixing rate, τ_{ij}^{sgs-1}.

3.2.3 Eddy-Dissipation-Concept Model

The EDC model, which is an extension of the eddy-dissipation model, incorporates detailed Arrhenius chemical kinetics in turbulent flows (Magnussen, 1981). It assumes that the reaction takes place in small turbulent structures called the fine scales. The reaction source term for the species α is modelled as,

$$\bar{\omega}_\alpha = \frac{\bar{\rho}(\xi^*)^2}{\tau^*[1-(\xi^*)^3]} (Y_\alpha^* - \bar{Y}_\alpha), \quad \textbf{(3-16)}$$

where Y_α^* represents the fine-scale species mass fraction, the time scale, τ^*, is modelled as,

$$\tau^* = C_\tau \left(\frac{\mu}{\bar{\rho}\varepsilon}\right)^{1/2}, \tag{3-17}$$

and the length fraction of the fine scales is expressed as,

$$\xi^* = C_\xi \left(\frac{\mu\varepsilon}{\bar{\rho}k^2}\right)^{1/4}, \tag{3-18}$$

where C_τ is the time scale constant set at 0.4082 and C_ξ is the volume fraction constant which is equal to 2.1377.

3.2.4 Non-Premixed Combustion Model

In the non-premixed combustion modelling approach, the chemical reaction rate is assumed to be faster than the mixing rate of the fuel and oxidiser. Therefore, combustion occurs once the fluids mix. Species concentrations are not obtained by solving the transport equations individually. Instead, they are derived from a scalar quantity used to describe the local mass fraction of the burnt and unburnt fuel called the mixture fraction (Pitsch, 2006).

Hence, the non-premixed combustion model is simplified to a mixing problem. This involves solving the mixture fraction transport equation which can be written as (Peters, 2000),

$$\frac{\partial \bar{\rho}\bar{Z}}{\partial t} + \frac{\partial (\bar{\rho}\bar{u}_i\bar{Z})}{\partial x_i} = -\frac{\partial \bar{J}_{z,i}}{\partial x_i} - \frac{\partial M_{z,i}}{\partial x_i}, \tag{3-19}$$

where $\bar{J}_{z,i}$ denotes the filtered mixture fraction mass flux and $M_{z,i}$ is the subgrid mixture fraction mass flux which requires closure modelling as similar to M_i^α.

For a system with one fuel stream, the filtered mixture fraction, $\bar{Z}$, is defined as (Sivathanu and Faeth, 1990),

$$\bar{Z} = \frac{\bar{Y}_\alpha - \bar{Y}_{\alpha,O}}{\bar{Y}_{\alpha,F} - \bar{Y}_{\alpha,O}}, \quad \textbf{(3-20)}$$

where $\bar{Y}_{\alpha,F}$ and $\bar{Y}_{\alpha,O}$ denote the filtered mass fraction of the species at the fuel and oxidiser inlets respectively. The value of Z is 1 for pure fuel, 0 for pure oxidiser and ranges between the two values depending on the extent of mixing. The Z transport equation does not contain a source term because Z is a conserved scalar and independent of the chemistry.

Probability density function (PDF), which links the instantaneous values of the species mass fractions to the filtered values, is used to describe the interaction between turbulence and chemistry in the non-premixed combustion model. For the equilibrium chemistry, the reactions are assumed to be infinitely fast and reversible so that the species are in equilibrium at each value of mixture fraction.

Therefore, the instantaneous species mass fractions, as well as the temperature and density, are only a function of the mixture fraction (Bilger, 1976, 1980). The filtered species mass fractions, temperature and density can then be obtained from the following relationships (Libby and Williams, 1980; O'Brien, 1980; Pope, 1985; Pitsch, 2006):

$$\bar{Y}_\alpha = \int_0^1 Y_\alpha^e(Z)\bar{f}(Z)dZ, \quad \textbf{(3-21)}$$

$$\bar{T} = \int_0^1 T^e(Z)\bar{f}(Z)dZ, \quad \textbf{(3-22)}$$

$$\frac{1}{\bar{\rho}} = \int_0^1 \frac{1}{\rho(Z)}\bar{f}(Z)dZ. \quad \textbf{(3-23)}$$

The filtered density function, $\bar{f}(Z)$, which requires closure modelling, represents the statistical properties of the mixing of the fuel and oxidiser by quantifying the probability of finding $\bar{Y}_\alpha$. The shape of $\bar{f}(Z)$ is assumed to be that of the beta-function (β-function) which can be mathematically expressed as a function of $\bar{Z}$ and its variance, $\overline{Z'^2}$ (Rhodes *et al.*, 1974; Kolbe and Kollmann, 1980; Cook and Riley, 1994),

$$\bar{f}(Z) = \frac{Z^{a-1}(1-Z)^{b-1}}{\int_0^1 Z^{a-1}(1-Z)^{b-1}dZ}, \tag{3-24}$$

$$a = \bar{Z}\left[\frac{\bar{Z}(1-\bar{Z})}{\overline{Z'^2}} - 1\right], \tag{3-25}$$

$$b = (1-\bar{Z})\left[\frac{\bar{Z}(1-\bar{Z})}{\overline{Z'^2}} - 1\right]. \tag{3-26}$$

For LES, $\overline{Z'^2}$ is modelled as,

$$\overline{Z'^2} = C_v L_s^2 |\nabla \bar{Z}|^2, \tag{3-27}$$

where L_s denotes the subgrid length scale. The value of the constant, C_v, is 0.5 for the current research. In FLUENT, the chemistry calculations and PDF integrations are pre-processed and stored in the look-up tables which are then used to obtain the mixture faction and other scalar quantities, making this approach highly computational efficient.

3.2.5 Flamelet Models

The flamelet models assume that the chemical reactions are so fast that they take place in a thin layer near the stoichiometric mixture on a scale smaller than the Kolmogorov scale. As a result, the reaction zone structure remains laminar and the diffusive transport occurs in the normal direction to the stoichiometric mixture surface.

Therefore, the scalar transport equations can be expressed such that the mixture fraction is an independent coordinate (Peters, 1983, 1984),

$$\frac{\partial Y_\alpha}{\partial t} = \frac{1}{2}\rho\chi\frac{\partial^2 Y_\alpha}{\partial Z^2} + \omega_\alpha. \quad \textbf{(3-28)}$$

For the steady laminar flamelet model, the flame structure is assumed to be in the steady state. Hence, the time derivative term on the left-hand side of Equation 3-28 can be neglected. The scalar dissipation rate, χ, is expressed as $\chi = 2D|\nabla Z|^2$, where D is the scalar diffusivity which represents the rate of local mixing. The relationship between Z and χ is assumed to be (Peters, 1984),

$$Y_\alpha = Y_\alpha^{fl}(Z, \chi_{st}), \quad \textbf{(3-29)}$$

where fl represents flamelet, st denotes stoichiometry. The filtered species mass fractions can be obtained from the integral,

$$\bar{Y}_\alpha = \int_0^1 Y_\alpha^{fl}(Z, \chi_{st})\tilde{f}(Z, \chi_{st})dZd\chi_{st}. \quad \textbf{(3-30)}$$

Since, it is assumed that Z and χ_{st} are statistically independent, the joint PDF, $\tilde{f}(Z, \chi_{st})$, can be simplified to $\tilde{f}(Z)\tilde{f}(\chi_{st})$ (Peters, 1984). The integration in Equation 3-30, as similar to the equilibrium chemistry, is pre-calculated and stored in a look-up table. The shape of $\tilde{f}(Z)$ is assumed to be β-function, and a function of $\bar{Z}$ and $\overline{Z'^2}$. The PDF of χ_{st} is described by a delta-function and modelled as,

$$\overline{\chi_{st}} = C_\chi\frac{(\mu_t + \mu)}{\rho\sigma_t}|\nabla\bar{Z}|^2, \quad \textbf{(3-31)}$$

where C_χ and σ_t are constants with the values of 2 and 0.85 accordingly.

3.3 NO_x Model

The assumption of equilibrium chemistry is not appropriate for NO_x modelling because the NO_x reaction rates are slow. Instead, the concentration of NO_x is calculated from the computed combustion flow fields using the FLUENT NO_x post-processor. Since the NO_x emissions consist mainly of NO and much less NO_2, the NO_x model only takes into account the chemical kinetic processes responsible for the NO formation. In non-premixed hydrocarbon combustion, the thermal and prompt NO mechanisms contribute to most of the NO formed (Bowman, 1992). Therefore, only these two NO formation mechanisms are considered for the current research. The NO_x emissions from the two mechanisms are predicted by solving the species transport equation in Equation 3-3 for the NO mass fraction.

The formation of thermal NO_x is highly temperature-dependant and dictated by the following chemical reactions which are known as the extended Zeldovich mechanism:

$$N_2 + O \rightleftharpoons NO + N, \tag{3-32}$$

$$N + O_2 \rightleftharpoons NO + O, \tag{3-33}$$

$$N + OH \rightleftharpoons NO + H. \tag{3-34}$$

With sufficient oxygen, a quasi-steady state can be assumed since the free nitrogen consumption rate becomes equal to its formation rate. Therefore, the net NO formation rate is obtained from

$$\frac{d[NO]}{dt} = 2k_{f,1}[O][N_2]\frac{\left(1 - \frac{k_{r,1}k_{r,2}[NO]^2}{k_{f,1}[N_2]k_{f,2}[O_2]}\right)}{\left(1 + \frac{k_{r,1}[NO]}{k_{f,2}[O_2] + k_{f,3}[OH]}\right)}, \tag{3-35}$$

where k is the reaction rate constant, the square brackets represent the concentration of a species, f and r denote forward and reverse reactions respectively. The subscript number 1, 2 and 3 of k denote the reactions in Equations 3-32 – 3-34 respectively. The k values selected for the NO_x model are obtained from the evaluation of Hanson and Salimian (1984):

$k_{f,1} = 1.8 \times 10^8 e^{-38370/T}$, $\quad k_{r,1} = 3.8 \times 10^7 e^{-425/T}$,

$k_{f,2} = 1.8 \times 10^4 T e^{-4680/T}$, $\quad k_{r,2} = 3.81 \times 10^3 T e^{-20820/T}$,

$k_{f,3} = 7.1 \times 10^7 e^{-450/T}$, $\quad k_{r,3} = 1.7 \times 10^8 e^{-24560/T}$.

To solve Equation 3-35, the [O] and [OH] are required in addition to the [O_2] and [N_2] which can be obtained from the combustion simulation results. Since the O atoms are more abundant than their equilibrium levels, their concentration is determined by employing the partial equilibrium approach in which third-body reactions are responsible for the O_2 dissociation-recombination process,

$$O_2 + M \rightleftharpoons O + O + M. \tag{3-36}$$

Hence, the following expression is substituted into Equation 3-35 (Warnatz, 2001),

$$[O] = 36.64 T^{1/2} [O_2]^{1/2} e^{-27123/T}. \tag{3-37}$$

When $k_2[O_2]_e \gg k_3[OH]_e$, the reaction in Equation 3-34 is assumed negligible and the calculation of OH concentration can be excluded. The source term due to the thermal NO_x mechanism in the NO transport equation is then computed from the rate of NO formation as,

$$S_{thermal,NO} = W_{NO} \frac{d[NO]}{dt}, \tag{3-38}$$

where W_{NO} represents the molecular weight of NO. The interaction between turbulence and the NO_x formation is taken into account by employing the PDF approach in terms of the mixture fraction.

The prompt NO mechanism is responsible for the rapid NO production in the flame front. For most hydrocarbon fuels, the prompt NO formation rate can be expressed as (De Soete, 1975; Backmier *et al.*, 1973),

$$\frac{d[NO]}{dt} = f k_{pr}[O_2]^a[N_2][FUEL]e^{-E_a/RT}, \quad \textbf{(3-39)}$$

where f denotes the correction factor which incorporates the effect of fuel type, a represents the oxygen reaction order, pr denotes the prompt NO mechanism and E_a has the value of 303474.125 J/gmol. The formation rate is then used to compute the source term due to the prompt NO mechanism in the same manner as the thermal NO source term expressed in Equation 3-38.

4 TEST CASES

4.1 Introduction

Simulation results of four test cases are presented in this chapter. The first and second test cases, which are LES of a non-reacting jet and a coaxial jet combustor respectively, are carried out with the focal aim of studying the mixing characteristics jet flows. This is important because for the combustion process, the reaction rate depends on the mixing and entrainment rates. Furthermore, the scalar mixing of the jet exhaust is important particularly when considering aircraft emissions since it influences the pollutants dispersion and interaction between the exhaust and ambient air. Therefore, accurate predictions of the flow-field and mixing characteristics are necessary in order to provide a better understanding of such flows, and enhance the design and development of more environmentally-friendly aircraft engines with reduced emissions. Hitherto, only structured grids have been employed in the simulations. Therefore, the third test case which is LES on an unstructured grid is carried out to assess the validity of using the unstructured grid for combustion LES prior to its actual application in the next chapter. Finally, the last test case is carried out to test the key chemical reaction and its kinetic parameters selected for the modelling of a helicopter exhaust in Chapter 7.

4.2 LES of a Non-Reacting Jet

Non-reacting LES is carried out to study the performance of the current LES in capturing the complex jet development and mixing characteristics of scalar properties. The computational setup will be described and the simulation results presented will be for the velocity and passive scalar fields.

4.2.1 Computational Domain and Setup

The computational domain consists of a round jet with co-flowing air, which is a representative of the jet engine exhaust configuration. The jet diameter, *D*, is 0.00635 m which is the same as that in the experiment (Garry and Holt, 2008; Poll *et al.*, 2009). The outer domain extends 40*D* radially and 110*D* axially. Three structured grids comprising approximately 1.0, 2.0 and 4.4 million elements are created for the grid sensitivity analysis. They will, henceforth, be referred to as the coarse, medium and fine grids respectively. All grids are refined near the jet exit and interface between the two fluid streams to ensure that the mesh is sufficiently fine for LES to capture the flow with rapid changes in the flow properties in the regions.

For the upstream boundary, the jet and co-flow inlets are specified as velocity inlets while the downstream boundary is an outflow. The surrounding cylindrical boundary is specified as the symmetry to avoid the flow from reflecting back into the domain and interfering with the jet flow. The computational grid and specified boundary conditions are illustrated in Figure 4-1. The flow conditions employed in the simulations are similar to those in the experiment. The velocity profile of the jet at the inlet is specified by the 1/7th power law defined as,

$$U_{jet} = U_{bulk} C \left(1 - \frac{r}{r_{jet}}\right)^{\frac{1}{7}}. \quad \textbf{(4-1)}$$

The constant, *C*, is 1.28 for a fully developed turbulent pipe flow condition. The bulk velocity of the jet, U_{bulk}, is 23 m/s and the velocity of the co-flowing air is 5 m/s.

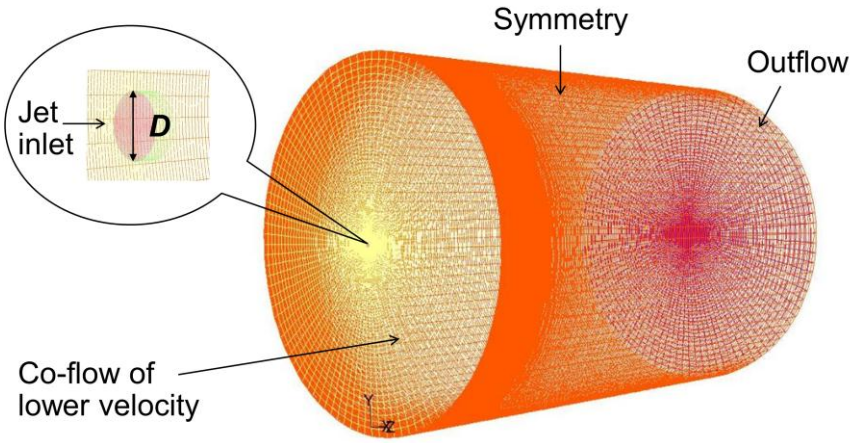

Figure 4-1 Computational mesh and boundary conditions of the round jet.

The simulations have been performed employing LES with the standard Smagorinsky-Lilly SGS treatment. The jet inlet velocity profile has been written as a UDF. The time step size selected for this study is 1.0×10^{-4} seconds. After the simulations have been performed initially for 5 flow-through times, samples are collected for 20 flow-through times to ensure mean statistics are sufficiently converged. The flow-through time is calculated based on the mean velocity and geometry length. Another UDF has been written to collect the statistics of the passive scalar fields, and time-average them. The radius, r, and axial distance, x, are normalised by D. The current simulation results in terms of the time-averaged axial velocity and passive scalar profiles are validated against the measurements from the low-speed wind tunnel experiment carried out at Cranfield University (Garry and Holt, 2008; Poll *et al.*, 2009), and compared with the LES results on a computational grid consisting of approximately 2.3 million elements from the previous LES code, PUFFIN, which has been developed by Kirkpatrick *et al.* (2003a, 2003b) and extended by Ranga-Dinesh (2007, 2010a, 2010b).

4.2.2 Results and Discussion

Figure 4-2 and 4-3 compare, respectively, the time-averaged axial velocity and passive scalar profiles obtained from LES on the three grids at the stations *x/D* = 15 and 30. The comparison reveals that the LES predictions are highly sensitive to the grid density especially in the near-field regions. As depicted in Figure 4-2 and 4-3, at *x/D* = 15, the results of the time-averaged axial velocity and passive scalar are over-predicted in the jet core region while the spreading rates are slightly under-predicted. However, these deviations from the experimental data reduce as the grid resolution increases because the finer grids are able to resolve more small-scale structures present in the jet core and shear layers.

In addition, the comparison of the axial velocity and passive scalar profiles at *x/D* = 30 suggests that the LES results become less sensitive to the grid resolution downstream of the jet. This is because of the higher grid requirements near jet nozzle where the velocity is higher, and the mixing is more intense.

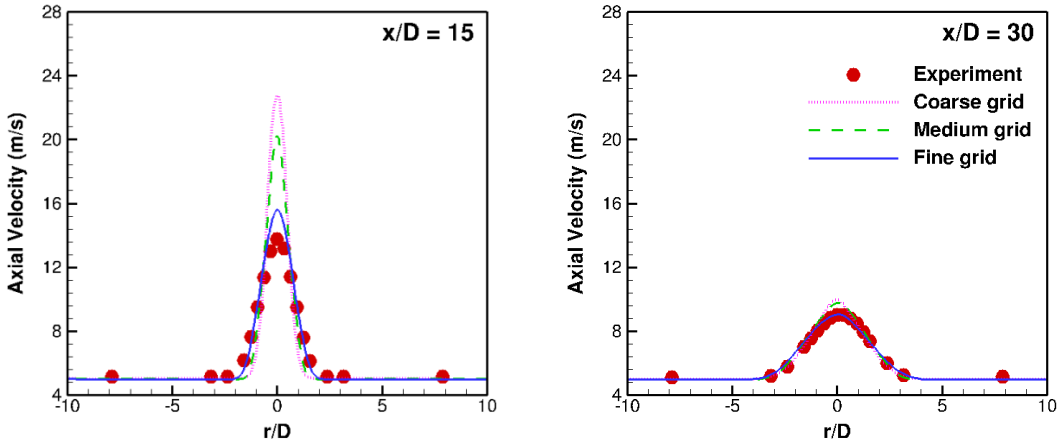

Figure 4-2 Time-averaged axial velocity profiles from the coarse, medium and fine grids at *x/D* = 15 and 30.

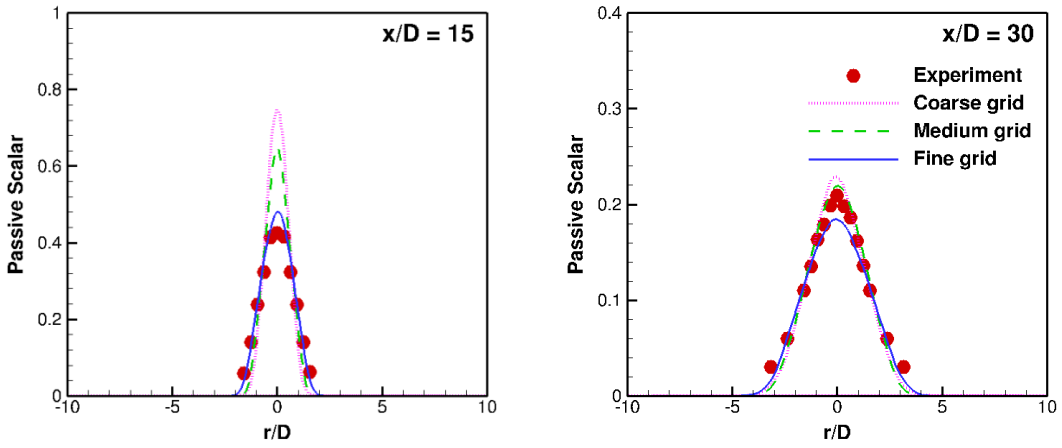

Figure 4-3 Time-averaged passive scalar profiles from the coarse, medium and fine grids at *x/D* = 15 and 30.

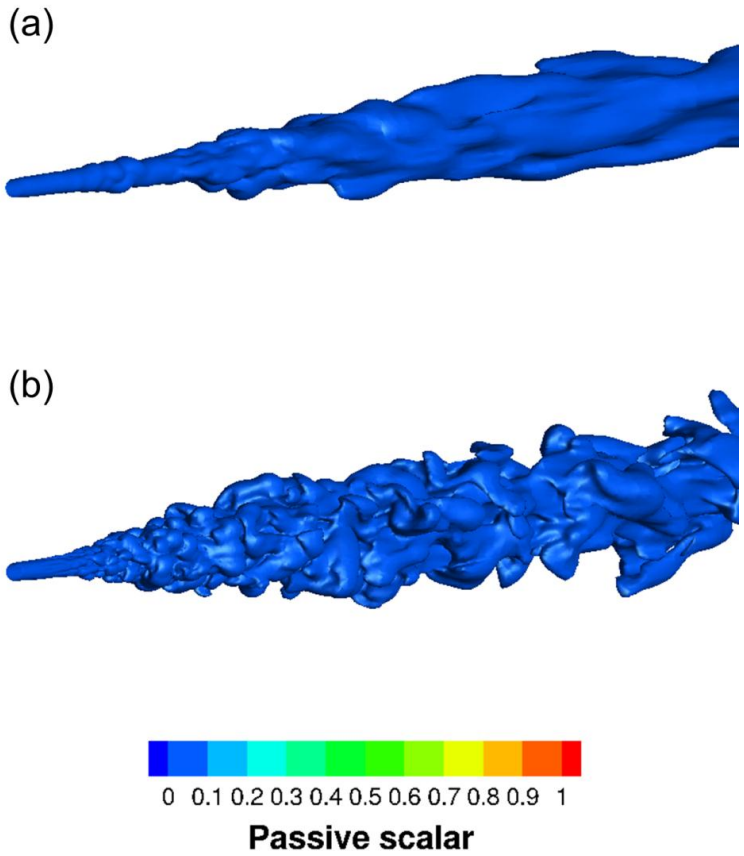

Figure 4-4 Instantaneous passive scalar iso-surfaces of LES on the (a) coarse and (b) fine grids at 3.13 s.

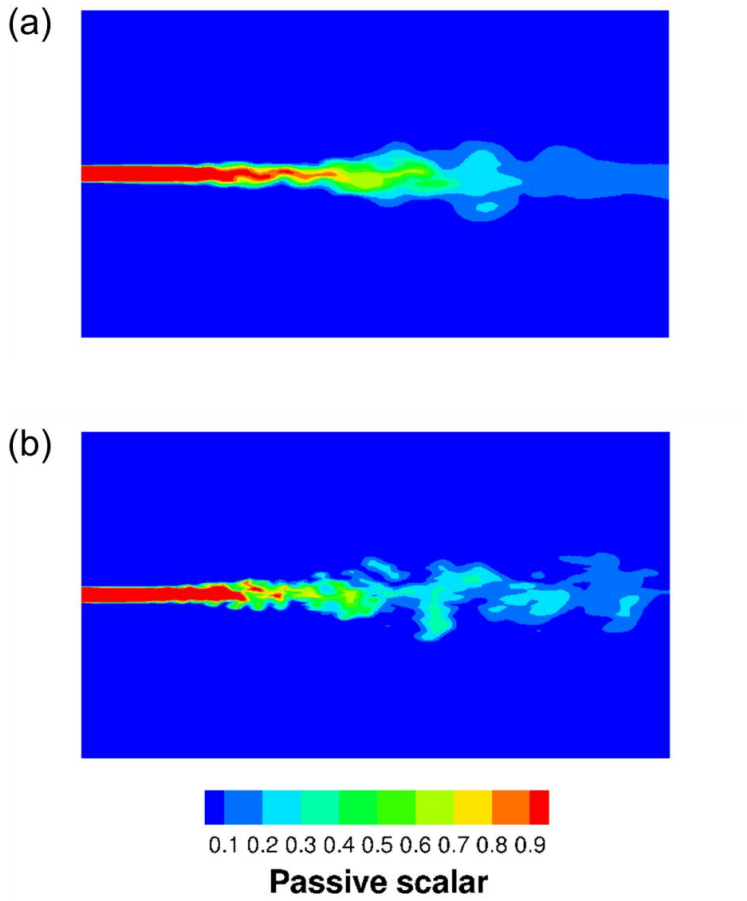

Figure 4-5 Instantaneous passive scalar contours on the centre-plane of LES on the coarse and fine grids at 3.13 s.

Figure 4-4 and 4-5 compare the instantaneous passive scalar iso-surfaces and contours on the centre-plane respectively from LES on the coarse and fine grids. The comparison in Figure 4-4 demonstrates the superiority of the fine grid over the coarse grid in capturing small-scale structures. As further exhibited in Figure 4-5, the fine grid is able to capture more detailed mixing, jet core tip breakup, vortex shedding and entrainment of the co-flowing fluid into the jet.

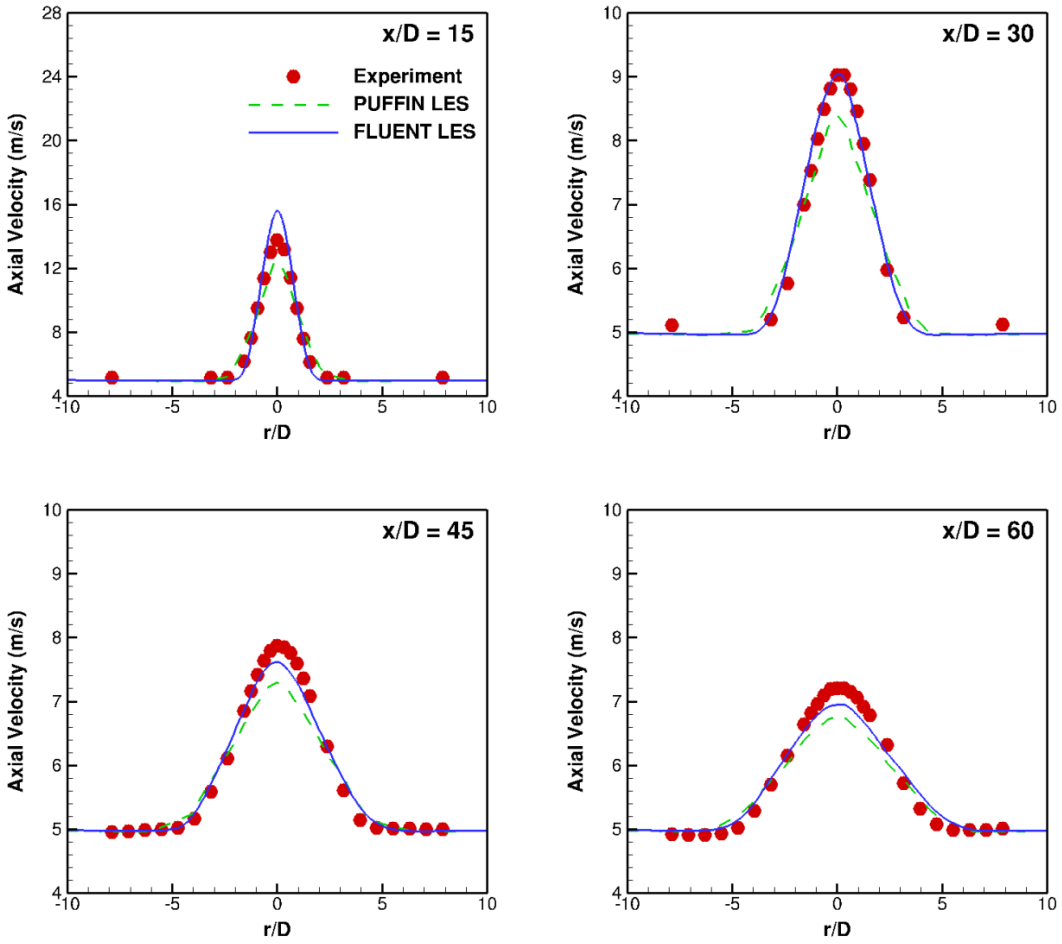

Figure 4-6 Comparison of time-averaged axial velocity profiles from FLUENT and PUFFIN LES at *x/D* = 15, 30, 45 and 60.

The results of LES on the fine grid are subsequently validated against the experimental data and compared with the solutions of the PUFFIN LES code. The comparison of time-averaged axial velocity profiles at stations *x/D* = 15, 30, 45 and 60 is illustrated in Figure 4-6. The simulation results exhibit the jet development along the streamwise direction. At the station *x/D* = 15, the current FLUENT LES over-predicts the velocity values in the jet centre slightly. However, at other downstream locations, the current LES predictions agree well with the experimental data.

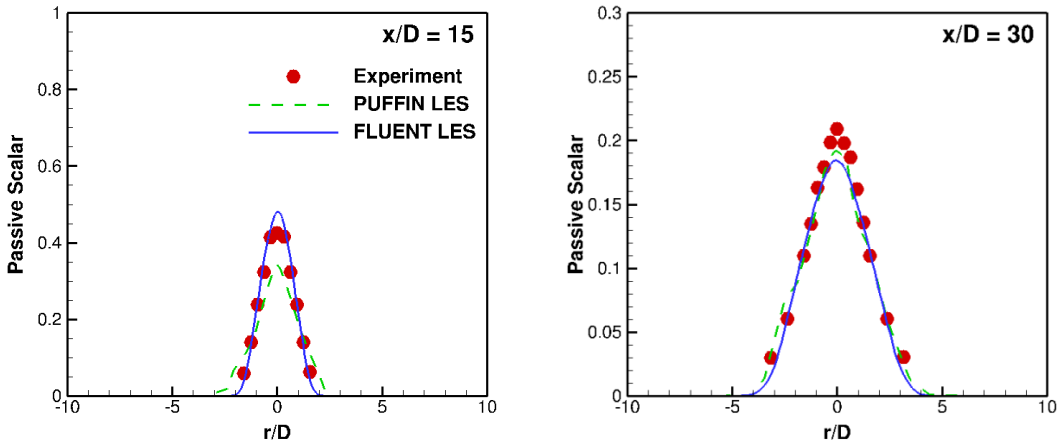

Figure 4-7 Comparison of time-averaged passive scalar profiles from FLUENT and PUFFIN LES at *x/D* = 15 and 30.

Figure 4-7 compares the time-averaged passive scalar profiles from the current FLUENT LES, PUFFIN LES and experiment at *x/D* = 15 and 30. As similar to the velocity comparison displayed in Figure 4-6, the current LES over-predicts the passive scalar values slightly in the core region at *x/D* = 15. Compared to the PUFFIN LES which employs a higher-order discretisation scheme and more advanced SGS model, the current LES is able to capture the jet peak and width better overall. This is because the current LES has been carried out on the finer mesh which allows more small-scale structures in the jet core and shear layers to be resolved. The capabilities of LES to predict flow fields, and capture the mixing and spreading behaviours of a round jet with a co-flow are demonstrated in this test case. Since the fidelity of LES solutions relies on the grid resolution, the simulation results in the core region can be further improved by the local grid refinement.

4.3 LES of a Coaxial Jet Combustor

The coaxial jet combustor employed in this test case is similar to the one in the experiment carried out by Owen *et al.* (1976). This configuration is selected because it has relatively simple geometry and boundary conditions yet manifests complex flow patterns which resemble those in a real gas turbine combustor.

The objectives of this study are to evaluate the capability of the current FLUENT LES code to model non-premixed turbulent combustion, and test the sensitivity of the simulation results to the grid resolution and chemistry model. The performances of LES and RANS are compared to demonstrate the superiority of LES over RANS in capturing realistic flame behaviours. This is followed by the description of LES flame structure and the sensitivity analysis. The results of this test case have been published in a scientific journal (Dumrongsak and Savill, 2012b).

4.3.1 Computational Domain and Setup

The LES simulations have been carried out for a coaxial jet combustor with the operating conditions similar to those in the experiment of Owen *et al.* (1976). The central inflow is a pure methane stream with the velocity of 0.93 m/s. The annular inflow is a non-swirling air stream with the bulk velocity, U, of 20.63 m/s. The operating pressure of the combustor is 3.8 atm. The fuel and air temperatures are 300 K and 750 K respectively. The two inflow streams are separated by a thin splitter plate with the thickness of 0.018 cm. The splitter plate creates the vortex shedding and instabilities which initiate turbulence in the jet mixing layer. The centre radius, annular outer radius, R, and combustor radius are 3.157 cm, 4.685 cm and 6.115 cm accordingly. The domain extends $0.2R$ upstream and $8.1R$ downstream.

Two O-type grids of 2.3 and 6.2 million hexahedral elements are created for the grid sensitivity analysis. These will, hereinafter, be referred to as the coarse and fine grids respectively. The grid is clustered axially near the jet exit and radially near the splitter plate wall to capture the mixing in these regions. The upstream boundary is specified as multiple velocity inlets. The fuel inlet is a fully developed pipe flow with the velocity described by the $1/7^{th}$ power law as shown in Equation 4-1. The downstream boundary is specified as a pressure outlet. All solid boundaries, including the splitter plate, are specified as walls and assumed to be adiabatic and impermeable. The schematic of the computational grid and boundary conditions is shown in Figure 4-8.

Turbulence modelling approaches employed in this study are LES and RANS k-ε. For LES, the unresolved subgrid scales are treated with the standard Smagorinsky-Lilly model. The chemistry models being compared in the sensitivity analysis are the equilibrium chemistry and steady flamelet models. For the LES grid sensitivity study, only the equilibrium chemistry is employed. The filtered transport equations are spatially discretised using the finite volume method. The momentum equations are solved applying the bounded central differencing scheme. The second order upwind scheme is used to solve the filtered mixture fraction transport equation. The time step size employed in LES is 1.0×10^{-5} seconds. To allow for the initial flow development, the simulations are performed for $220R/U$ seconds before samples are collected for another $1760R/U$ seconds to ensure adequately converged statistics are obtained.

The current LES results from this test case are validated against the data from the experiment carried out at the United Technologies Research Center (Owen *et al.*, 1976), and compared with the solutions from the modified LES which employs a more advanced chemistry modelling approach, the steady flamelet/progress variable chemistry model, on a computational grid consisting of approximately 2.5 million elements (Pierce and Moin, 2004). The profiles of mixture fraction, chemical species mass fractions, temperature and axial velocity are compared at various stations inside the combustor. The length and velocity presented are normalised by R and U respectively.

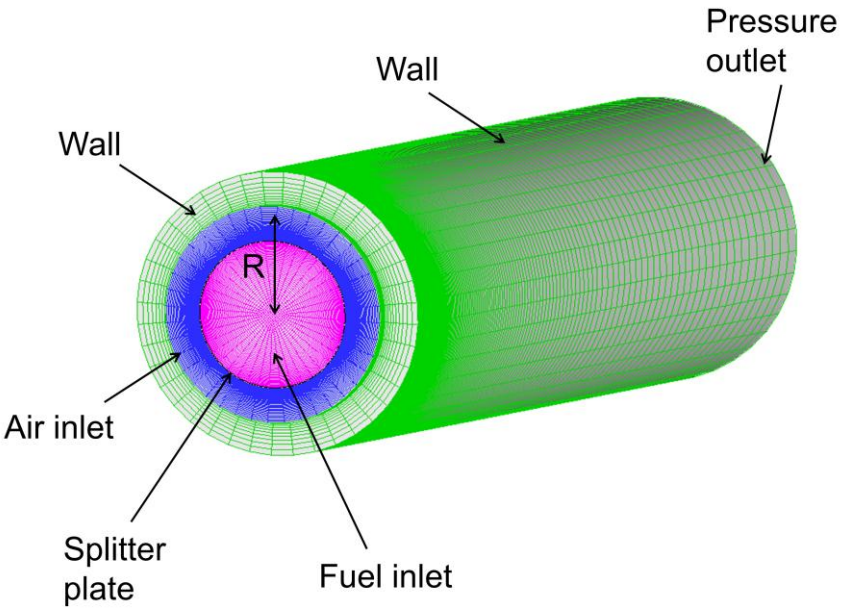

Figure 4-8 Coaxial jet combustor mesh and boundary conditions.

4.3.2 Results and Discussion

LES and RANS Comparison

The simulations have been carried out employing the current LES and RANS with the equilibrium chemistry model on the coarse grid to compare the capabilities of the transient and steady turbulence modelling approaches to capture the flame structure. Figure 4-9 compares the mixture fraction contours on the midplane. At this instance, the LES approach predicts asymmetric mixing behaviours with more mixing on the upper side than the lower side of the fuel port. However, the mixture fraction contours obtained from RANS are smooth and symmetric. This is because RANS is able to provide only the mean flow fields.

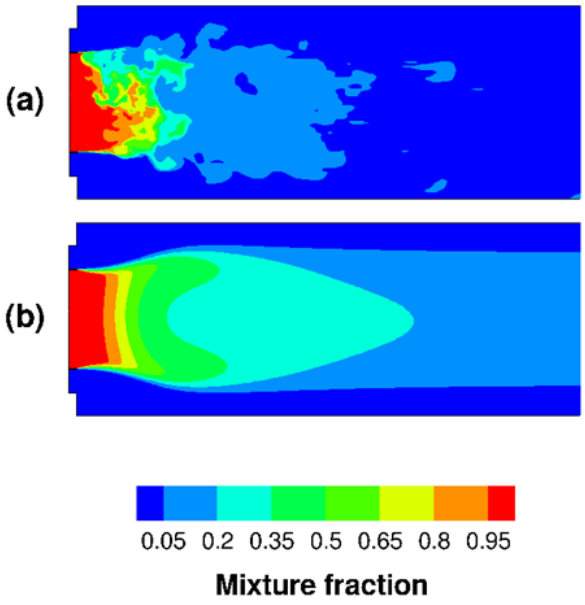

Figure 4-9 Instantaneous mixture fraction contours from (a) LES at 2.54 s and (b) RANS.

Figure 4-10 compares the corresponding contours of product mass fraction which is calculated from the sum of CO_2 and H_2O mass fractions. The regions with higher product concentrations mark the flame location. As indicated by irregular, wavy contours, the LES approach is able to capture a wider range of unsteady flame behaviours which agree with the observation made in the experiment (Owen *et al.*, 1976). At the instance shown, more products are formed in the upper region near the fuel port than the lower region which is consistent with the mixture fraction predictions of LES. It is also demonstrated that some unburnt reactants are able to penetrate into the flame. The RANS approach, on the other hand, predicts a symmetric flame which does not exhibit the unsteady nature of combustion. Both LES and RANS predict flame attached to the splitter plate. However, as suggested by the thicker and longer attached contours, the attached flame predicted by RANS is more intense than that predicted by LES. For this case, the highest product mass fraction attainable in theory is approximately 0.275 which occurs at the stoichiometric mixture fraction (Pierce and Moin, 2004). The RANS approach, as illustrated in Figure 4-10 under-predicts the maximum product mass fraction significantly.

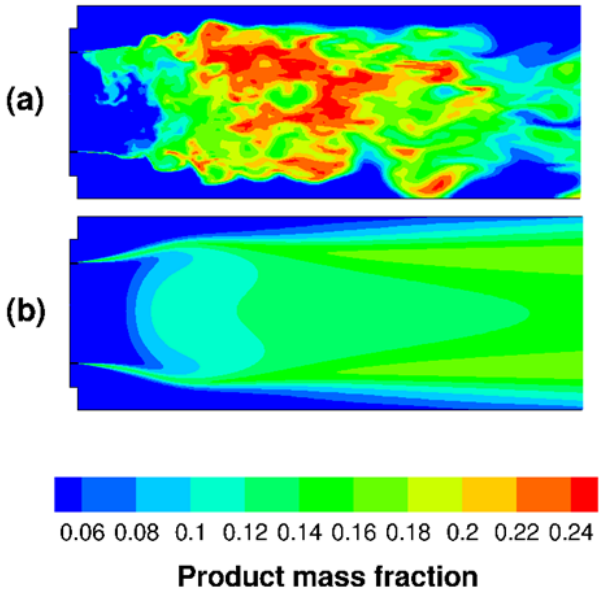

Figure 4-10 Instantaneous product mass fraction contours from (a) LES at 2.54 s and (b) RANS.

To support the qualitative comparison in Figure 4-9, the mixture fraction profiles predicted by LES and RANS are compared in Figure 4-11. The predictions from LES are time-averaged. At the station x/R = 0.21, the LES approach offers improvements over the RANS approach which under-predicts the mixing rates significantly. At the downstream station, x/R = 3.84, RANS still under-predicts the mixing rates. However, the near-wall mixture fraction predictions from the RANS approach agree with the experimental data better than the LES approach which is known to experience difficulties predicting the near-wall flows accurately (Pope, 2000; Langford and Moser, 1999; Sagaut, 2001; Wegner *et al.*, 2004). This is because LES requires very high grid resolution to sufficiently resolve the flow in viscous near-wall regions. At x/R = 3.84, LES over-predicts the mixing rates, and produces the mixture fraction profile which is almost level, suggesting that the mixing is essentially complete. The mixture fraction profile from the modified LES (Pierce and Moin, 2004), on the other hand, agrees very well with the experimental data at this station.

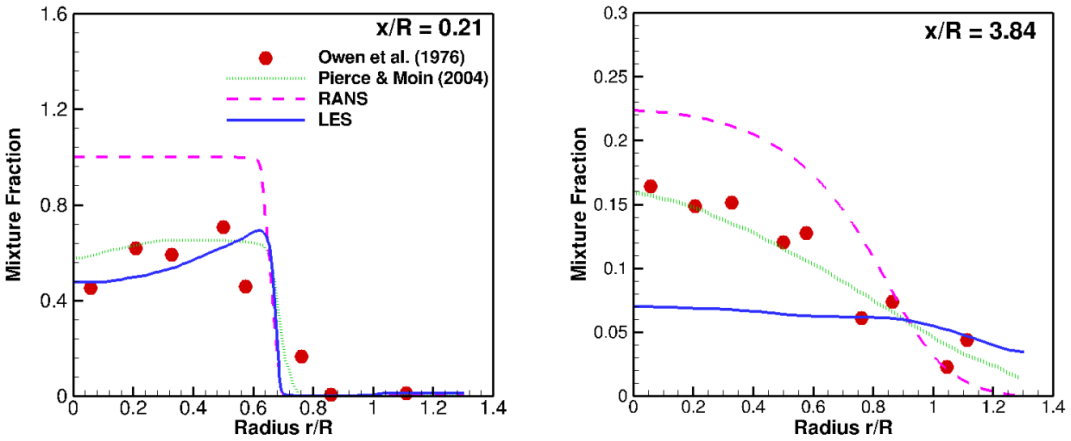

Figure 4-11 Profiles of time-averaged mixture fraction from LES and RANS.

Figure 4-12 compares the temperature profiles predicted by LES and RANS. At the upstream station, *x/R* = 0.89, the temperature profile obtained from LES agrees better with the experimental data than RANS in the inner and mixing regions. However, the LES predictions deviate from the experimental data more than the RANS predictions in the near-wall region. The sharp peak in the mixing layer predicted by RANS corresponds to the flame attached to the splitter plate exhibited in Figure 4-10(b) and the lower mixing rates illustrated in Figure 4-11. The flame reproduced by RANS remains attached to the splitter plate at the downstream station, *x/R* = 1.57, as indicated by a spike in the temperature profile. The temperature profile computed by the current LES, on the other hand, agrees generally well with the experimental data in the inner flame region. However, as similar to the upstream predictions, the current LES results in the near-wall region deviate from the experimental measurements considerably.

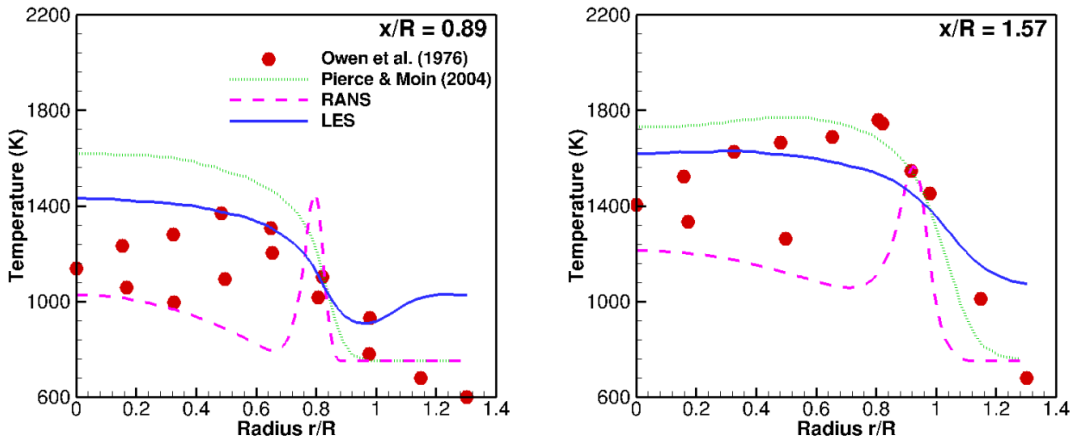

Figure 4-12 Profiles of time-averaged temperature from LES and RANS.

LES Flame Structure

The instantaneous temperature iso-surfaces and radial cross sectional contours predicted by the current LES with the fine grid and the equilibrium chemistry model are illustrated in Figure 4-13. The regions with the higher temperature indicate the flame location. As depicted in Figure 4-13(a), the flame is contained in the central region behind the fuel port, and extends in the axial direction along the combustor. The recirculation of combustion products caused by the high air-to-fuel velocity ratio provides a continuous ignition source and stabilises the flame. This is consistent with the flame configuration observed in the experiment of Owen *et al.* (1976). However, in this study, the flame is predicted to be attached to the splitter plate whereas the flame in the experiment lifted off from the nozzle lip and reattached intermittently in an extremely unsteady manner. This is due to the incapability of the equilibrium chemistry and steady flamelet models to cope with the non-equilibrium effects such as extinction, ignition and flame lift-off.

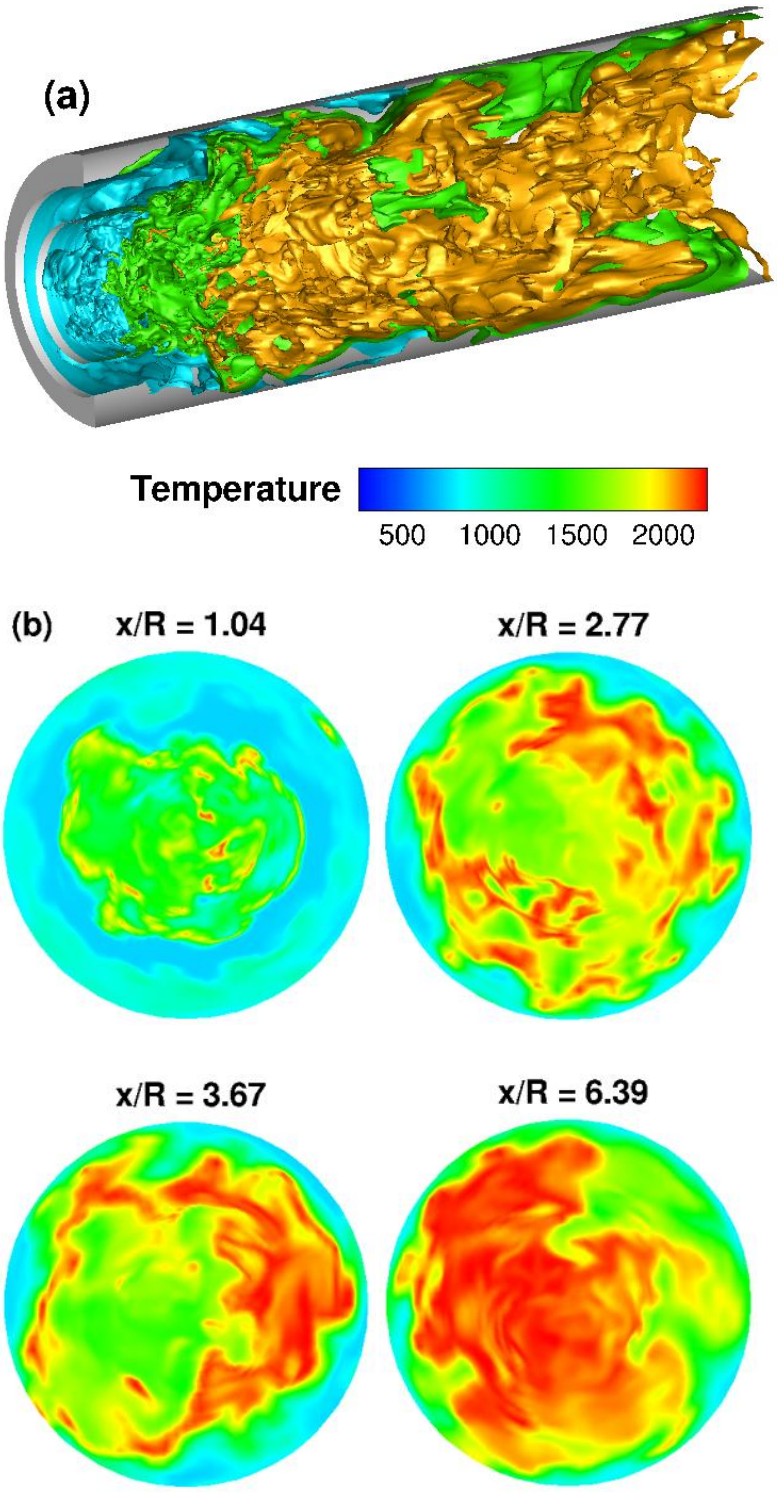

Figure 4-13 Instantaneous temperature (a) iso-surfaces and (b) radial cross sectional contours from LES with the fine grid at 3.59 s.

Figure 4-13(b) exhibits the radial cross-sectional contours of the temperature. The contours at the upstream locations display distinct temperature zones. The cold annular air stream is forced outward towards the wall by the reaction, and forms a lower temperature layer which enfolds the inner higher temperature region. The thickness of this outer cold air layer reduces as the axial distance increases. The flame is made up of separate high temperature zones within the fuel-air shear layer. Near the fuel port, there are many small, isolated high temperature pockets. However, the segregated high temperature pockets become larger and more amalgamated along the combustor length.

LES Sensitivity Analysis

The sensitivity analysis has been carried out to assess the effects of the grid resolution and chemistry model on the combustion LES solutions. For the grid sensitivity analysis, LES is performed on the coarse and fine grids employing only the equilibrium chemistry model. The sensitivity of the LES results to the chemistry model is evaluated by employing the equilibrium chemistry and steady flamelet models on the coarse grid. The instantaneous iso-surfaces of the mixture fraction predicted by the current LES on the coarse and fine grids are exhibited in Figure 4-14. The qualitative comparison reveals that the fine grid is able to capture more smaller-scale mixing in the inner flame than the coarse grid, especially in the upstream region behind the fuel port.

For the non-premixed combustion model, it is crucial to predict the mixture fraction accurately since it is used to derive other quantities such as the temperature, density and species mass fractions. The time-averaged mixture fraction profiles obtained from the current LES are depicted in Figure 4-15. At the station x/R = 0.21, the simulation results from different grids and chemistry models are similar and agree generally well with the experimental data. However, at the station x/R = 3.16, LES with both chemistry models on the coarse grid significantly under-predicts the mixture fraction values in the inner flame. This suggests that the grid resolution is inadequate for capturing the mixing in this region.

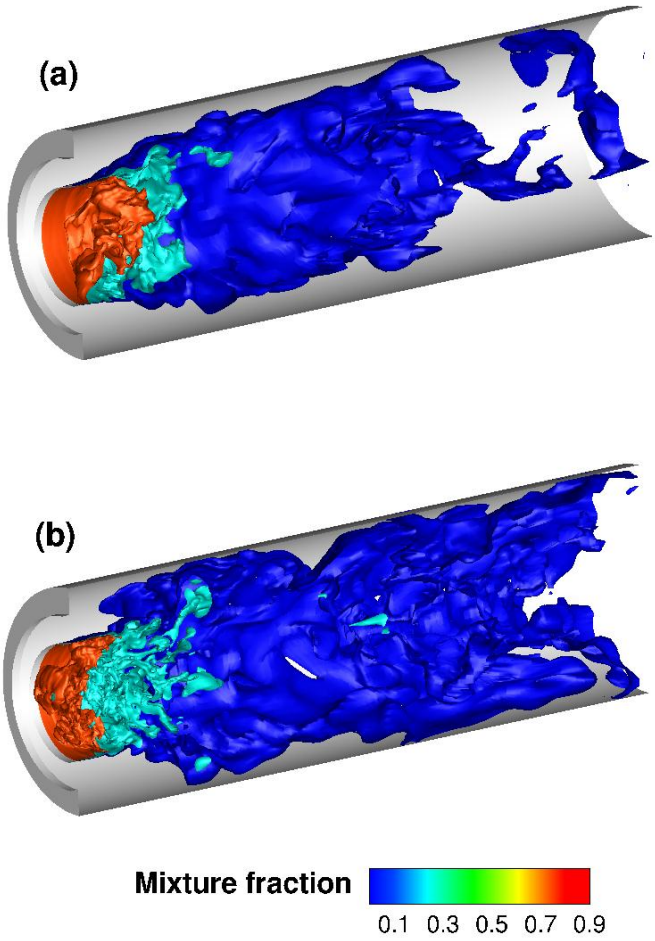

Figure 4-14 Instantaneous mixture fraction iso-surfaces (a) from the coarse and (b) fine grids at 3.59 s.

As illustrated in Figure 4-15, at the station *x/R* = 3.16, the current LES predictions improve, especially in the central and near-wall regions, when the grid is refined. The predictions from the modified LES with the more advanced chemistry modelling approach (Pierce and Moin, 2004), on the other hand, are in excellent agreement with the experimental data at this station.

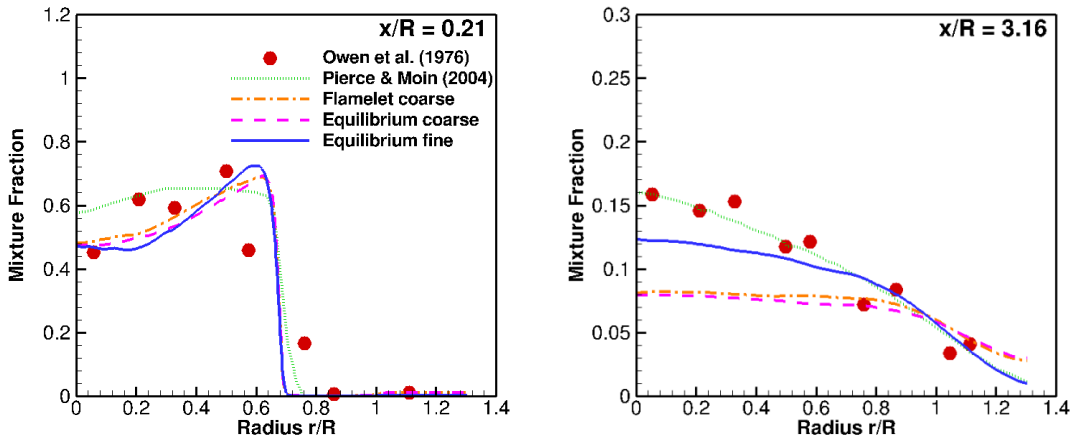

Figure 4-15 Comparison of time-averaged mixture fraction profiles.

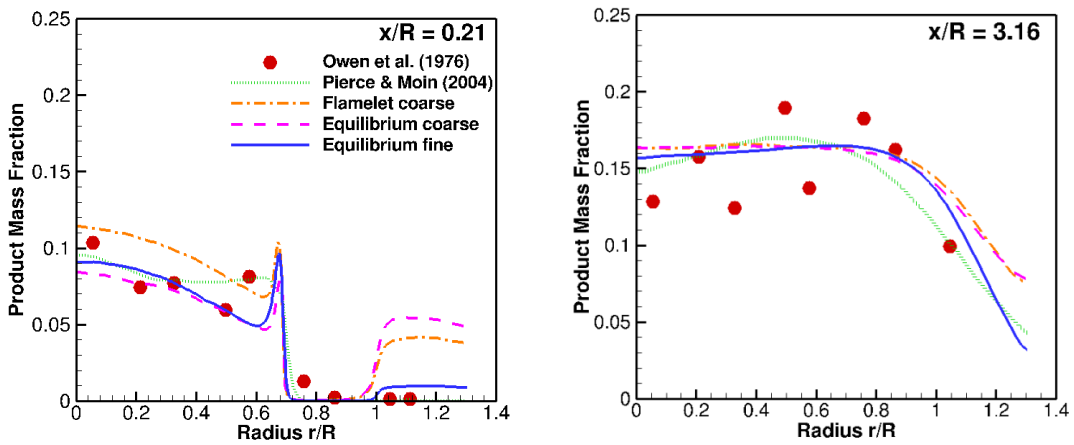

Figure 4-16 Comparison of time-averaged product mass fraction profiles.

The comparison of time-averaged product mass fraction profiles is illustrated in Figure 4-16. The equilibrium chemistry and steady flamelet models predict a spike in the thin mixing layer at the station x/R = 0.21. High product formation predicted in this region by both chemistry models corresponds to the attached flame exhibited in Figure 4-10(a).

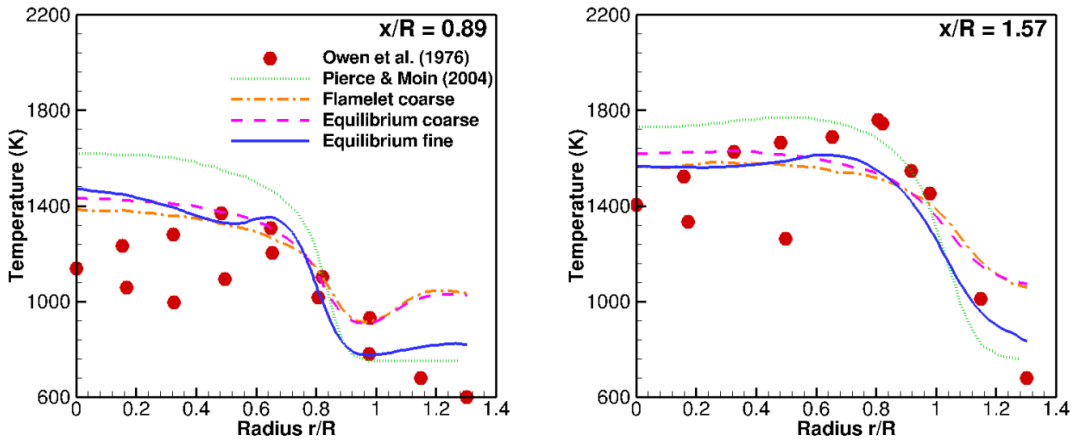

Figure 4-17 Comparison of time-averaged temperature profiles.

The products found in the inner region at *x/R* = 0.21 are the result of the product recirculation from the reaction downstream. In this region, the steady flamelet model predicts higher product mass fraction than the equilibrium chemistry model. Furthermore, both chemistry models predict higher product mass fraction near the wall. These discrepancies are reduced significantly when the fine grid is employed. At the station *x/R* = 3.16, the simulation results from both chemistry models are in excellent agreement with the experimental data. An improvement in the near-wall predictions, again, can be observed when the finer grid is employed.

Figure 4-17 compares the time-averaged temperature profiles obtained from the simulations. The predicted temperature profiles from the current LES with both chemistry models and the experimental measurements are in good agreement. Discrepancies between the predicted near-wall temperature and the experimental data at all stations are due to the adiabatic wall assumption applied in the study. In the experiment, the combustor wall was isothermal, and cooled to the temperature of approximately 500 K. Therefore, the near-wall temperature in the simulations can be affected by the thermal boundary layers. However, as exhibited in Figure 4-17, the temperature predictions near the wall can still be improved when a higher grid resolution is employed.

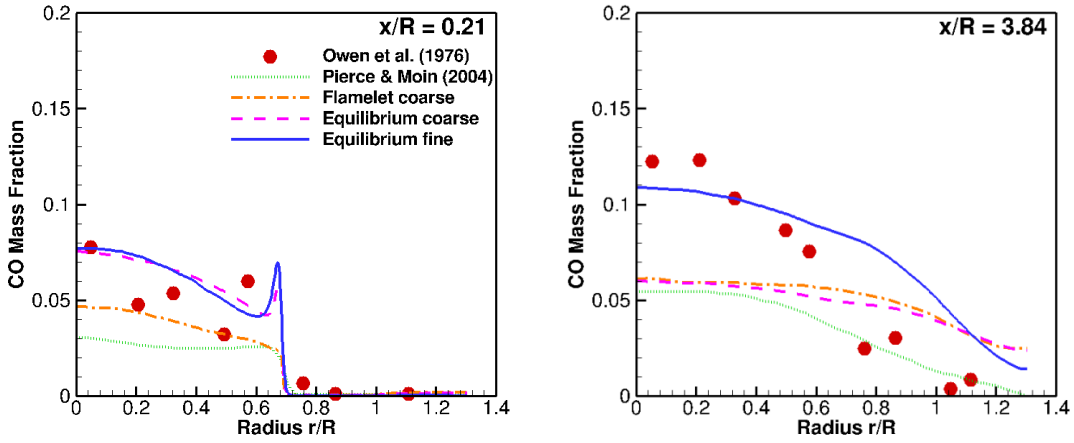

Figure 4-18 Comparison of time-averaged CO mass fraction profiles.

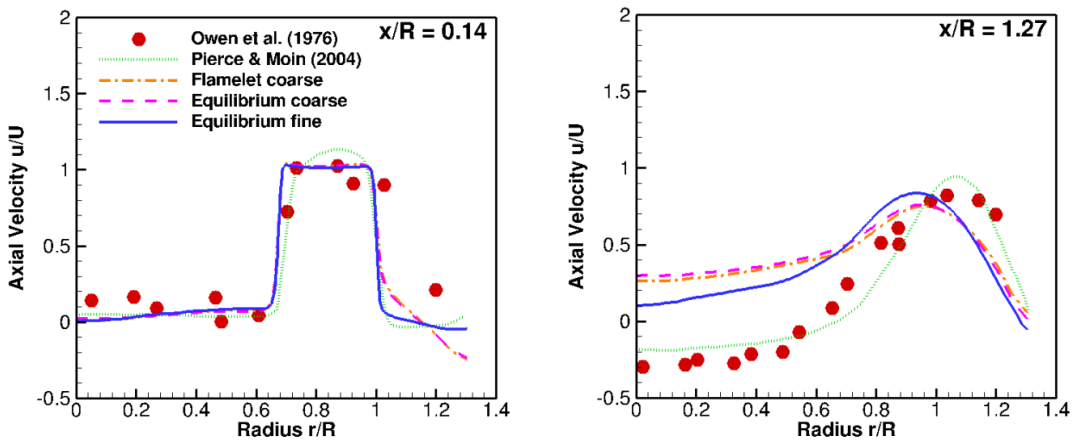

Figure 4-19 Comparison of time-averaged axial velocity profiles.

The time-averaged profiles of CO mass fraction are compared in Figure 4-18. At the station *x/R* = 0.21, the equilibrium chemistry model predicts a spike in CO mass fraction in the mixing layer as similar to the product mass fraction predictions. However, there is no such peak in the CO mass fraction profile predicted by the steady flamelet model. At the station *x/R* = 3.84, there are discrepancies between the simulation results from both chemistry models and the experimental data. Especially in the inner region, these deviations reduce when the fine grid is employed.

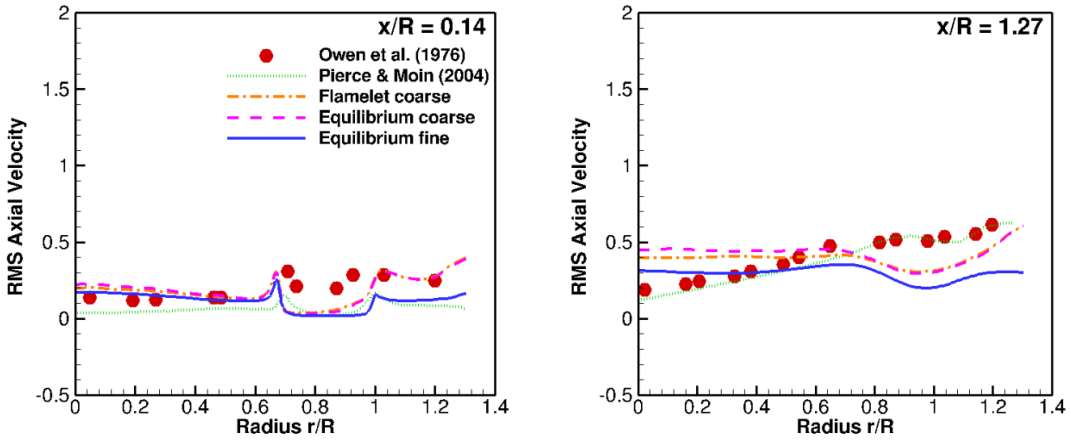

Figure 4-20 Comparison of time-averaged RMS axial velocity profiles.

Figure 4-19 and 4-20 depict the profiles of time-averaged axial velocity and RMS velocity respectively. Although the mixture fraction is sensitive to the rate of chemical heat release, the predictions of axial velocity and its RMS are found to be rather insensitive to the chemistry model. This is because the effects of the heat release on the velocity field are likely to be accumulative. At the station x/R = 0.14, the axial velocity profiles from the equilibrium and steady flamelet models are almost identical with a slight improvement in the near-wall predictions when the fine grid is employed. At the station x/R = 1.27, there are discrepancies between the predicted axial velocity profiles from both chemistry models and the experimental data, particularly in the inner region. The recirculation in this region is not well captured by the current LES. However, the modified LES with the advanced chemistry model is able to predict the axial velocity profile which is closer to the experimental data at this station.

4.4 LES on an Unstructured Grid

Another test case has been carried out to validate the application of LES with unstructured grids for non-premixed combustion simulations. The combustor configuration, operating and boundary conditions employed in this test case are the same as those of the coaxial jet combustor in the previous section. Due to the complexity of fitting the tetrahedral elements around the thin splitter plate and the difficulty in achieving numerical stability, the splitter plate is simplified to a solid surface with negligible thickness. The computational grid consists of 3.8 million tetrahedral elements. The LES computations are compared with the experimental data (Owen *et al*., 1976), modified LES calculations (Pierce and Moin, 2004) and results from the current LES code on the structured grid consisting of 2.3 million elements.

4.4.1 Results and Discussion

Figure 4-21 compares the instantaneous mixture fraction contours on the combustor midplane captured by the structured and unstructured grids. As expected, there is a delay in the upstream mixing on the unstructured grid as illustrated in Figure 4-21(b) whereas for the structured grid, as exhibited in Figure 4-21(a), the mixing process takes place immediately behind the fuel port. This is mainly due to the simplification of the combustor configuration on the unstructured grid which changes the flow physics in the combustor. Since the splitter plate plays a key role in initiating the flow instability at the interface between the two fluid streams, altering the thickness of the splitter plate will affect the mixing and recirculation processes of the flow inside the combustor. Nevertheless, compared to the structured grid, the fluid displayed on the unstructured grid appears to mix more vigorously downstream as indicated by the highly irregular and wavy shape of the mixture fraction contours.

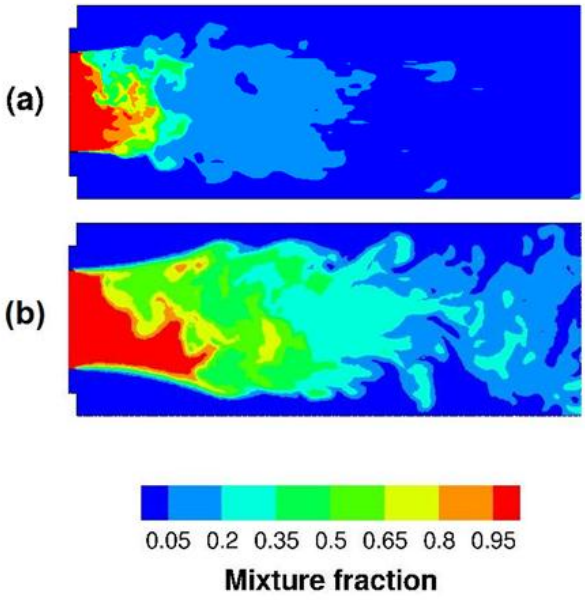

Figure 4-21 Instantaneous mixture friction contours at 2.54 s from (a) structured grid with a thin splitter plate and (b) unstructured grid with negligible splitter plate thickness.

The profiles of mixture fraction and product mass fraction at various stations along the combustor are compared in Figure 4-22. At x/R = 0.21, the mixing rate is significantly under-predicted by LES on the unstructured grid. Since the splitter plate has a great influence on the flow behaviours upstream, eliminating its thickness causes the flow to be smoother, more stable and thus difficult to mix. Nevertheless, since the combustor operating and boundary conditions are the same in both cases, the profiles are expected to be uniform towards the exit of the combustor where the mixing completes. As illustrated in Figure 4-22, the mixture fraction profiles exhibited on the unstructured grid agree better with the experimental data downstream.

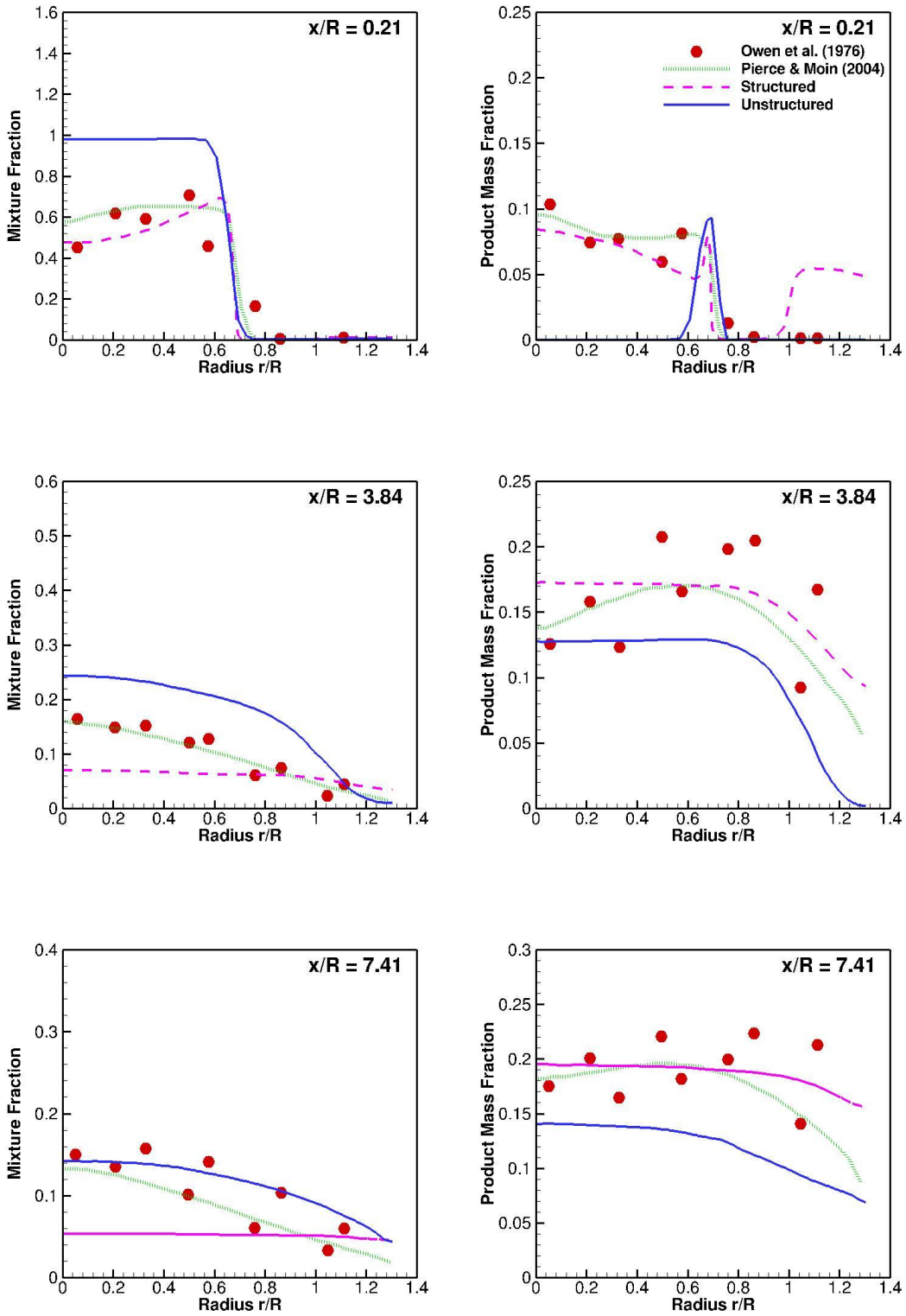

Figure 4-22 Profiles of time-averaged mixture fraction (left) and product mass fraction (right) from structured grid with a thin splitter plate and unstructured grid with negligible splitter plate thickness.

At *x/R* = 7.41, the LES predictions on the unstructured grid and the experimental data agree reasonably well. Contrarily, the LES predictions on the structured grid deviate from the experimental data more in the downstream region. This may be due to two reasons. Firstly, the unstructured grid consists of more elements than the structured grid. Secondly, the structured mesh is refined near the inlets but much coarser downstream while for the unstructured mesh, the elements are more uniformly distributed throughout the whole combustor. As a result, the unstructured mesh has finer grid elements near the combustor exit, less abrupt change in the cell size, and thus is able to capture more mixing in this region.

The comparison of product mass fraction profiles on the right-hand side of Figure 4-22 reveals that at the station *x/R* = 0.21, LES on the unstructured grid is able to predict products formed only at the interface between the two fluids, whereas in the experiment, as well as the current LES on the structured grid, there are also products present in the core region. However, the predictions of LES with the unstructured grid match the experimental data better towards the combustor exit as demonstrated at the locations *x/R* = 3.84 and 7.41.

Figure 4-23 compares the time-averaged temperature profiles obtained from LES on both grids. For the unstructured grid, at the upstream location, *x/R* = 0.89, the LES approach predicts generally constant temperature in the central and annular streams, suggesting that the mixing and thus reaction have not reached these regions. The peak in the predicted temperature indicates that the reaction takes place only in the shear layer. As similar to the predictions of mixture fraction and product mass fraction, the temperature profiles from LES on the unstructured mesh agree better with the experimental data downstream.

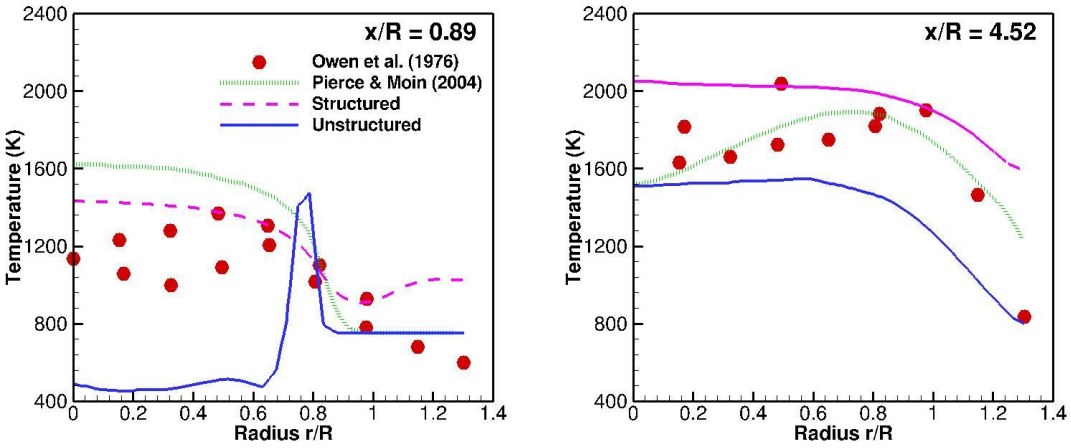

Figure 4-23 Profiles of time-averaged temperature from structured grid with a thin splitter plate and unstructured grid with negligible splitter plate thickness.

The simulation results from this test case reveal that an acceptable level of fidelity can be achieved from LES with the unstructured grid. The purpose of this comparison is for validation and not to suggest that the unstructured grid is superior or inferior to the structured grid. For the coaxial jet combustor which is a simple configuration, the application of the structured grid is more efficient. However, an unstructured grid provides more flexibility and can be easily applied to more complex geometries such as the simplified helicopter combustor in the next chapter.

4.5 Chemical Reaction in a Jet

The chemical transformation of the hot aircraft exhaust species during the cooling and mixing with the ambient air involves numerous complex chemical processes. Of particular importance is the transformation of NO to NO_2. This is because, although NO is predominantly emitted in the engine exhaust, it is the levels of NO_2 that are controlled by the regulations. Excessive NO_2 causes serious harms to plants and human health. NO_2 prevents plant growth and causes defoliation. For humans, breathing NO_2 at a concentration of 3 ppm causes bronchial constriction. Furthermore, NO_2 exposures at 150 ppm and above cause changes in the lungs which can be fatal (Moore *et al*., 2008). Therefore, the key gas-phase reaction selected for the current research is,

$$NO + O_3 \rightarrow NO_2 + O_2. \quad \textbf{(4-2)}$$

The simulations have been carried out for a simple round jet with the geometry and flow conditions similar to those in the experiment of Shea (1976, 1977). The aim of this test case is to perform CFD simulations of the selected chemical process and test its kinetic parameters. In addition, the effects of different reaction models on the numerical results are also investigated. The results from this test case are necessary in order to lay the ground for the modelling of the reactive helicopter exhaust in Chapter 7.

4.5.1 Computational Domain and Setup

The computational domain consists of a round jet which has the diameter, *d*, of 0.5 cm. The jet nozzle is located at the centre of a large circular cylindrical tank with the diameter of 50.0 cm and the height of 200.0 cm. The flow Reynolds number based on the nozzle diameter is 4000 and the co-flow velocity is 0.1 cm/s. The jet enters the domain vertically from the top of the tank. The central jet carries O_3 diluted in O_2 while the surrounding co-flow contains NO mixed with inert N_2. The concentration ratio of NO to O_3 is 20. Wherever the gasses mix, O_3 and NO react as in Equation 4-2. The operating temperature and pressure are 295 K and 4.06 atm respectively.

An O-type grid consisting of approximately 350,000 hexahedral elements has been created for this test case. Since it was observed in the experiment that the reaction length was only slightly over 5*d* (Shea, 1976, 1977), the grid is clustered near the nozzle exit to capture the reaction in this region. The jet nozzle and its surrounding co-flow inlet are specified as the velocity inlets. The jet is a fully developed pipe flow with the velocity profile described by Equation 4-1. The downstream boundary is a pressure outlet. The tank surface is specified as wall and assumed to be adiabatic. The computational mesh and boundary conditions are summarised in Figure 4-24.

Considering the experimental measurements were taken at the steady-state operation, the turbulence modelling approach employed in this test case is the steady RANS k-ε model. The jet was observed by Shea (1976, 1977) to be highly reactive. For the sensitivity study, two reaction models are compared. These are the laminar finite-rate and eddy dissipation models. The chemical kinetic parameters employed in this test case are presented in Table 4-1. The numerical results are validated against the experimental measurements of Shea (1976, 1977) in terms of the profiles of O_3 concentration normalised by its initial value.

Table 4-1 Chemical kinetic parameters for the NO + O_3 reaction.

	A ($cm^3mol^{-1}s^{-1}$)	**β**	**E_a ($Jmol^{-1}$)**
$NO + O_3 \rightarrow NO_2 + O_2$ (Mallard *et al*., 1994)	2.14×10^{-12}	0.0	11707

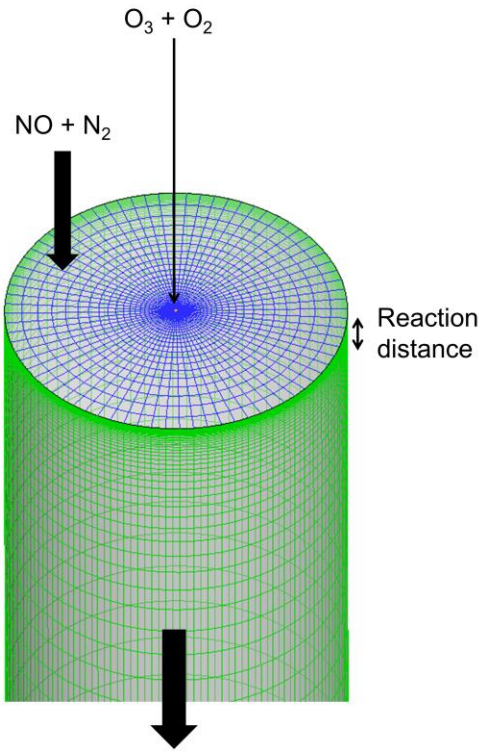

Figure 4-24 Computational mesh of the circular cylindrical tank.

4.5.2 Results and Discussion

Figure 4-25 illustrates the normalised O_3 concentration profiles obtained from RANS with the two reaction models along the centreline. The RANS predictions are validated against the experimental measurements recorded at the same operating conditions. In addition, the simulation results are compared to the mean experimental data which have been averaged from different experimental runs at five Reynolds numbers ranging from 4000 to 32000, and the pressures of 1.34 and 4.06 atm.

As demonstrated in Figure 4-25, the normalised O_3 concentrations along the centreline predicted by both chemistry models remain at the maximum value until the distance of approximately 2*d* which agree very well with the experimental data. After this point, the mixing reaches the jet core, and the reaction begins to consume O_3, leading to the drop in its concentration. The RANS predictions, as well as the experimental data, exhibit a drop in the O_3 concentration but at different rates. The results from the eddy dissipation model match the experimental measurements well. The results from the laminar finite-rate model, on the other hand, start to deviate from the experimental data after 2*d*. The model predicts a slower reaction rate, and the drop in the O_3 concentration becomes evident only after 3*d*. This is due to the fact that the laminar finite-rate model does not take into account the effects of turbulence on the reaction rate. In the case where the chemistry is fast and the reaction is controlled by the turbulence, this assumption does not hold.

Figure 4-26 compares the normalised O_3 concentration profiles obtained from RANS with the two reaction models across the tank at x/d = 1. At this location, there is a distinct separation between the jet and co-flow. Both reaction models predict highest O_3 concentration in the jet core and zero O_3 concentration in the annular stream, which agree with the experimental data. However, at the interface where the two fluid streams meet, the eddy dissipation model predicts lower O_3 concentrations than the experiment. This is owing to its fast reaction assumption, and thus O_3 is consumed more by the reaction. The laminar finite-rate model, on the other hand, over-predicts the O_3 concentrations in this region. As demonstrated in both Figures 4-25 and 4-26, the model tends to under-predict the reaction rate because it neglects the turbulence-chemistry interaction.

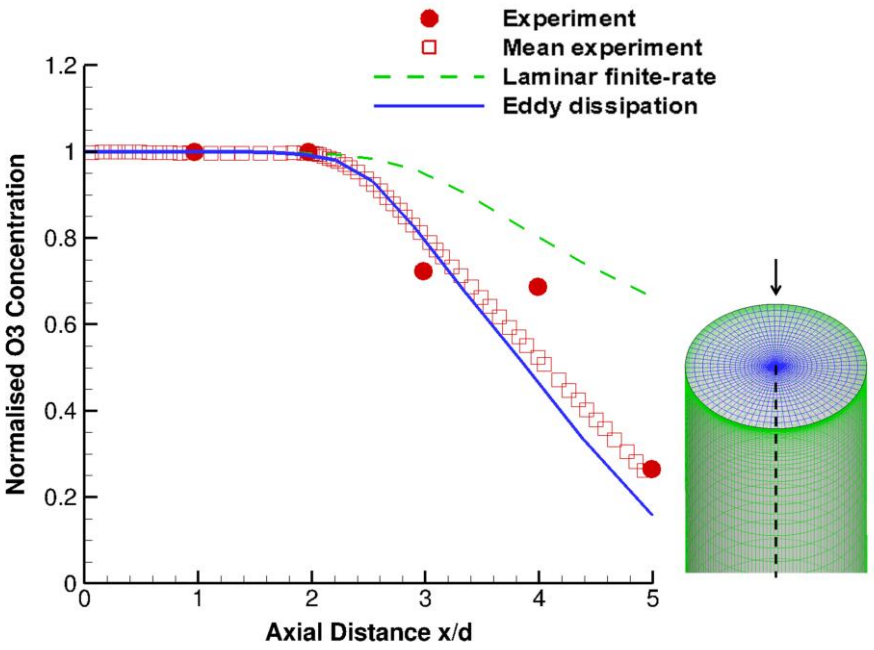

Figure 4-25 Normalised O_3 concentration profiles obtained from RANS with different reaction models along the centreline.

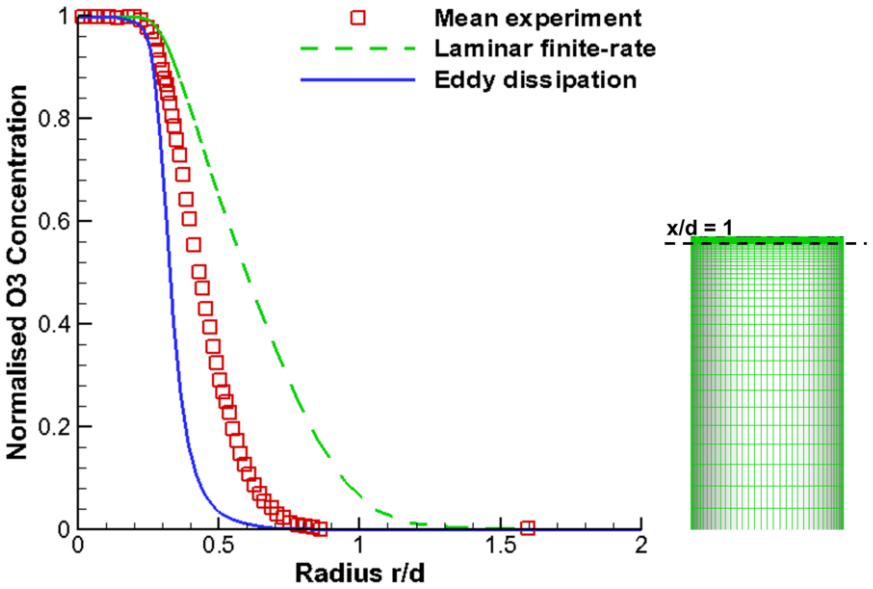

Figure 4-26 Normalised O_3 concentration profiles obtained from RANS with different reaction models across *x/d* = 1.

4.6 Conclusions

The findings from the first test case of this chapter have demonstrated the potential of LES for capturing detailed mixing characteristics of a round jet. Despite the simple chemistry models employed, the results from the second and third test cases reveal the good capabilities of the current LES, with both structured and unstructured grids, to reproduce the flame and flow characteristics of non-premixed turbulent combustion. This is owing to the fact that LES directly resolves the large-scale motions which control the rate of mixing and reaction. As demonstrated by the results, the current LES calculations are found to be sensitive to the grid resolution, especially in the inner and near-wall regions. Nevertheless, important aspects of the combustion process, such as the main reactions and pollution formation, usually take place far away from the wall. Therefore, an acceptable fidelity level of LES predictions for future engineering design applications such as optimisation investigations can be achieved with moderate grid refinement. In the last test case of this chapter, the NO reaction and its chemical kinetic parameters selected for the helicopter exhaust modelling in Chapter 7 have been successfully validated.

5 LES OF A HELICOPTER COMBUSTOR

5.1 Introduction

Although a notable amount of work on LES of simple academic flames has been carried out and communicated to the open public, hitherto LES of a helicopter combustor has only been considered by a limited number of researchers. Boudier *et al*. (2007, 2008) studied the effects of grid resolution on LES of reacting flows in a helicopter combustor employing their specialised higher order scheme LES code on meshes consisting of 1.2 to 44 million elements. Other work includes the study of combustion instabilities carried out on meshes composing of 38 to 336 million elements (Staffelbach *et al.*, 2009; Wolf *et al*., 2012), and the incorporation of detailed chemistry in the LES code (Auzillon *et al.*, 2013). All of these studies employed very dense mesh, higher order numerical methods or both.

The purpose of this work is to numerically study the Jet A/air reaction in a helicopter combustor, and predict NO_x emissions employing the current LES code. To investigate the sensitivity of the LES results to the grid resolution, the simulations have been carried out on three computational meshes with different sizes. The LES results in terms of the flame structure, temperature distributions, maximum flame temperature, exit temperature and $EINO_x$ are compared with those from the combustor design, analytical solutions, previous LES and test measurements.

5.2 Combustor Configuration

The combustor configuration employed in this study, as illustrated in Figure 5-1, is a 30° section of an annular combustor simplified from a reference combustor designed within the Curtiss-Wright Corporation (1974). The combustor size and performance resemble those of the high-performance combustor for small gas turbine engine developed and tested within the United States Army Aviation Material Laboratories (1970). The relative shaft length of the combustor is 145 mm, and the housing diameter is 370 mm. The combustor consists of primary and dilution zones.

The operating conditions considered for the current research are those of the reference combustor at 100% rated power, and an in-house gas turbine engine performance code, TURBOMATCH (Pachidis *et al*., 2007; Li *et al*., 2009), at 32% power. These combustor operating conditions are presented in Table 5-1. The helicopter combustor operating at the maximum power will be employed as the baseline case for the current research.

The fuel and primary air inlets are located on the combustor dome. The central inflow is a pure Jet A stream at the temperature of 300 K while the annular co-flow is non-swirling air, making up 29% of the primary zone airflow. The cup-shaped flame stabiliser serves to reduce the velocity of the Jet A/air mixture and reverse the flow direction. Furthermore, it creates a recirculation zone in its wake which entraps the hot combustion products and stabilises the flame. To ensure complete combustion and reinforce the flow recirculation, the remaining primary zone airflow is introduced into the combustor through two primary air slots located on the combustor dome. The total primary zone airflow makes up 35.4% of the total combustor airflow. At the exit of the primary zone, the hot combustion products are cooled by the dilution air which makes up 35.4% of the combustor airflow and is introduced into the combustor through two inner liner holes and two outer liner holes. The film cooling bands have not been explicitly modelled in this study but the required film cooling airflow is accounted for by distributed it through the primary air slots and dilution holes.

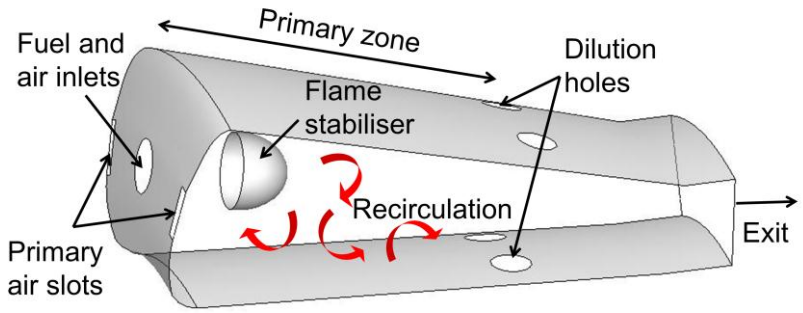

Figure 5-1 Schematic of the combustor configuration.

Table 5-1 Helicopter combustor operating conditions.

Power	Inlet pressure (atm)	Fuel flow rate (kg/s)	Airflow rate (kg/s)	Inlet temperature (K)
100%	10.0	0.0588	2.270	625
32%	5.8	0.0244	1.439	525

5.3 Computational Setup

The numerical study has been carried out for the simplified helicopter combustor employing the current LES code which has been successfully validated against the classical experimental data (Owen *et al.*, 1976) for a coaxial jet combustor in Chapter 4. Furthermore, it has been successfully applied in a sensitivity analysis (Dumrongsak and Savill, 2012a, 2012b), and predicts combustion quantities as well as the specifically calibrated LES code (Pierce and Moin, 2004). By post-processing the combustion results, the NO_x model calculates NO_x formation through the thermal and prompt NO mechanisms.

For LES grid sensitivity analysis, the simulations have been performed on three unstructured meshes consisting of approximately 0.2, 1.8 and 5.0 million tetrahedral elements which will, hereinafter, be referred to as the coarse, medium and fine grids respectively. The grid is refined near the flame stabiliser, and primary air and fuel inlets where rapid changes in the fluid properties are expected to take place. The comparison of the grid resolution on the midplane is displayed in Figure 5-2. The coaxial jet inlets, primary air slots and dilution holes are specified as the mass flow inlets. The downstream boundary is a pressure outlet. The side boundaries are periodic while all solid boundaries, including the flame stabiliser, are assumed to be no-slip, adiabatic and impermeable walls. The time step size employed is 1.0×10^{-4} seconds for the coarse grid, and 1.0×10^{-5} seconds for the medium and fine grids. To allow for the initial flow development, the simulations have been performed on all grids for 40 flow-through times based on the mean velocity of the coaxial jets and the combustor length. Subsequently, temporal averaging has been performed over another 40 flow-through times to ensure adequately converged statistics with regards to the main flow direction are obtained.

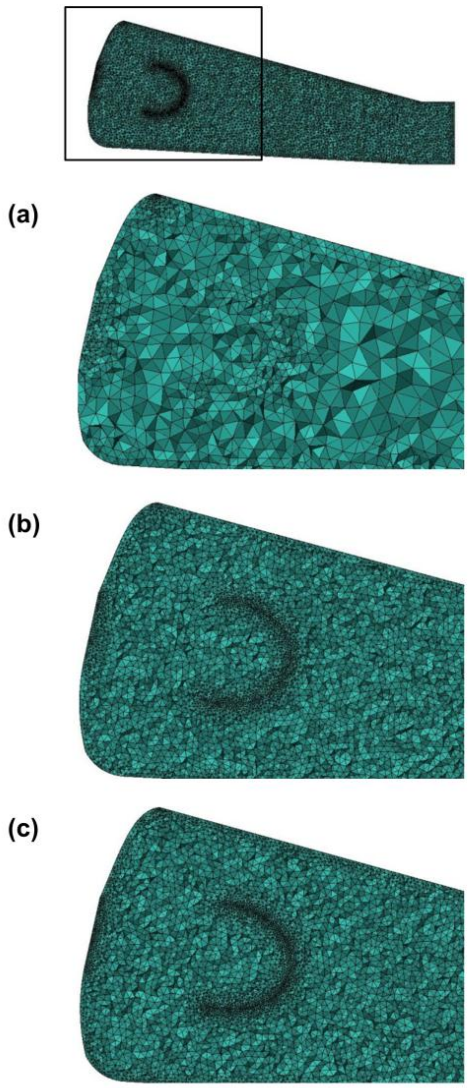

Figure 5-2 Resolution on the axial midplane of the (a) coarse, (b) medium and (c) fine grids.

5.4 Results and Discussion

5.4.1 Instantaneous Temperature and Flame Structure

Figure 5-3 illustrates the mixture fraction iso-surfaces in the helicopter combustor operating at 100% power obtained from LES on the coarse and fine grids. The comparison reveals that the fine grid is able to retrieve more detailed mixing and small turbulent structures than the coarse grid. The corresponding instantaneous iso-surfaces of the temperatures at 800 K, 1600 K and 2400 K obtained from LES on the two grids are illustrated in Figure 5-4. The comparison reveals that the fine grid depicts more irregular and spread-out flame which is a result of better mixing resolved. As demonstrated by the lower-temperature iso-surfaces, the coarse grid displays strong and almost straight penetration of the cooling air through the slots whereas the fine grid exhibits the cooling air penetrating up to the downstream of the primary zone where it becomes perturbed, starts to shed and mix with the hot combustion products. This agrees with the results of previous LES on finer meshes (Boudier *et al.*, 2008).

Figure 5-5 depicts the instantaneous temperature distributions on the midplane of the three grids. The comparison in Figure 5-5 reveals that the key flow features captured by the three grids are similar overall. The flow path of fresh gases entering the combustion chamber is obstructed by the flame stabiliser, resulting in a reduction of the flow velocity, and increased mixing. The flame, as indicated by the contours of highest temperature, is attached behind the flame stabiliser, and encompasses mostly in the primary zone where the flow recirculation has been designed to take place. In addition, the three grids are able to capture the wavy flame structure which indicates that the combustion is a highly unsteady process. Despite similar combustion characteristics captured, the instantaneous temperature distributions from all grids are different locally. As the grid resolution increases, the temperature contours become more pronounced, and more flame front wrinkling is resolved.

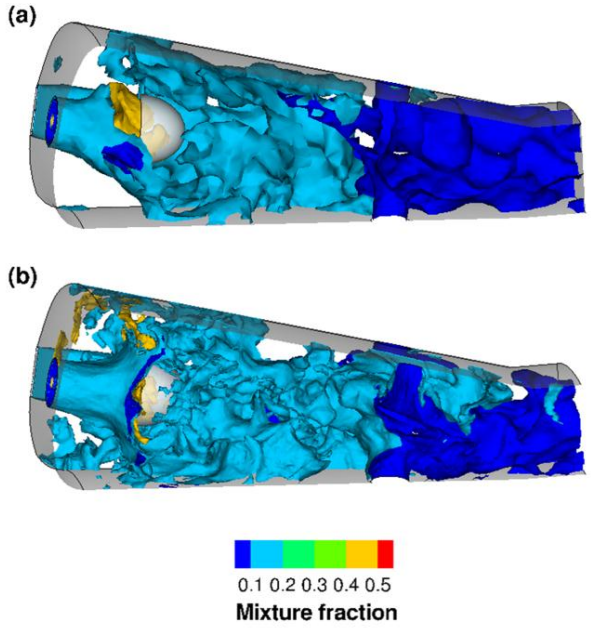

Figure 5-3 Instantaneous mixture fraction iso-surfaces from the (a) coarse and (b) fine grids at 5.12 s.

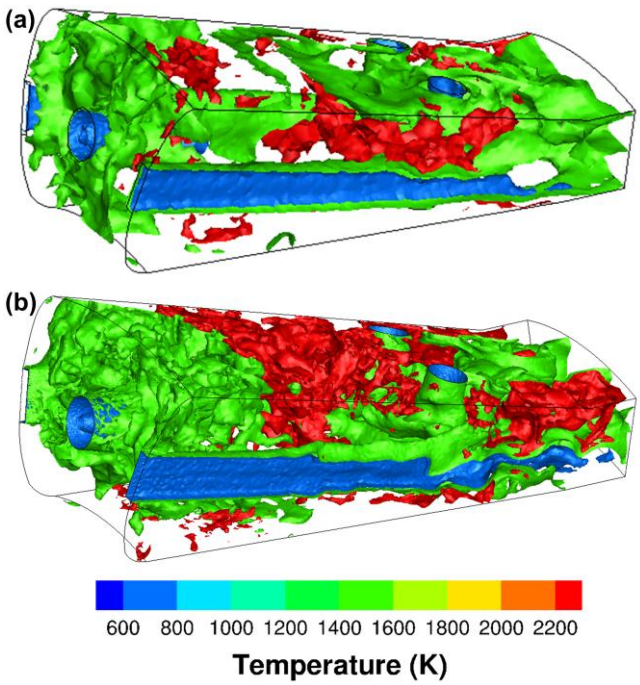

Figure 5-4 Instantaneous temperature iso-surfaces from the (a) coarse and (b) fine grids at 5.12 s.

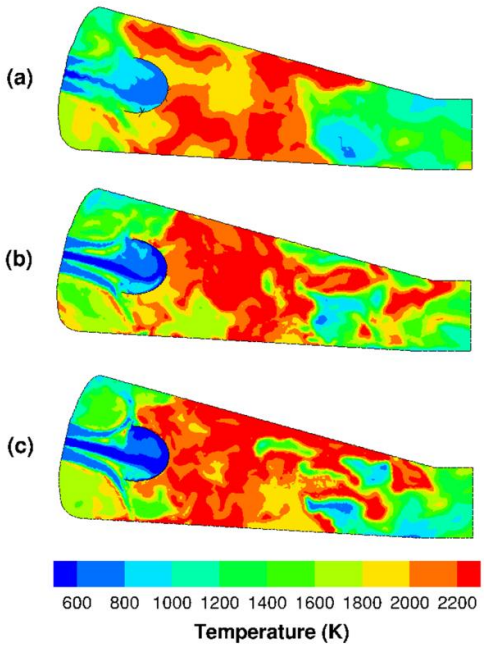

Figure 5-5 Instantaneous temperature contours on the axial midplane from the (a) coarse, (b) medium and (c) fine grids at 5.12 s.

5.4.2 Time-Averaged Temperature

Although instantaneous flow fields in the combustor are different, the LES solutions are expected to converge towards the same temporal statistics which should be independent of the grid resolution. Therefore, the comparison of the time-averaged flow fields is a good indicator of the effects of the mesh resolution on the LES results. The time-averaged temperature distributions from LES on different grids are illustrated in Figure 5-6. All grids exhibit similar mean flame location which matches that of the initial combustor design (Curtiss-Wright Corporation, 1974). This highlights the proper performance of the combustion model employed which appears to be independent of the grid resolution. Despite the agreement in the flame position, the main discrepancy between the simulation results seems to be the area of highest flame temperature which is larger on the fine grid than the other two grids. As the rate of reaction in non-premixed combustion is controlled by the mixing rate, more

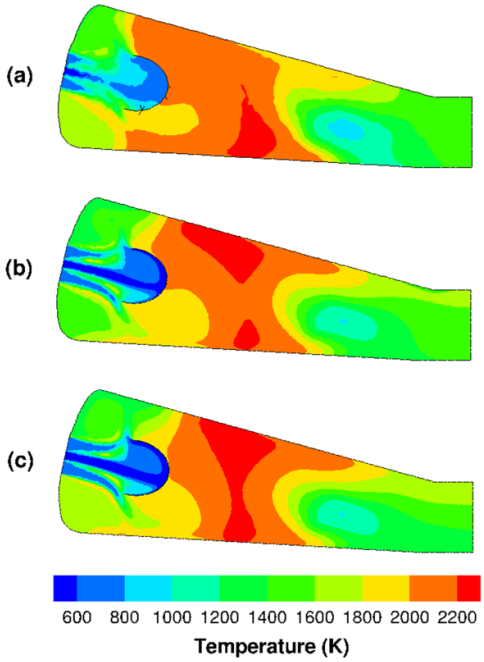

Figure 5-6 Time-averaged temperature contours on the axial midplane from the (a) coarse, (b) medium and (c) fine grids.

detailed mixing captured by the fine grid leads to more intense reaction between the gases and thus higher temperature. Similar mean combustion behaviours overall suggest that grid independence is achieved for the medium and fine meshes. The results demonstrate that, even without employing very high grid resolution or advanced numerical approaches such as those applied in the previous helicopter combustor studies of Boudier *et al*. (2007, 2008), Staffelbach *et al*. (2009), Wolf *et al*. (2012) and Auzillon *et al*. (2013) the current LES code, in conjunction with moderate grid refinement, simple combustion and chemistry models, is able to provide results with an acceptable level of fidelity. This economic advantage makes it a promising tool for the design and emissions optimisation investigations of helicopter combustors. These findings are consistent with the conclusions of the previous studies carried by Dumrongsak and Savill (2012a, 2012b).

5.4.3 NO_x Emissions

The contours of time-averaged NO mass fraction are compared in Figure 5-7. The NO mass fraction is normalised by its maximum value. The LES results obtained from the three grids depict the highest NO mass fraction location in the primary zone where the flame is restrained, and the temperature peaks. Since the thermal NO formation proceeds at a significant rate at the temperatures approximately above 1850 K (Lefebvre and Ballal, 2010), this consistency of NO predictions highlights the appropriateness of the NO_x model employed. Furthermore, there is overall agreement between the solutions on the medium and fine grids in terms of the NO levels, contour shape and position of the highest NO mass fraction which corresponds to the predicted time-averaged peak temperature illustrated in Figure 5-6.

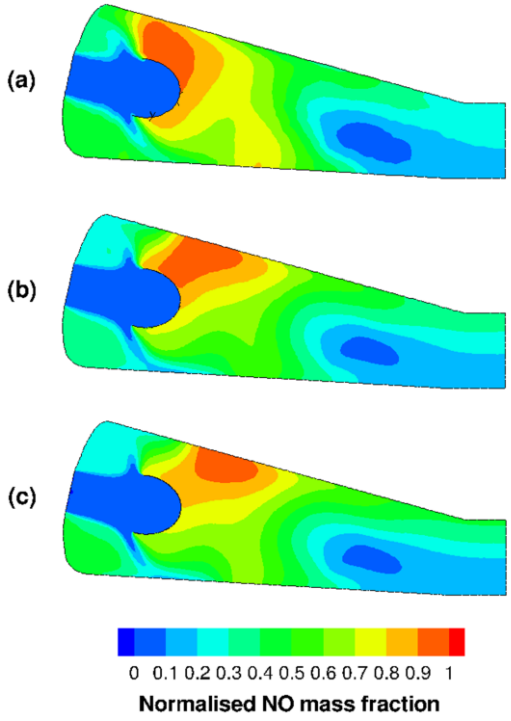

Figure 5-7 Time-averaged NO mass fraction contours on the axial midplane from the (a) coarse, (b) medium and (c) fine grids.

Table 5-2 Comparison of flame temperature, exit temperature and $EINO_x$.

	Flame temperature (K)	Exit temperature (K)	Exit $EINO_x$ (g/kg)
Coarse grid	2435	1503	10.69
Medium grid	2465	1490	10.90
Fine grid	2487	1478	13.31
EQLBRM code	2485	-	-
Curtiss-Wright Corp.	-	1477	-
FOCA	-	-	11.66
Naval Air Propulsion Centre	-	-	11.60

For quantitative comparison, Table 5-2 presents the flame temperature, exit temperature and $EINO_x$ obtained from LES on the three grids at 100% engine power. The values of the flame temperature computed from the current LES are compared with the flame temperature for Jet A/air reaction calculated by the EQLBRM code at the similar operating pressure and inlet temperature (Heiser and Pratt, 1994; Oates, 1997). As shown in Table 5-2, the grid refinement increases the flame temperature, which agrees with the comparison made in Figure 5-6. This is due to the fact that LES on the fine grid is able to capture better mixing which leads to the higher reaction rate and thus flame temperature in the primary zone. Contrarily, in the dilution zone where the reaction has completed, an increase in mesh resolution leads to lowered exit temperature. This is because the finer grids are able to capture more interaction between the hot combustion products and cooling air, which results in the increased heat transfer and lowered gas temperature. The values of predicted exit temperature are compared to the combustor design value from the Curtiss-Wright Corporation (1974).

For the evaluation of aviation NO_x, the parameter commonly used is its emission index, $EINO_x$, which is defined as (USEPA, 1977),

$$EINO_x = \frac{Mass\ of\ emitted\ NO_x}{Mass\ of\ fuel\ burnt}.$$

Since aircraft engines use a relatively large amount of fuel compared to the amount of NO generated, the unit of $EINO_x$ is more conveniently expressed as g/kg. The $EINO_x$ values obtained from LES are compared with those from the emissions approximation approach developed within the Federal Office of Civil Aviation (FOCA, 2009) for turboshaft engines at the take-off condition, and the emissions measurements carried out within the Naval Air Propulsion Centre for the General Electric T58-GE-16 engine at the maximum power (AESO, 1987). The predicted value of $EINO_x$ from LES increases as the grid resolution increases. This is associated with the prediction of the maximum flame temperature since the thermal NO formation is influenced considerably by the flame temperature (Snyder *et al*., 1994).

It should be noted that the $EINO_x$ values used for this comparison are not endorsed by ICAO. There are uncertainties associated with the estimation which are the consequences of the fuel flow approximation, selection of time in mode and power settings. Furthermore, the measurements are normally obtained during the tests carried out under the standard ground conditions which may not be the same as the flight conditions. Since there are not any $EINO_x$ data of a helicopter combustor with the size, power and operating conditions which exactly match those of the reference helicopter combustor employed in the current research, these $EINO_x$ values from the approximation approach and test measurements provide a reasonable range of the helicopter $EINO_x$ values which can be used for LES result validation.

Figure 5-8 compares the time-averaged temperature contours on various transverse planes in the helicopter combustor at 100% and 32% powers on the medium grid. As expected, the overall mean temperature at 100% power is considerably higher than that at 32% power. However, the temperature distributions at both power settings exhibit a similar trend. The first plane from the left displays relatively high mean temperature compared to other regions, indicating that some reaction has already taken place at this location. However, among the four planes, the mean temperature on the second plane is the highest. This is because this plane is located in the recirculation zone behind the flame stabiliser where the flame is contained, and the temperature peaks. The third plane, which is located in the upstream of the dilution zone, depicts the penetration of the dilution air as indicated by the contours of lower temperatures. As the gases proceed towards the exit, they are mixed with the cooling air, and the mean temperature decreases as demonstrated on the last plane.

The $EINO_x$ predictions from the current LES at these two operating points are compared with the values from the FOCA's emissions approximation approach in Figure 5-9. It is shown that both approaches predict a similar trend in the NO_x production which increases as the engine operates at a higher power setting. This is a result of the increase in fuel flow which raises the flame temperature and thus the amount of NO_x generated. At the maximum engine power, LES predicts $EINO_x$ which is slightly higher than that obtained from the FOCA's approximation. On the other hand, at 32% power, LES predicts relatively low $EINO_x$ compared to the FOCA's approximation. The airflow rate for this case is almost half of that for the maximum power setting. Since the primary air inlet area is the same for these two cases, the significant reduction in the airflow rate leads to a considerably lower flow velocity which contributes to inadequate mixing and thus limited reaction. Hence, the flame temperature is lower, and less NO_x is generated.

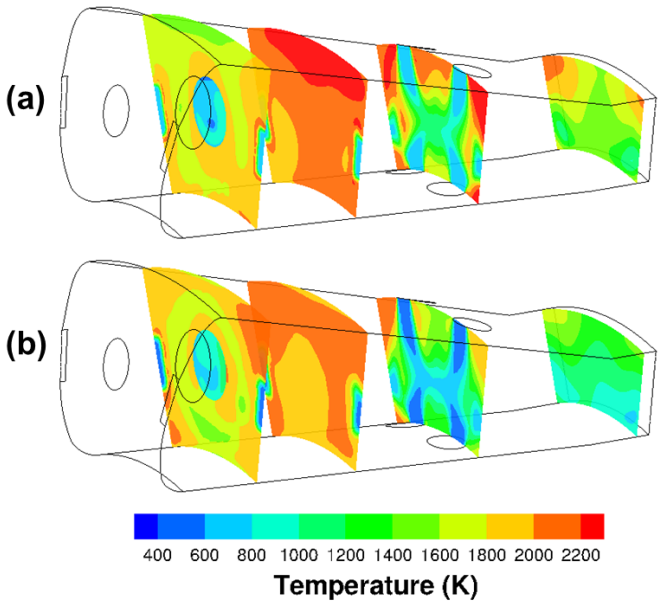

Figure 5-8 Time-averaged temperature contours at (a) 100% and (b) 32% powers.

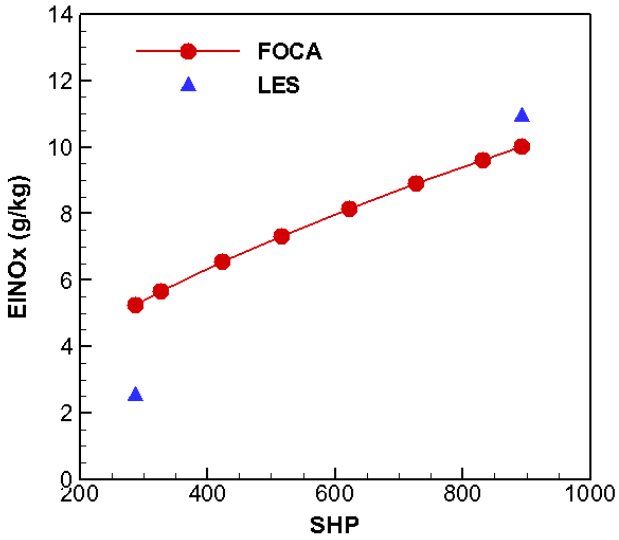

Figure 5-9 Comparison of $EINO_x$ predictions from LES and FOCA.

5.5 Conclusions

The simulation results from this chapter demonstrate the capability of the current LES code to capture the flame characteristics which match those of the reference helicopter combustor design as well as previous LES requiring ten to one hundred times larger meshes. Furthermore, the flame temperature, exit temperature and $EINO_x$ computed from LES agree generally well with the analytical solutions and test measurements. The current LES predicts a similar NO_x production trend as the FOCA's emissions approximation approach. The $EINO_x$ increases as the engine operates at a higher power setting. This is a result of the increase in the fuel flow which raises the flame temperature and thus the amount of NO_x generated. The results from this chapter highlight the possibility of employing the current LES code with a minimal grid resolution of only a few million elements for the design and emissions optimisation studies as well as its use to calibrate simpler performance and emissions models.

6 LES FOR CALIBRATION

6.1 Introduction

The aim of this chapter is to assess the potential of LES and its application for the calibration of other simpler performance and emissions models for future optimisation investigations. The model being studied is HEPHAESTUS, a 1-D in-house code developed within Cranfield University Department of Power and Propulsion, which calculates the combustor performance and emissions based on the stirred reactor concept (Celis, 2010).

This chapter consists of two main parts. The first part compares the simulation results of kerosene/air reaction in a generic combustor obtained from LES with those from HEPHAESTUS (Mazlan, 2012). In the latter part of this chapter, the LES predictions of the helicopter combustor at the maximum power setting presented in Chapter 5 are compared with the computations obtained from HEPHAESTUS.

6.2 Generic Combustor

Simulations have been carried out to study the kerosene/air reaction in a generic aircraft engine combustor employing LES. The predicted temperature and $EINO_x$ values are compared with those obtained from HEPHAESTUS (Mazlan, 2012).

6.2.1 HEPHAESTUS Combustor Model

The flow assumptions employed in the HEPHAESTUS generic combustor model are represented in Figure 6-1. The combustor model is divided into the flame front, primary, intermediate and dilution zones. Except for the dilution zone, all zones are further separated into the core and near-wall regions.

The fuel and air mixture first enters the combustor into the core and near-wall regions of the flame front zone which is assumed to be a partially-stirred reactor. The gases subsequently leave the flame front zone and enter the primary zone where the cooling air is injected to provide more oxygen for complete combustion, and cool the hot combustion products. Similarly, the gases enter and leave the intermediate zone. Finally, all gasses, including the additional cooling air, enter the dilution zone and leave the combustor. The primary, intermediate and dilution zones are represented by perfectly-stirred reactors.

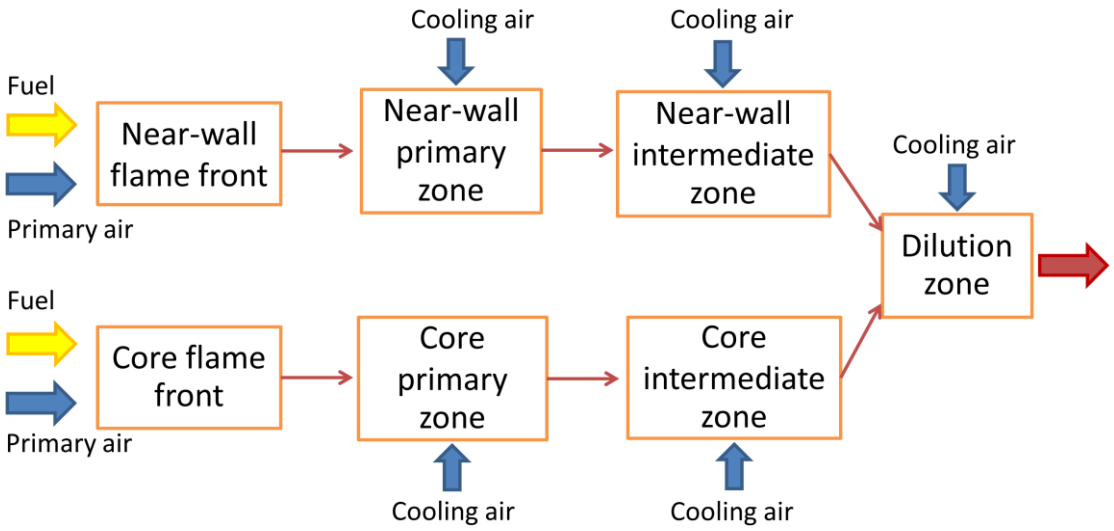

Figure 6-1 Schematic of the generic combustor model in HEPHAESTUS.

6.2.2 Computational Domain and Setup

The generic combustor configuration employed for LES is a 36° section of an annular combustor as illustrated in Figure 6-2. To allow for the comparison of results, the LES generic combustor is modelled in such a way that it represents the combustor model in HEPHAESTUS. The dimensions of the generic combustor are presented in the work of Mazlan (2012). The combustor is separated into the flame front, primary, intermediate and dilution zones. The length of each zone corresponds to the zone length assumed in

HEPHAESTUS. The flame front zone starts at the fuel and primary air inlets. In this zone, there is no separation of the near-wall and core regions as in HEPHAESTUS. The fuel and primary air are introduced into the combustor through the injector orifices and swirler respectively. In the primary and intermediate zones, the cooling air is injected into the core and near-wall regions through the plunged dilution holes and film cooling bands accordingly. For the dilution zone, the cooling air enters the combustor through eight film cooling bands.

The simulations are carried out on an unstructured mesh consisting of approximately 540,000 tetrahedral elements. All fuel and air inlets are specified as mass flow inlets. The amount of fuel and air entering each combustor zone are similar to those in the HEPHAESTUS model. The fuel is kerosene with the temperature of 288 K and the mass flow rate of 0.417 kg/s. The air has the temperature of 737 K and the total mass flow rate of 19.535 kg/s. The combustor exit is a pressure outlet and the two side boundaries are periodic. The wall is assumed to be no-slip and adiabatic. The simulations have been performed employing the current LES code. The time step size employed in the simulations is 1.0×10^{-4} seconds. The simulations have been carried out for 10 flow-through times to allow for the initial flow development and another 15 flow-through times for temporal averaging.

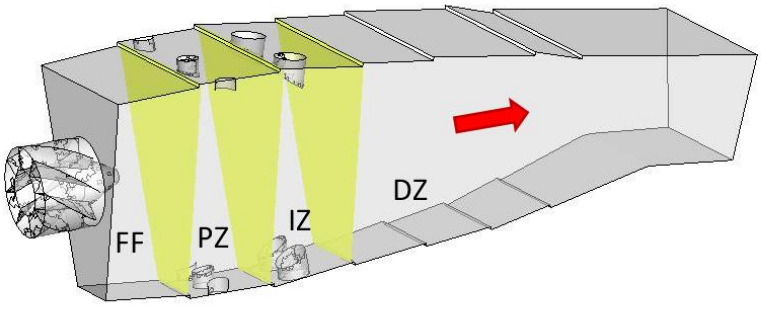

Figure 6-2 Schematic of a 36° section of the generic annular combustor.

6.2.3 Results and Discussion

Figure 6-3 displays the instantaneous temperature iso-surfaces obtained from LES of the generic combustor. The time-averaged temperature contours on the middle axial and various transverse planes are depicted in Figure 6-4. As exhibited in both figures, the flame is restrained primarily in the intermediate zone, and extends to the upstream of the dilution zone. Figure 6-5 compares the zone temperatures obtained from LES with those from HEPHAESTUS. For LES, the flame front, primary and intermediate zone temperatures are the average temperatures of the cross-sectional planes located in the middle of these zones. The last point is the average temperature at the combustor outlet. While the peak in temperature predicted by LES is located in the intermediate zone, HEPHAESTUS reports the maximum flame temperature to be in the primary zone (Mazlan, 2012). The difference in the locations of the maximum flame temperature is mainly due to the specific assumptions made in HEPHAESTUS.

The flame front zone in HEPHAESTUS is assumed to be a partially-stirred reactor to take into account the heterogeneities of the initial mixing between the fuel and air. As the reaction is limited by the inadequate mixing, the flame temperature does not reach its maximum value in this zone. However, as the gases enter the primary zone where they are assumed to be perfectly mixed, the reaction takes place spontaneously, consuming most of the reactants. As a result, most heat is produced, and thus the maximum flame temperature is reached in this zone. As the hot combustion products progress towards the dilution zone, their temperatures drop. The perfectly-stirred reactor assumption established in HEPHAESTUS implies that the cooling air introduced into each combustion zone is able to efficiently mix with the hot combustion products, and hence the gas temperature is lowered rapidly.

For LES of the generic combustor, the mixing between the fuel and air is enhanced through the swirling primary air, turbulence, flow recirculation and difference in fluid velocities. Since the flame front zone has relatively short residence time, the mixing between the fuel and air is minimal. As the gases enter the primary and subsequently intermediate zones, they have more time to mix. Furthermore, they are perturbed by the injection of cooling air though the plunged dilution holes. The strong penetration of the cooling jet, along with the extended rims of the dilution holes, obstructs the flow path, changes the flow direction and creates recirculation regions. This is demonstrated in Figure 6-6 which depicts the flow streamlines near the plunged dilution hole in the upper liner of the intermediate zone. Due to the vigorous mixing and recirculation, the flame is stabilised in this zone, leading to the highest temperature predicted. As the hot gases proceed towards the dilution zone, they are cooled by the dilution air. Despite the difference in the locations of the maximum temperature, and the significant discrepancy in the intermediate zone temperature predictions, the outlet temperatures obtained from LES and HEPHAESTUS are fairly close to each other.

Figure 6-7 exhibits the instantaneous NO mass fraction iso-surfaces in the generic combustor. It is shown that a significant amount of NO is produced in the intermediate zone and upstream of the dilution zone where the temperature is relatively high. The exit $EINO_x$ values obtained from LES and HEPHAESTUS are 10.0 and 3.7 g/kg respectively. Since the NO generation is associated with the flame temperature, the lower $EINO_x$ value computed from HEPHAESTUS corresponds to the lower flame temperature predicted.

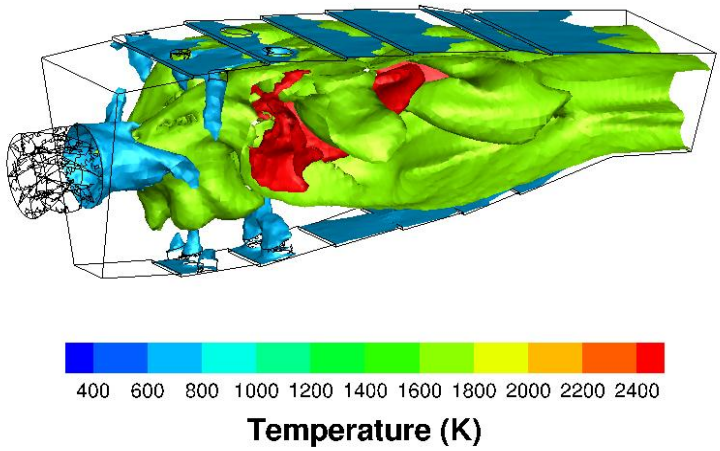

Figure 6-3 Instantaneous temperature iso-surfaces of the generic combustor at 6.71 s.

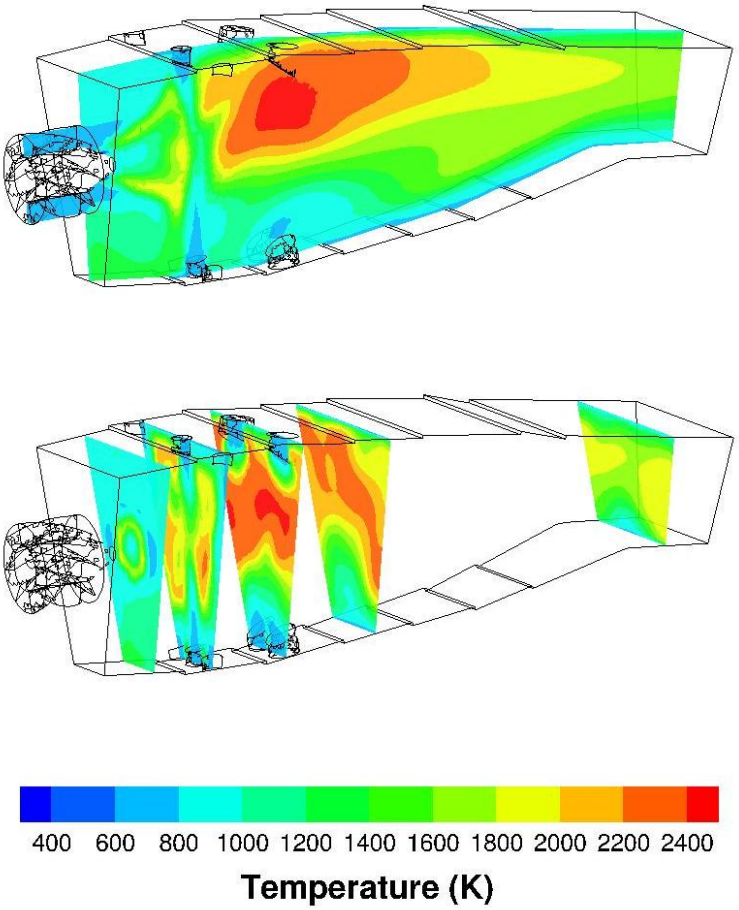

Figure 6-4 Contours of time-averaged temperature on combustor middle axial and various transverse planes.

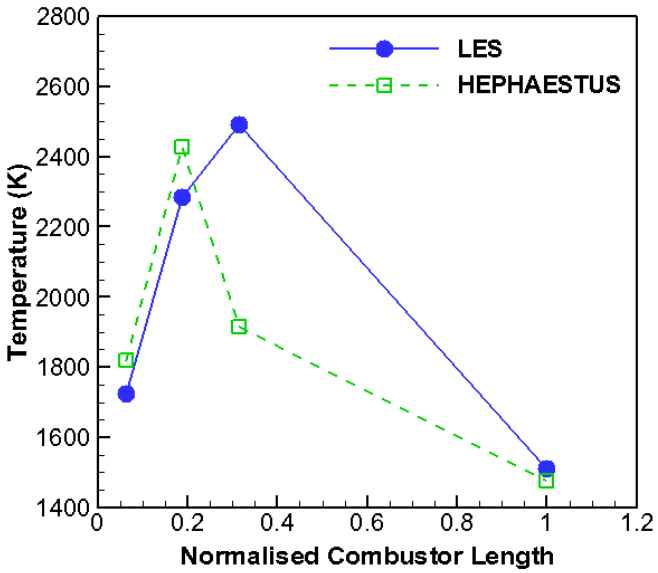

Figure 6-5 LES cross-sectional plane-averaged temperatures compared with HEPHAESTUS combustor zone temperatures.

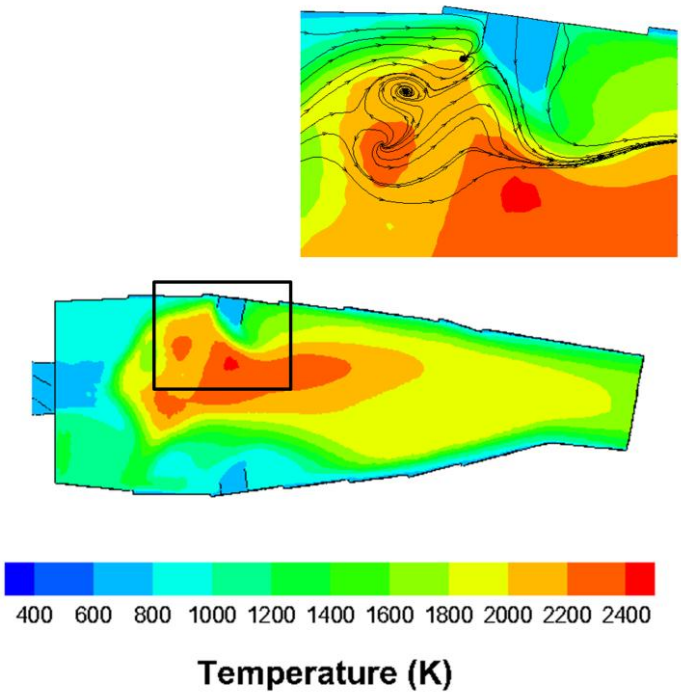

Figure 6-6 Streamlines of flow near the outer dilution hole in the intermediate zone displayed on the time-averaged temperature contours.

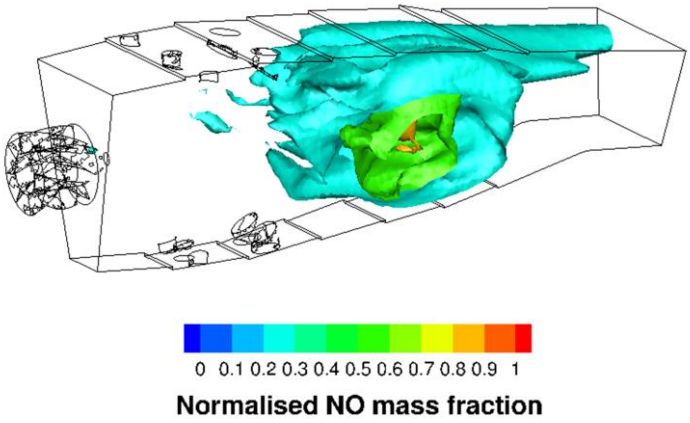

Figure 6-7 Instantaneous NO mass fraction iso-surfaces at 6.71 s.

6.3 Helicopter Combustor

A study has been carried out to compare the performance of LES and HEPHAESTUS in modelling the reaction in a small helicopter combustor. The values of $EINO_x$ computed from both approaches are compared.

6.3.1 HEPHAESTUS Combustor Model

The helicopter combustor model in HEPHAESTUS is illustrated in Figure 6-8. As similar to the HEPHAESTUS generic combustor model, the helicopter combustor is divided into the flame front, primary, intermediate and dilution zones. However, unlike the generic combustor, all helicopter combustor zones are represented by perfectly-stirred reactors, and there is no separation between the core and near-wall regions. The equivalent ratio is fixed at 0.9 for all operating conditions. It is assumed in the model that 90% of the fuel is introduced into the flame front zone where it reacts with the primary air. The gases then leave the flame front zone and enter the primary zone where another 10% of the fuel is added. The remaining air is distributed into the primary, intermediate and dilution zones to cool the hot gases. The combustor operating pressure, fuel and air flow rates, and inlet temperatures are the same as those employed in LES of the helicopter combustor in Chapter 5.

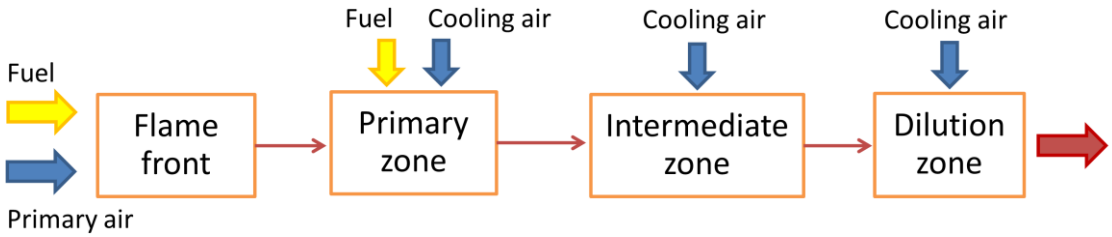

Figure 6-8 Schematic of the helicopter combustor model in HEPHAESTUS.

Since the LES helicopter combustor only has the primary and dilution zones, the HEPHAESTUS flame front, primary and intermediate zones combined are assumed to be equivalent to the primary zone of the LES combustor. For the baseline HEPHAESTUS model, the flame front zone volume is assumed to be 20% of the total LES combustor volume. The airflow distributions of LES and baseline HEPHAESTUS combustors are compared in Table 6-1.

Table 6-1 Comparison of airflow distributions in the helicopter combustor.

Zone	Airflow distributions	
	LES	HEPHAESTUS (baseline)
Flame front	-	20%
Primary	52%	22%
Intermediate	-	10%
Dilution	48%	48%

6.3.2 Computational Domain and Setup

The LES combustor configuration, computational mesh, boundary conditions, operating conditions, and numerical methods employed in this study correspond to those of the helicopter combustor operating at the maximum engine power, which are presented in Chapter 5.

6.3.3 Results and Discussion

The $EINO_x$ predictions from LES on the fine grid and HEPHAESTUS are compared in Table 6-2. The $EINO_x$ value obtained from HEPHAESTUS with the baseline combustor model is considerable lower than that computed from LES. The NO_x calculation in HEPHAESTUS is based on the input parameters such as the equivalence ratio, flame front zone area, length and airflow. However, for LES of the helicopter combustor, as well as the actual combustion inside helicopter combustors, it is difficult to determine the flame front volume. Since the values of flame front zone area, length and airflow employed in the baseline HEPHAESTUS combustor model are assumed, they may not provide the comparable representative of the combustion inside the helicopter combustor.

Another factor which may contribute to the discrepancy between the results is the assumption that the fuel and air mix instantly and completely once they enter the HEPHAESTUS combustor model. For LES, the fuel and air enter the helicopter combustor domain through separate inlets in the upstream of the primary zone where limited reaction takes place due to the inadequate mixing between the reactants. However, most of the reaction occurs downstream of the primary zone behind the flame stabiliser where the flow recirculation is present as demonstrated by the streamlines on the combustor midplane in Figure 6-9. Hence, the perfectly-stirred reactor assumption established at the flame front zone of the helicopter combustor model in HEPHAESTUS is unrealistic because it does not take into account the heterogeneities of the initial mixing between the fuel and air.

Table 6-2 Comparison of $EINO_x$ predictions from LES and HEPHAESTUS.

Approach	Exit $EINO_x$ (g/kg)	Deviation
LES (fine grid)	13.31	-
HEPHAESTUS (baseline)	1.74	86.9%
HEPHAESTUS (modified)	10.14	23.8%

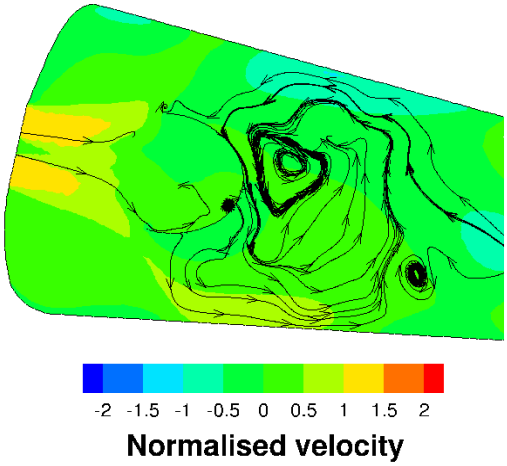

Figure 6-9 Streamlines on time-averaged contours of velocity normalised by the inlet air velocity demonstrating flow recirculation behind the flame stabiliser inside the LES helicopter combustor.

Moreover, it is assumed in HEPHAESTUS that the equivalence ratio at all operating points is fixed at 0.9. For LES, the equivalence ratio is calculated based on the actual amount of fuel and air ratio in the primary zone which is approximately 1.07 at 100% power. A decrease in the equivalence ratio leads to a drop in the flame temperature and thus the NO_x produced. Therefore, HEPHAESTUS predicts lower $EINO_x$ than LES at this operating point.

An improvement on the HEPHAESTUS helicopter combustor model has been attempted by adjusting the inputs for the flame front zone area and length. Increasing these values has the effect of increasing the NO_x generation. As demonstrated in the $EINO_x$ comparison presented in Table 6-2, the discrepancy between the LES and HEPHAESTUS predictions reduces significantly when the modified HEPHAESTUS is employed. Despite the result improvement, the important question now is whether the increased flame front zone volume is actually a real representative of the flame in the helicopter combustor.

6.4 Conclusions

The discrepancies between the results obtained from LES and HEPHAESTUS are found to be primarily due to specific simplification and assumptions established in the HEPHAESTUS models. While LES computes the temperature and NO based on the fluid mixing and flow fields captured, HEPHAESTUS assumes that the mixing in the primary, intermediate and dilution zones is spontaneous and perfect, which is a condition difficult to achieve in the real gas turbine combustor. Especially for the helicopter combustor model, the perfectly-stirred reactor assumption established at the flame front zone is unrealistic because it neglects the heterogeneities of the initial mixing between the fuel and air. Since the reaction and heat transfer rates depend on the rate of mixing, this perfect mixing assumption influences the $EINO_x$ predictions.

Although the assumption of four combustor zones can be applied to the generic combustor, it may not be appropriate for the helicopter combustor since most of the actual helicopter combustors are relatively small and short compared to the aircraft engine combustors. Therefore, the helicopter combustors typically have less number of zones. Furthermore, fixing the equivalence ratio at one value for all operating conditions may not provide the realistic representation of the reaction in helicopter combustors. As the power setting changes, the fuel flow rate and thus the equivalence ratio change. These shortcomings affect the fidelity level of HEPHAESTUS results.

As demonstrated in this chapter, LES can be employed to explore the limitations of simpler performance and emissions modelling approaches such as HEPHAESTUS. Being a higher-fidelity modelling approach, LES has proven its potential to be employed in the calibration of HEPHAESTUS. By using the LES results as the standard, the input parameters such as the flame front zone area, length and airflow which control the NO_x calculation in HEPHAESTUS can be adjusted to improve its predictive capabilities.

7 LES OF REACTIVE HELICOPTER EXHAUST

7.1 Introduction

Reliable assessments of the impacts of aviation emissions on the climate and air quality primarily require detailed knowledge about the chemical evolution and dilution processes which take place at the first stage of the exhaust plume dispersion. In addition, modelling the chemical reaction in the jet exhaust is of great significance because the exhaust species are currently inaccessible to measurements. The purpose of this study is to gain an insight into a NO chemical process in a helicopter jet exhaust employing LES. The plume reaction considered is the transformation of NO to NO_2. For the grid sensitivity analysis, the simulations have been performed on three computational meshes. The effects of helicopter exhaust temperature on the chemical reaction have also been investigated. Since much of the chemistry takes place very early in the jet (Karcher *et al.,* 1996), this study focuses on the early plume regime up to 20 m downstream of the exhaust exit.

7.2 Computational Domain and Setup

The simulations have been performed on a cone-shaped computational domain illustrated in Figure 7.1. The central inlet which represents the helicopter exhaust exit has the diameter of 0.5 m. This dimension is comparable to that of the turboshaft engine which has similar rated power as the reference helicopter combustor employed in this research (Daly, 2010). The jet is surrounded by an annular ambient air inlet with the outer diameter of 5.0 m. The domain extends 35.0 m downstream. The exit diameter increases to 30.0 m. Three O-type grids which consist of approximately 175,000, 777,000 and 1,654,000 hexahedral elements have been created for the grid sensitivity analysis. They will, henceforth, be referred to as the coarse, medium and find grids respectively. As exhibited in Figure 7.2, the grid is clustered near the centre of the exhaust plane radially and the exhaust exit axially to capture the reaction in the region of interest.

The current LES code has been employed in conjunction with the EDC model. The plume reaction considered is the transformation of NO to NO_2, which has previously been validated in Chapter 4. The time step sizes employed for the coarse, medium and fine grids are 8.0×10^{-4}, 1.0×10^{-4} and 5.0×10^{-5} seconds respectively. The simulations have been carried out for 5 flow-through times to allow for the initial flow development and another 10 flow-through times for temporal averaging.

The jet inlet is specified as the mass flow inlet. By assuming the fuel mass flow is negligible, the mass flow rate at the exhaust exit is taken to be equal to that of the air at the helicopter engine inlet. For the sensitivity study, the exhaust total temperatures considered are 422 K and 600 K. The annular inlet is set as the pressure inlet with the total pressure of 10 Pa above the ambient pressure, and total temperature of 290 K. The conical side boundary is specified as the pressure inlet with the total pressure equals to the ambient pressure, and the total temperature of 290 K. The outlet of the domain is the pressure outlet. This setup corresponds to that of the exhaust plumes modelling of Garmory *et al*. (2008) and Gursoy (2009).

For the initial background composition, the O_3, NO and NO_2 concentrations are representative of the values at sea level in the United Kingdom (Garmory *et al*., 2008). The value of the background O_2 is obtained from the study of Karcher *et al.* (1996). These values are presented in Table 7.1. The remaining air is assumed to be composed of only N_2 which does not take part in the reaction. The helicopter exhaust chemical composition is assumed to consist of only NO, O_2 and N_2. The concentrations of NO and O_2 in the jet exhaust are obtained from the LES results of the helicopter combustor in Chapter 5. The computed values of NO concentration are normalised by the initial NO concentration at the exhaust exit.

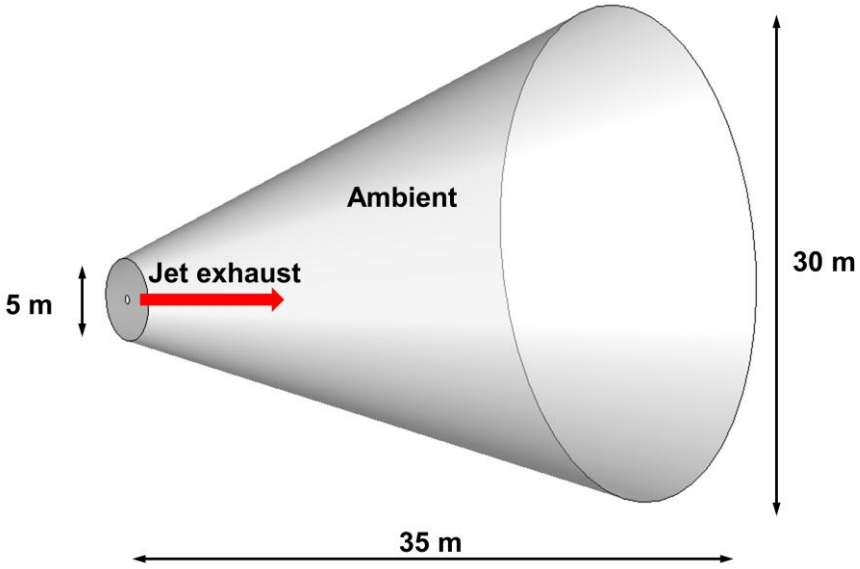

Figure 7-1 Dimensions of the jet exhaust domain.

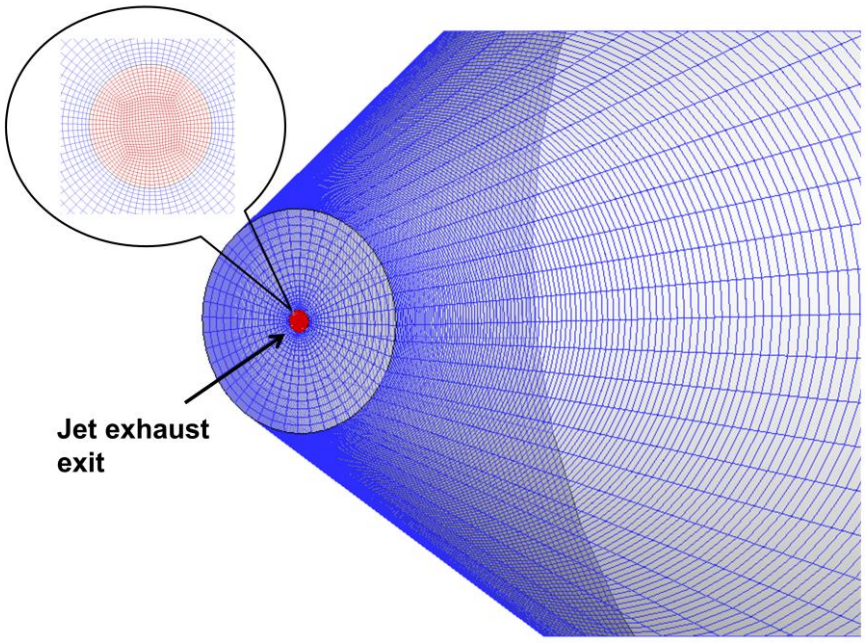

Figure 7-2 Computational mesh of the domain behind the exhaust exit.

Table 7-1 Initial chemical compositions.

Species	Exhaust (ppmv)	Background air (ppmv)
O_2	1.71×10^{5}	2.10×10^{5}
O_3	-	3.86×10^{-2}
NO	5.39×10^{1}	1.86×10^{-2}
NO_2	-	3.14×10^{-2}

7.3 Results and Discussion

7.3.1 Grid Sensitivity Analysis

Figure 7-3 compares the contours of NO mass fraction, normalised by its initial value at the exhaust exit given in Table 7-1, on the midplane of the three grids. The comparison reveals that as the grid resolution increases, more reaction at the interface between the exhaust plume and ambient air is captured. This can be observed by the green colour contours which suggest that some NO has already been mixed and consumed by the reaction. Particularly from 3 m to 8 m, compared to the coarser meshes, the fine grid exhibits thicker shear layers where small-scale structures and strong mixing are present. In addition, as suggested by the shorter red contours, the reaction in the jet core depicted on the finer grids takes place earlier than the coarse grid. Further downstream, the coarse grid appears to be rather dissipative. Its resolution is inadequate to resolve the vertex shedding and entrainment of the ambient air into the exhaust plume as well as the fine grid which exhibits separate pockets of higher NO mass fractions after the distance of approximately 10 m.

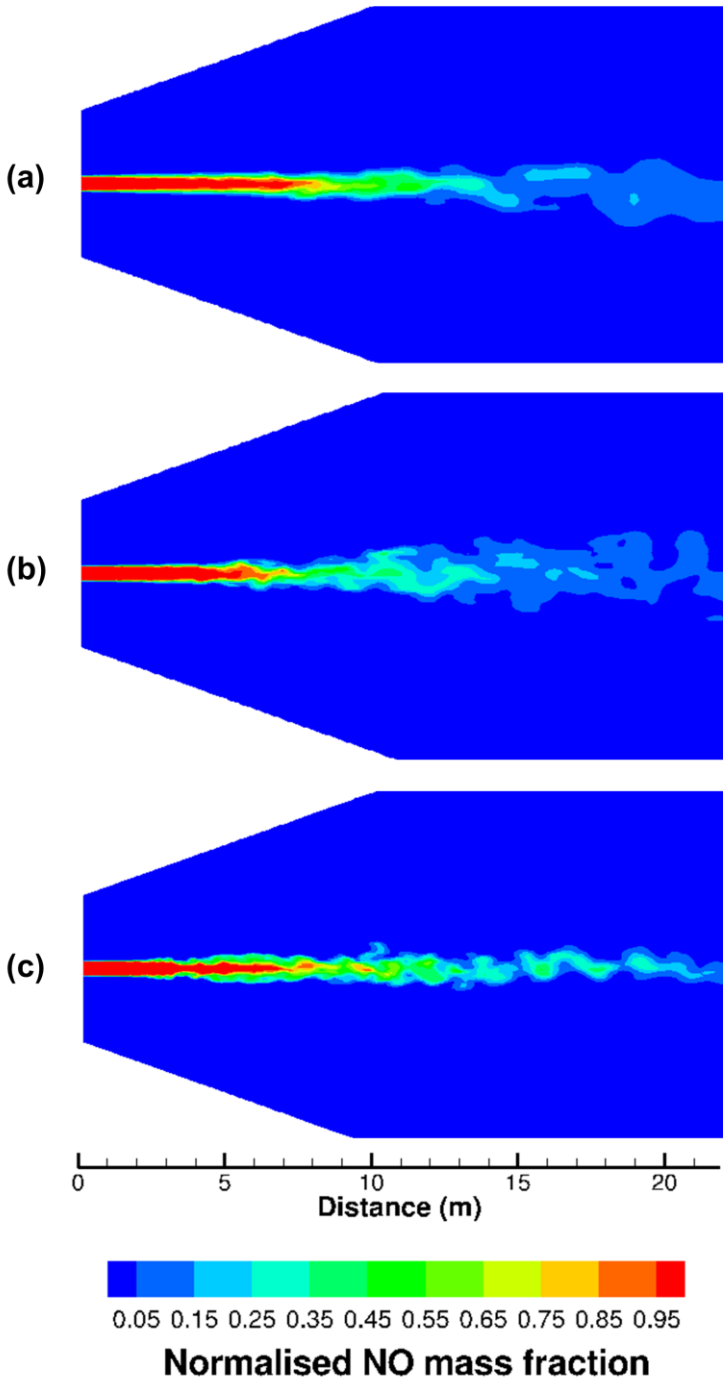

Figure 7-3 Instantaneous contours of NO mass fraction, normalised by the initial value of the exhaust, on the (a) coarse, (b) medium and (c) fine grids at 30.62 s.

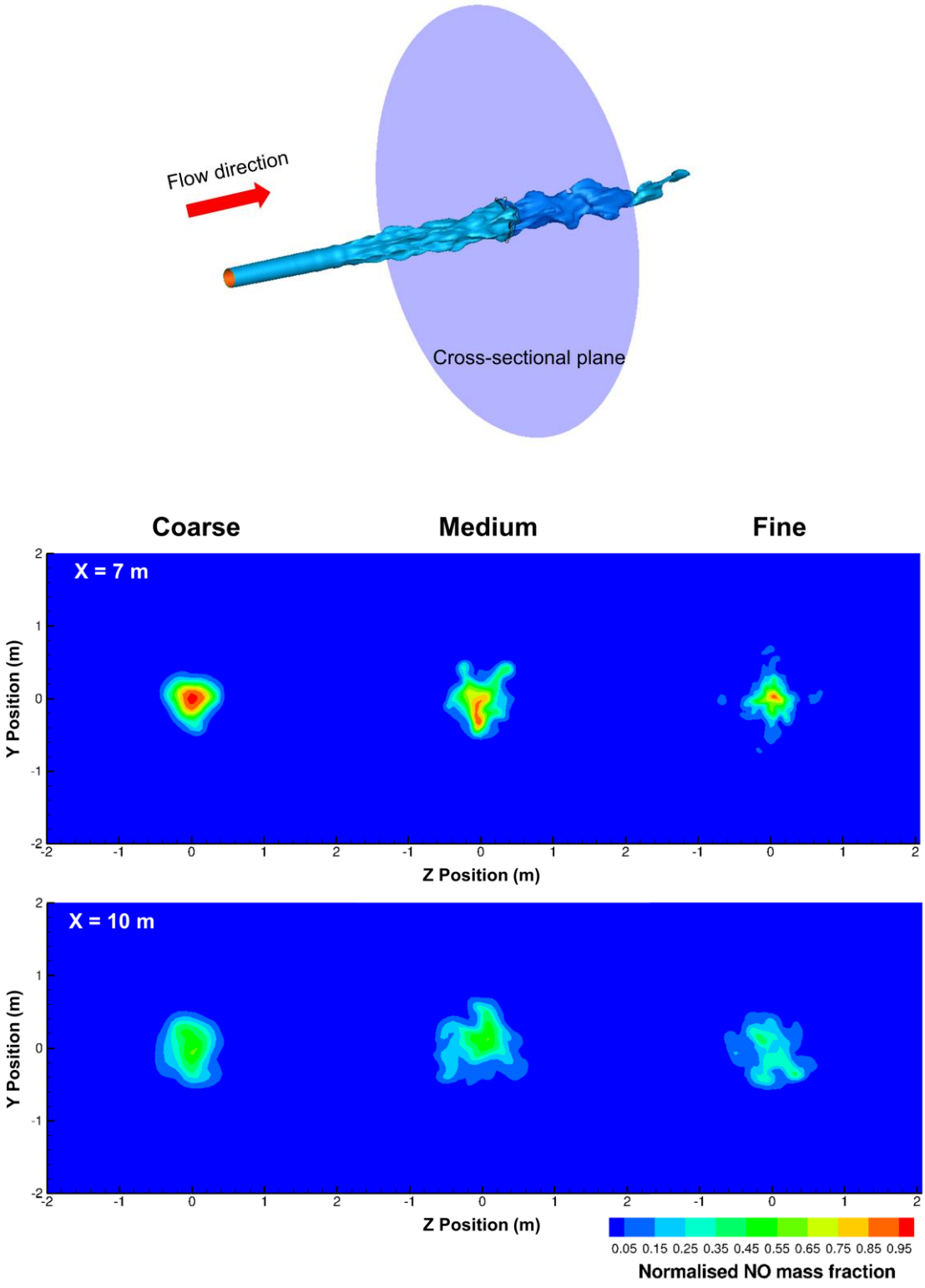

Figure 7-4 Comparison of instantaneous contours of NO mass fraction, normalised by the initial value of the exhaust, on the cross-sectional planes at *x* = 7 m and 10 m from all grids at 30.62 s.

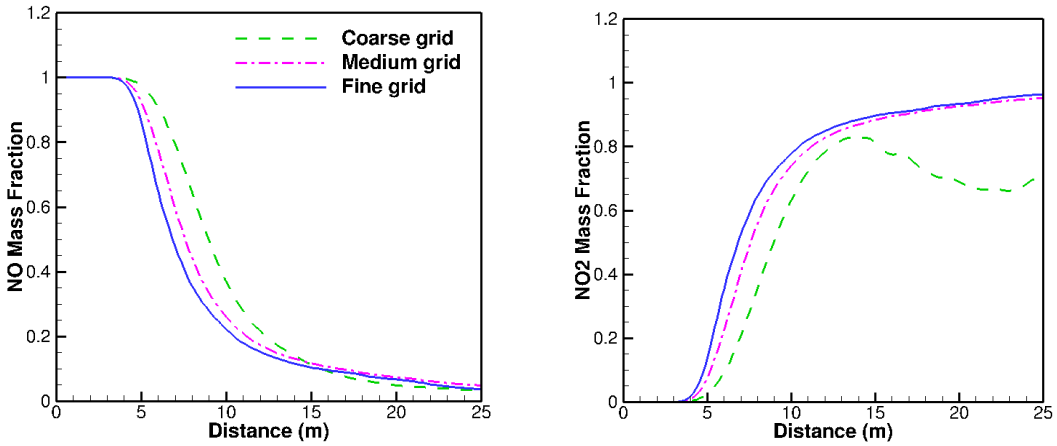

Figure 7-5 Profiles of time-averaged NO (left) and NO_2 (right) mass fractions along the jet centreline on different grids.

Figure 7-4 compares the normalised NO mass fraction contours on the cross-sectional planes of the three grids. At x = 7 m, the three grids exhibit a region of maximum NO mass fraction in the jet core. However, the coarse grid depicts the largest area of the maximum NO region. There are distinct NO layers with the jet core concentrated at the centre and enclosed by thin shear layers. This is because the mixing between the jet exhaust and ambient air at this location has not been well captured by the coarse grid. The medium and fine grids, on the other hand, display the entrainment of the ambient air into the exhaust plume which leads to the consumption of NO by the reaction and thus smaller maximum NO region. At x = 10 m, all grids no longer exhibit the maximum NO zone. This is consistent with the NO contours in Figure 7-3 which depicts the length of jet core to be less than 10 m for all grids. The coarse grid still displays concentrated jet enfolded by the ambient air whereas the medium and fine grids exhibit more mixing between the jet exhaust and surrounding air.

Profiles of time-averaged normalised NO and NO_2 mass fractions along the jet centreline obtained from different grids are compared in Figure 7-5. Behind the exhaust exit, LES on the three grids initially predict maximum NO mass fraction until the distance of about 5 m, after which the surrounding air begins to be entrained into the exhaust plume, and the reaction starts to take place, leading to the drop in the NO mass fraction. However, different grids exhibit different NO decreasing rates. As the grid resolution increases, the drop in the NO level becomes more rapid. This is due to the fact that the finer grids are able to capture smaller-scale mixing better. As a result, the entrainment of the ambient air and, hence, the reaction reach the jet core quicker. Furthermore, it can also be observed that in the reaction zone between 5 m to 15 m, the increase in NO consumption rate from the coarse grid to the medium grid is higher than that from the medium grid to the fine grid. Since similar initial chemical compositions are employed in the three cases, the NO levels are expected to reach the same value after the reaction completes. This is illustrated on the left of Figure 7-5 where the NO mass profiles approach the same level in the downstream region after the distance of approximately 22 m.

On the right of Figure 7-5, the corresponding rise in NO_2 mass fraction from the reaction is demonstrated. The increase in the grid resolution from the medium mesh to the fine mesh raises the NO_2 generation rate slightly in the reaction zone. This is consistent with the increase in the NO consumption rate exhibited on the left. The NO_2 profiles from the two grids reach the same level after the distance around 15 m. The coarse grid, on the other hand, is too dissipative and displays a non-physical drop in NO_2 mass fraction after the distance of 15 m. This suggests that the resolution of the coarse grid is inadequate in this region.

7.3.2 Effects of the Exhaust Temperature

To compare the effects of temperature on the chemical transformation of NO to NO_2, LES has been performed on the medium grid for the helicopter exhaust temperature of 422 K and 600 K. The NO mass fraction contours obtained from the simulations are compared in Figure 7-6. The comparison reveals that the increase in the exhaust temperature increases the chemical reaction rate. As illustrated in Figure 7-6 (a) for the exhaust temperature of 422 K, the length of the jet core is significantly longer compared to that in the higher exhaust temperature case. While the exhaust plume of lower temperature is narrower and has higher NO concentration, the simulation results of the higher exhaust temperature depict more dispersed helicopter exhaust plume with lower NO level downstream. This is owing to the fact that the rise in the temperature increases the energy of NO particles, which in turn allows them to react more readily when colliding with the O_3 particles.

Figure 7-7 compares the profiles of time-averaged normalised NO and NO_2 mass fractions along the jet centreline obtained from LES for the two exhaust temperatures. The NO level remains constant at the beginning until the distance of approximately 5 m and 6 m for the exhaust temperature of 600 K and 422 K respectively, after which the NO mass fraction starts to drop. However, the rate of NO consumption by the reaction is higher for the 600 K exhaust temperature than the 422 K counterpart. This is consistent with the NO contours in Figure 7-6 which displays a shorter jet core in the case of the higher exhaust temperature. In the downstream region where the profiles start to level, it can be observed that the final NO level of the 600 K exhaust temperature case is slightly lower than that of the 422 K exhaust temperature. The profiles of NO_2 mass fraction correspond to the NO predictions. The higher NO consumption rate for the 600 K exhaust temperature illustrated in the left figure leads to a higher NO_2 generation rate on the right figure. Furthermore, the final NO_2 level is slightly higher for the case of the higher helicopter exhaust temperature.

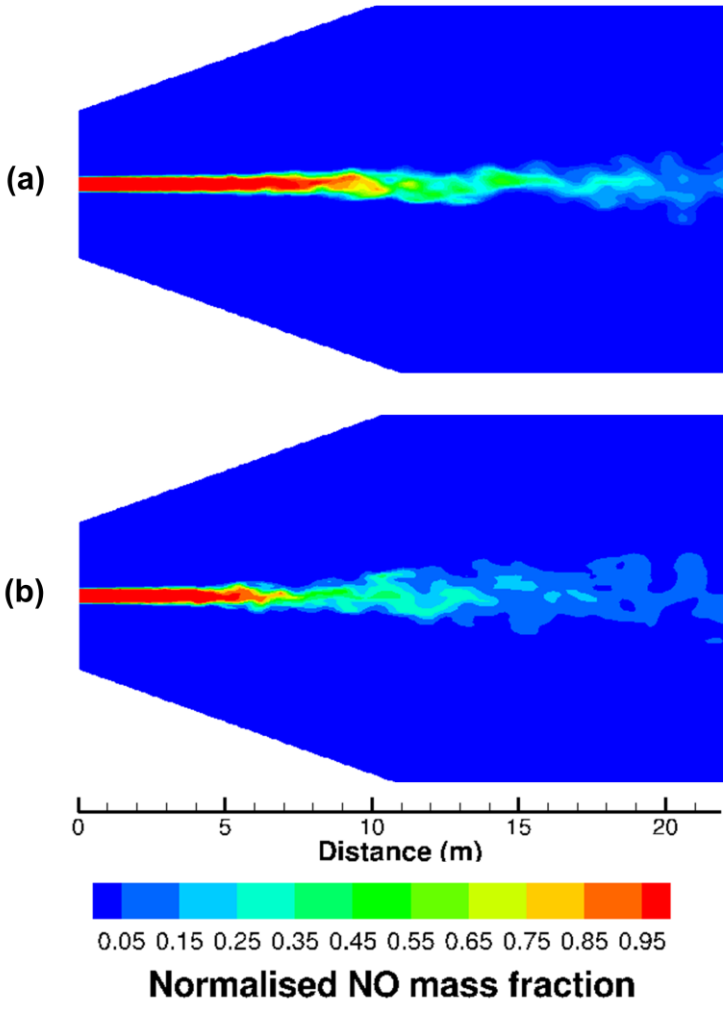

Figure 7-6 Instantaneous contours of NO mass fraction, normalised by the initial value of the exhaust, for the exhaust temperature of (a) 422 K and (b) 600 K at 30.62 s.

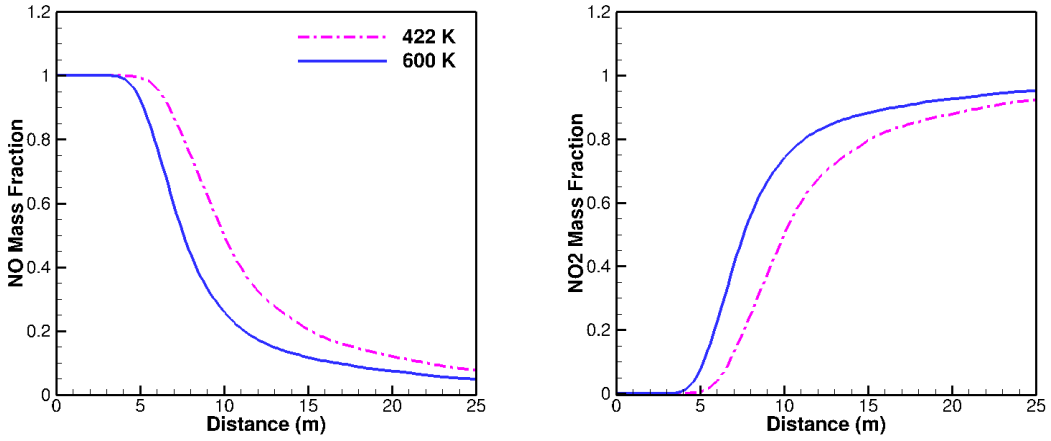

Figure 7-7 Profiles of time-averaged NO (left) and NO_2 (right) mass fractions along the jet centreline from different helicopter exhaust temperatures.

7.4 Conclusions

The performance of LES in modelling the chemical transformation of NO to NO_2 in the helicopter exhaust plume has been demonstrated in this chapter. The medium and fine grids exhibit more mixing and thus reaction in the shear layers. In addition, the entrainment of the surrounding air into the exhaust plume downstream is well captured on these grids. The coarse mesh, on the other hand, is found to be too dissipative, and provides non-physical NO_2 formation trend downstream. Comparing the two exhaust temperatures, the increase in the exhaust temperature raises the reaction rate and the amount of products generated. This is because the NO particles gain more energy from the rise in temperature, and thus are able to react with the O_3 particles more readily.

8 CONCLUSIONS AND FUTURE WORK

8.1 Conclusion

The increasing environmental concerns over the impacts of aviation emissions on the climate and air quality have led to the development of more stringent policies and significant world-wide efforts to reduce aviation emissions, particularly the harmful NO_x emissions. However, the lack of publicly accessible helicopter engine emission data and information on the chemical evolution of important species in the helicopter exhaust plume impedes the design and development of more environmentally-friendly helicopter engines with reduced emissions.

The findings from the current research highlight the good capabilities of the current commercial LES at minimal grid resolution and computational resource requirements in terms of the number of processors utilised and execution time, with simple combustion and chemistry models, to capture main combustion characteristics in a helicopter combustor, predict helicopter NO_x emissions, and evaluate an important chemical reaction in a helicopter exhaust plume. This economic advantage makes it a promising tool for the design and emissions optimisation investigations of helicopter combustors and exhaust systems, which will diminish the reliance on the expensive parametric experimental studies. Another fundamental element of the current research has been the assessment of the potential application of LES for the calibration of other lower-fidelity combustion performance and emissions models.

The research begins with the validation of the current commercial LES code for a non-reacting round jet. Compared with a previous research LES code which tends to over-predict the jet spreading rate, the results from the current LES agree better with the experimental data. However, LES results are found to be very sensitive to the grid resolution in the upstream of the jet core. This is because of the higher grid requirements near jet nozzle where the velocity is higher, and the mixing is more intense. The capabilities of LES to predict flow

fields, capture mixing and spreading characteristics of a round jet with a co-flow have been demonstrated in this test case.

The second test case is LES of a coaxial jet combustor. The comparison of simulation results demonstrates the superiority of LES over RANS in capturing realistic flame characteristics. The current LES is able to predict the highest product mass fraction which agrees with the highest product mass fraction attainable in theory. The RANS approach, on the other hand, under-predicts the product mass fraction significantly because it is not able to capture the mixing well, and thus under-predicts the reaction rate. However, RANS performs better than LES near the wall due to the higher grid requirements of LES to resolve flow in viscous near-wall regions.

The LES results are then validated against the classical experimental data and compared with the computations obtained from a modified LES with a more advanced chemistry modelling approach. The current LES is able to capture highly unsteady flame behaviours which agree with the observation made in the experiment. The fine grid is able to capture more smaller-scale mixing in the inner flame than the coarse grid, especially in the upstream region behind the fuel port. In addition, improvements in the near-wall predictions have been observed when the finer grid is employed. Although the LES predictions are especially sensitive to the grid resolution near the wall, the current LES code is able to provide valuable results for future design and emissions optimisation investigations of combustors since important aspects of the combustion process, such as the main reactions and pollution formation, usually take place far away from the wall.

For the comparison of chemistry models, there are slight discrepancies between the upstream predictions behind the fuel port. However, these discrepancies diminish along the combustor length. Since the combustor operating and boundary conditions are the same in both cases, the profiles are expected to be uniform towards the exit of the combustor where the reaction completes. As demonstrated by the results, the downstream predictions from the two models are similar and agree generally well with the experimental measurements.

Another test case has been carried out to validate the application of the current LES with an unstructured grid for modelling non-premixed combustion. The results reveal that there is a delay in the upstream mixing and thus reaction on the unstructured grid which is mainly due to the simplification of the configuration. Since the splitter plate plays a key role in initiating the flow instability at the interface between the two fluid streams, altering the thickness of the splitter plate on the unstructured grid affects the mixing and recirculation process of the flow inside the combustor.

Compared to the structured grid, the mixture fraction, product mass fraction and temperature predictions of LES on the unstructured grid agree better with the experimental data downstream. This is because the unstructured mesh has finer grid elements near the combustor exit, and thus is able to capture more detailed mixing in this region. The purpose of the comparison in this test case is for validation and not to suggest that the unstructured grid is superior or inferior to the structured grid. For the coaxial jet combustor which is a simple configuration, the application of the structured grid is more efficient. However, an unstructured grid provides more flexibility and can be easily applied to more complex geometries such as the helicopter combustor employed in the current research.

For the last test case, the transformation of NO to NO_2, which is the key gas-phase chemical reaction selected for the reactive helicopter exhaust plume modelling, and its kinetic parameters have been validated for a round jet configuration. The two reaction models being compared are the laminar finite-rate and eddy dissipation models. The simulation results predicted by the eddy dissipation model agree generally well with the experimental data except at the fluid interface where the model over-predicts the reaction rate slightly. The laminar finite-rate model, on the other hand, tends to under-predict the reaction rate in the regions where the effects of turbulence become important. This is owing to the fact that the model does not take into account the turbulence-chemistry interaction.

The validated LES code is then employed to model the Jet A/air reaction in the helicopter combustor. The current LES is able to capture the flame characteristics which match those of the reference helicopter combustor design as well as previous LES requiring ten to one hundred times larger meshes. In addition, the flame temperature, outlet temperature and $EINO_x$ computed by the current LES agree generally well with the analytical solutions and test measurements. The grid sensitivity analysis reveals similar mean flame location on all grids, which matches that of the initial combustor design. This highlights the proper performance of the combustion model employed which appears to be independent of the grid resolution. Furthermore, the three grids depict the highest NO mass fraction location in the primary zone where the flame is restrained, and the temperature peaks. Since the thermal NO formation proceeds at a significant rate at high temperatures, this consistency of NO predictions highlights the appropriateness of the NO_x model employed.

Despite similar combustion results predicted, the instantaneous temperature distributions from all grids are different locally. As the grid resolution increases, the temperature contours become more pronounced, and more flame front wrinkling is resolved. As demonstrated by the comparison, the fine grid displays more perturbation, shedding and mixing of the gas stream. This agrees with the previous LES results.

For the quantitative comparison, the flame temperature is found to increase with the grid refinement. This is due to the fact that LES on the fine grid is able to capture better mixing which leads to the higher reaction rate and thus flame temperature in the primary zone. However, the increase in mesh resolution decreases the exit temperature. This is because the finer grids are able to capture more interaction between the hot combustion products and cooling air, which results in the increased heat transfer and lowered gas temperature. For the comparison between the maximum and low engine powers, the predicted $EINO_x$ increases with the power settings. This is a result of the increase in fuel flow which raises the flame temperature and thus the amount of NO_x generated.

Subsequently, the potential application of LES for the calibration of simpler performance and emissions models has been assessed for the generic and helicopter combustors. The temperature and $EINO_x$ predictions obtained from LES are compared with those from an in-house performance and emissions modelling code, HEPHAESTUS. The discrepancies between the results are primarily due to specific simplification and assumptions established in the HEPHAESTUS model. While LES computes the reaction based on the mixing and flow fields captured, HEPHAESTUS assumes that the mixing in the primary, intermediate and dilution zones is spontaneous and perfect, which is a condition difficult to achieve in the real gas turbine combustor. Especially for the helicopter combustor model, the perfectly-stirred reactor assumption established at the flame front zone is unrealistic because it neglects the heterogeneities of the initial mixing between the fuel and air. Since the reaction and heat transfer rates depend on the rate of mixing, this perfect mixing assumption affects the temperature and $EINO_x$ predictions.

As demonstrated in the current research, LES can be employed to explore the limitations of simpler performance and emissions modelling approaches such as HEPHAESTUS. Being a higher-fidelity modelling approach, LES has proven its potential to be employed in the calibration of HEPHAESTUS. By using the LES results as the standard, the input parameters such as the flame front zone volume, airflow distributions and equivalence ratio which control the NO_x calculation in HEPHAESTUS can be adjusted to improve its predictive capabilities.

Finally, LES has been employed to model the transformation of NO to NO_2 in the helicopter exhaust plume. The current LES is able to capture the vortex shedding, entrainment of the ambient air in to the jet core and chemical reaction well. The grid sensitivity analysis reveals that as the mesh resolution increases, LES is able to capture more mixing and reaction, especially in the shear layers, leading to lower NO concentrations predicted. The comparison of the two exhaust temperatures reveals that the increase in the exhaust temperature raises the reaction rate and the amount of products generated. This is because the NO particles gain more energy from the rise in temperature, and thus are able to react with the O_3 particles more readily.

The results from the current research highlight the possibility of employing the LES code with a minimal grid resolution of only a few million elements for the design optimisation studies as well as its use to calibrate simpler performance and emissions models.

8.2 Future Work

The current research focuses on the modelling of NO_x emissions from the helicopter combustor and the chemical transformation of NO to NO_2 in the exhaust plume. It provides an insight into the NO_x formation characteristics, influences of important flow parameters on the NO_x generation, and reaction of NO in the hot exhaust with the ambient O_3. Another environmental concern associated with the helicopter operations is soot which is the second largest contributor to global warming. Exposure to soot leads to serious health problems, such as aggravation of respiratory, cardiovascular diseases, and premature mortality (USEPA, 1999). Soot contains polycyclic aromatic hydrocarbons (PAHs) which are hazardous chemical compounds and identified as carcinogenic. As the measurements of Chen *et al.* (2006) demonstrated, the PAHs emissions from the UH-1H turboshaft engine was the highest compared to those from the motor vehicle, heavy duty diesel and F101 aircraft engines.

This suggests that soot emissions from helicopter engines are not negligible, and thus appropriate measures should be taken to reduce these emissions. Therefore, in the future, it is necessary to carry out a high-fidelity numerical study of soot emissions from helicopter engines, soot dispersion characteristics in the environment and soot formation in the atmosphere by the transformation of NO_x, VOCs, SO_x in order to provide a better understanding of soot emissions.

To properly account for the interaction between the film cooling air and hot combustion products, the explicit modelling of helicopter combustor film cooling bands could also be included in the future work. However, since the film cooling thickness is generally too small for standard LES grids, the mesh generation issue involved will have to be taken into consideration.

The comparison between the results obtained from the current LES and HEPHAESTUS model for the helicopter combustor has demonstrated that by adjusting the input values of flame front zone area and length, the deviation of the HEPHAESTUS NO_x output from the predicted LES NO_x reduces significantly. Therefore, on the part of the HEPHAESTUS users, the LES results from the current research can be used as the standard for further calibrating the parameters controlling the NO_x calculation in HEPHAESTUS. The flame front zone area and length obtained after the calibration could be used as the baseline values for other helicopter combustor studies. On the other hand, the code developers could incorporate the heterogeneities of the initial mixing between the fuel and air in the flame front zone into the HEPHAESTUS model. Furthermore, the developers may modify the HEPHAESTUS code so that the actual equivalence ratio is calculated instead of using a constant equivalence ratio for different fuel and air mixtures. This will provide a more realistic representation of the reaction and thus the NO_x generation inside helicopter combustors.

For the exhaust study, this research only considers a circular aft exhaust face configuration which produces a straight plume during a forward flight mode. As suggested by the literature (O'Brien *et al*., 2008), the exhaust configuration affects the flow characteristics. This, in turn, influences the mixing and thus the reaction between the chemical species in the exhaust plume and ambient air. Therefore, LES could be carried out to investigate how different exhaust face shapes and angles affect the chemical reaction in the exhaust. The simulation results will be beneficial for the future design and optimisation processes of more environmentally-friendly exhaust systems.

In addition, the current research only focuses on one key chemical reaction in the helicopter exhaust plume. However, the actual chemical transformation of species in the jet exhaust involves numerous complex chemical processes. Although modelling these chemical processes employing LES is a challenge owing to the numerical complexity and high computational costs involved, it will provide insights into the dominant chemical reactions and the overall effects of these reactions on a particular exhaust species.

The NO_x measurements of the reference helicopter engine are not available in the public domain at present for the current research. However, there may be a future possibility to quantitatively compare helicopter exhaust NO_x predictions obtained from LES with the test data from new research programmes such as the Fibre-Laser Imaging of Gas Turbine Exhaust Species (FLITES) consortium which has been launched to build upon the expertise in chemical species tomography, fibre-lasers, and gas-detection opto-electronics for aero engine emission measurements (Johnson, 2013; Armstrong, 2013).

Due to the rising fuel price and environmental concerns associated with the petroleum combustion, the aviation industry has been exploring alternatives to conventional jet fuel. To achieve the emissions reduction goals, one of the most promising solutions is the use of biojet fuels, which will reduce the amount of greenhouse gases emitted. Experimental studies have been carried out to evaluate the engine performance and emissions from biofuel combustion. In addition, over 1500 flights have already been successfully and safely operated using biofuel-kerosene blends (IATA, 2013). Following the success of the biofuel application for civil aircraft, LES of biofuel-kerosene/air reaction in a helicopter combustor could be carried out to evaluate the engine performance and emissions in order to explore the possibility of extending the application of biofuels to power helicopters.

PUBLICATIONS, PRESENTATIONS AND AWARDS

- **Journal publications**

  - Dumrongsak, J. and Savill, A. M. (2012) Numerical analysis and sensitivity study of non-premixed combustion using LES. *World Academy of Sciences Engineering and Technology*, 72, pp. 1164-1175 (Appendix A.1).

  - Dumrongsak, J. and Savill, A. M. (2014) Prediction of NO_x Emissions from a Helicopter Combustor Using Large Eddy Simulation (submitted) (Appendix A.2).

- **Conferences**

  - Dumrongsak, J. and Savill, A. M. (2012) Large eddy simulation of a coaxial jet combustor. In: *9th European Fluid Mechanics Conference,* Rome, 9-13 September, pp. 497.

  - Dumrongsak, J. and Savill, A. M. (2012) Numerical analysis and sensitivity study of non-premixed combustion using LES. In: *33rd International Conference on Fluid Mechanics, Heat Transfer and Thermodynamics,* Phuket, 24-25 December, pp. 55-66.

- **Poster presentations**

  - Dumrongsak, J. and Savill, A. M. (2012) Combustion large eddy simulation of Jet-A fuel in a helicopter combustor. *The Royal Society of Chemistry Energy Sector Early Career Symposium*, Cranfield University, 27 November (Appendix B.1).

- Dumrongsak, J. and Savill, A. M. (2013) Large eddy simulation of helicopter combustor and exhaust emissions. *The Annual Engineering and Aerospace Doctoral Training Centre's Research Students' and Supervisors' Lunch and Poster Conference*, Cranfield University, 12 February (Appendix B.2).

- Dumrongsak, J. and Savill, A. M. (2013) Large eddy simulation of helicopter combustor and exhaust emissions. *The FLITES In-plume Imaging of Gas Turbine Exhaust Species Workshop*, Institution of Engineering and Technology, Savoy Place, 21-22 March.

- **Awards**

  - Best Fossil Fuel Poster Prize at the Royal Society of Chemistry Energy Sector Early Career Symposium November 2012.

  - American Society of Mechanical Engineers International Gas Turbine Institute Student Scholarship.

  - Funds for Women Graduates Foundation Grant.

- **Others**

  - ANSYS Hall of Fame Competition (submitted on 15 November 2012) Animation of transient temperature distributions of Jet-A fuel and air combustion inside a section of a helicopter annular combustor using Large Eddy Simulation model in ANSYS Fluent.

REFERENCES

Aircraft Environmental Support Office (AESO). (1987) *Gaseous Emissions from Aircraft Engines: A Handbook for the Calculation of Emission Indexes and Gaseous Emissions from Aircraft Engines.* California: Naval Environmental Protection Support Service, AESO Report no. 1-87.

Albouze, G., Poinsot, T. and Gicquel, L. (2009) Chemical kinetics modeling and LES combustion model effects on a perfectly premixed burner. *Comptes Rendus Mécanique,* 337 (6-7), pp. 318-328.

Armstrong, I. (2013) *CO_2 imaging and NO measurement in turbine exhaust using TFLAS*. Fibre-Laser Imaging of Gas Turbine Exhaust Species (FLITES), Institution of Engineering and Technology, Savoy Place, 22 March.

Auzillon, P., Riber, E., Gicquel, L. Y. M., Gicquel, O, Darabiha, N., Veynante, D. and Fiorina, B. (2013) Numerical investigation of a helicopter combustion chamber using LES and tabulated chemistry. *Comptes Rendus Mécanique*, 341(1-2), pp. 257-265.

Backmier, F., Eberius, K. H. and Just, T. (1973) The Formation of Nitric Oxide and the Detection of HCN in Premixed Hydrocarbon-Air Flames at 1 Atmosphere. *Combustion Science and Technology*, 7, pp. 77-84.

Bahr, D. W. (1992) Aircraft turbine engine NO_x emission limits—status and trends. In: *ASME TURBO EXPO 1992*, Cologne, Germany, 1-4 June, ASME, 92-GT-415.

Baik, J. J., Kang, Y. S. and Kim, J. J. (2007) Modeling reactive pollutant dispersion in an urban street canyon. *Atmospheric Environment*, 41, pp. 934-949.

Baker, J., Walker, H. L. and Cai, X. M. (2004) A study of the dispersion and transport of reactive pollutants in and above street canyons – a large eddy simulation. *Atmospheric Environment*, 38, pp. 6883-6892.

Barths, H., Peters, N., Brehm, N., Mack, A., Pfitzner, M. and Smiljanovski, V. (1998) Simulation of pollutant formation in a gas-turbine combustor using unsteady flamelets. *Symposium (International) on Combustion*, 27, pp. 1841-1847.

Benim, A. C. and Syed, K. J. (1998) Laminar flamelet modelling of turbulent premixed combustion. *Applied Mathematical Modelling,* 22(1-2), pp. 113-136.

Biava, M., Khier, W. and Vigevano, L. (2012) CFD prediction of air flow past a full helicopter configuration. *Aerospace Science and Technology*, 19(1), pp. 3-18.

Bilger, R. W. (1976) Turbulent jet diffusion flames. *Progress in Energy and Combustion Science*, 1, pp. 87-109.

Bilger, R. W. (1980) Turbulent flows with nonpremixed reactants. In: Libby, P. A. and Willians, F. A. (eds.) *Topics in Applied Physics*, New York: Springer-Verlag, pp. 65-113.

Boileau, M., Staffelbach, G., Cuenot, B., Poinsot, T. and Berat, C. (2008) LES of an ignition sequence in a gas turbine engine. *Combustion and Flame*, 154, pp. 2-22.

Boudier, G., Gicquel, L. Y. M., Poinsot, T., Bissières, D. and Bérat, C. (2007) Comparison of LES, RANS and experiments in an aeronautical gas turbine combustion chamber. *Proceedings of the Combustion Institute*, 31(2), pp. 3075-3082.

Boudier, G., Gicquel, L.Y.M. and Poinsot, T. (2008) Effects of mesh resolution on large eddy simulation of reacting flows in complex geometry combustors. *Combustion and Flame*, 155, pp. 196-214.

Bowman, C. T. (1992) Control of combustion-generated nitrogen oxides emissions: technology driven by regulations. *Symposium* (*International) on Combustion*, 24, pp. 859-878.

Branley, N. and Jones, W. P. (2001) Large eddy simulation of a turbulent non-premixed flame. *Combustion and Flame*, 127, pp. 1914-1934.

Brasseur, G. P., Cox, R. A., Hauglustaine, D., Isaksen, I., Lelieveld, J., Lister, D. H., Sausen, R., Schumann, U., Wahner, A. and Wiesen, P. (1998) European scientific assessment of the atmospheric effects of aircraft emissions. *Atmospheric Environment,* 32(13), pp. 2329-2418.

Bray, K. N. C., Libby, P. A. and Moss, J. B. (1985) Scalar length scale variations in premixed turbulent flames. *Symposium (International) on Combustion*, 20(1), pp. 421-427.

Bray, K. N. C., Champion, M. and Libby, P. A. (1989) Mean reaction rates in premixed turbulent flames. *Symposium (International) on Combustion,* 22(1), pp. 763-769.

Bray, K. N. C, Domingo, P. and Vervisch, L. (2005) Role of the progress variable in models for partially premixed turbulent combustion. *Combustion and Flame,* 141(4), pp. 431-437.

Broadwell, J. E. and Lutz, A. E. (1998) A Turbulent Jet Chemical Reaction Model: NO_x Production in Jet Flames. *Combustion and Flame,* 114(3-4), pp. 319-335.

Brown, G. L. and Roshko, A. (1974) On density effects and large structure in turbulent mixing layers. *Journal of Fluid Mechanics*, 64(4), pp. 775-816.

Buriko, Y. Y. and Kuznetsov, V. R. (1978) Possible mechanism of the formation of nitrogen oxides in turbulent diffusional combustion. *Combustion, Explosion, and Shock Waves,* 14(3), pp. 296-303.

Celis, C. (2010) *Evaluation and Optimisation of Environmentally Friendly Aircraft Propulsion Systems*. PhD thesis, Cranfield University, UK.

Chakravarthy, V. K. and Menon, S. (2000) Subgrid modelling of turbulent premixed flames in the flamelet regime. *Flow Turbulence and Combustion*, 65, pp. 133-161.

Chan, T. L., Dong, G., Cheung, C. S., Leung, C. W., Wong, C. P. and Hung, W. T. (2001) Monte Carlo simulation of nitrogen oxides dispersion from a vehicular exhaust plume and its sensitivity studies. *Atmospheric Environment*, 35, pp. 6117-6127.

Chen, J. and Kollmann, W. (1992) PDF modeling and analysis of thermal NO formation in turbulent nonpremixed hydrogen-air jet flames. *Combustion and Flame,* 88(3-4), pp. 397-412.

Chen, L. D., Roquemore, W. M., Goss, L. P. and Vilimpoc, V. (1991) Vorticity generation in jet diffusion flames. *Combustion Science and Technology,* 77, pp. 41-57.

Chen, Y., Lee, W., Uang, S., Lee, S. and Tsai, P. (2006) Characteristics of polycyclic aromatic hydrocarbon (PAH) emissions from a UH-1H helicopter engine and its impact on the ambient environment. *Atmospheric Environment*, 40(39), pp. 7589-7597.

Colucci, P. J., Jaberi, F. A., Givi, P. and Pope, S. B. (1998) Filtered density function for large eddy simulation of turbulent reacting flows. *Physics of Fluids*, 10, pp. 499-515.

Cook A. W. and Riley, J. J. (1994) A subgrid model for equilibrium chemistry in turbulent flow. *Physics of Fluids*, 6, pp. 2868-2870.

Cook, A. W., Riley, J. J. and Kosaly, G. (1997) A laminar flamelet approach to subgrid-scale chemistry in turbulent flows. *Combustion and Flame*, 109, pp. 332-341.

Curtiss-Wright Corporation (1974) *Analysis and design of combustors for high performance small gas turbines for advanced helicopters.* Ohio: NASA Lewis Research Center, Final Technical Report, NASA/CR-169486.

Daly, M. (ed.) (2010) *Jane's Aero-Engines: Issue 27*. Surrey: HIS Global Limited.

De Bonis, J. R. and Scott, J. N. (2002) Large-Eddy Simulation of a Turbulent Compressible Round Jet. *AIAA Journal*, 40(7), pp. 1346-1354.

De Soete, G. G. (1975) Overall Reaction Rates of NO and N_2 Formation from Fuel Nitrogen. *International Symposium on Combustion*, 15, pp. 1093–1102.

Derksen, M. A. F., Kok, J. B. W. and van der Meer, T. H. (2003) Modelling of Turbulent Combustion with Reaction Progress Variables and CSP. *Proceedings of the European Combustion Meeting,* pp. 1-5.

Di Mare, F., Jones, W. P. and Menzies, K. R. (2004) Large eddy simulation of a model gas turbine combustor. *Combustion and Flame*, 137, pp. 278-294.

Dimotakis, P. E., Miake-Lye, R. C. and Papantoniou, D. A. (1983) Structure and dynamics of round turbulent jets. *Physics of Fluids*, 26, pp. 3185–3192.

Doolan, C. and Mi, J. (2007) Unsteady Reynolds Averaged Simulation of the Passive Scalar Field in the Turbulent Near-Wake of a Circular Cylinder. *Proceedings of the Australian Combustion Symposium,* pp. 154-157.

Drake, M. C. and Blint, R. J. (1989) Thermal NO_x in stretched laminar opposed-flow diffusion flames with $CO/H_2/N_2$ fuel. *Combustion and Flame,* 76(2), pp. 151-167.

Drake, M. C. and Blint, R. J. (1991) Relative importance of nitric oxide formation mechanisms in laminar opposed-flow diffusion flames. *Combustion and Flame,* 83(1-2), pp. 185-203.

Duchamp de Lageneste, L. and Pitsch, H. (2001) Progress in large-eddy simulation of premixed and partially-premixed turbulent combustion. *Center for Turbulence Research Annual Research Briefs*, pp. 97-107.

Duchamp de Lageneste, L. and Pitsch, H. (2001) *Progress in large-eddy simulation of premixed and partially-premixed turbulent combustion*. Stanford: Center for Turbulence Research, Annual Research Briefs, NASA Ames, pp. 97-107.

Dumrongsak, J. and Savill, A. M. (2012a) Large eddy simulation of a coaxial jet combustor. *In: 9th European Fluid Mechanics Conference*, Rome 9-13 September.

Dumrongsak, J. and Savill, A. M. (2012b) Numerical analysis and sensitivity study of non-premixed combustion using LES. *World Academy of Sciences Engineering & Technology*, 72, pp. 1164-1175.

Duwig, C. and Fureby, C. (2007) Large eddy simulation of unsteady lean stratified premixed combustion. *Combustion and Flame,* 151(1-2), pp. 85-103.

Eastwood, S., Tucker, P., Xia, H., Dunkley, P. and Carpenter, P. (2010) Large-Eddy Simulations and Measurements of a Small-Scale High-Speed Coflowing Jet. *AIAA Journal,* 48(5), pp. 963-974.

Eidson, T. M. (1985) Numerical simulation of the turbulent Rayleigh-Benard problem using subgrid modelling. *Journal of Fluid Mechanics*, 158, pp. 245-268.

Federal Office of Civil Aviation (FOCA). (2009) *Guidance on the determination of helicopter emissions*. Switzerland: Federal Department of the Environment, Transport, Energy and Communications (DETEC).

Forkel, H. and Janicka J. (2000) Large-eddy simulation of a turbulent hydrogen diffusion flame. *Flow Turbulence and Combustion*, 65, pp. 163-175.

Frank, J. H., Barlow, R. S. and Lundquist, C. (2000) Radiation and nitric oxide formation in turbulent non-premixed jet flames. *Proceedings of the Combustion Institute,* 28(1), pp. 447-454.

Freeman, C. E. and Mineck, R. E. (1987) *Fuselage surface pressure measurements of a helicopter wind tunnel model with a 3.15-meter diameter single rotor*. Virginia: NASA Langley Research Center, Technical Memorandum, TM-80051, VA 23665-5225.

Gardner, R. M., Adams, K., Cook, T., Deidewig, F., Ernedal, S., Falk, R., Fleuti, E., Herms, E., Johnson, C. E., Lecht, M., Lee, D. S., Leech, M., Lister, D., Massé, B., Metcalfe, M., Newton, P., Schmitt, A., Vandenbergh, C. and van Drimmelen, R. (1997) The ANCAT/EC global inventory of NO_x emissions from aircraft. *Atmospheric Environment*, 31(12), pp. 1751-1766.

Garmory, A., Britter, R. E. and Mastorakos, E. (2008) Simulation of the evolution of aircraft exhaust plumes including detailed chemistry and segregation. *Journal of Geography Research D: Atmospheres*, 113(8).

Garmory, A., Mastorakos, E. and Bilger, R. W. (2010) Simulations of the chemical transformations in a jet engine exhaust plume. In: *48th AIAA Aerospace Sciences Meeting Including the New Horizons Forum and Aerospace Exposition*, Orlando, 4-7 January, pp. 5026-5037, AIAA 2010-429.

Garry, K. P. and Holt, J. (2008) *Modelling the dispersion of aircraft engine efflux in proximity to airports in an atmospheric boundary layer wind tunnel*. Cranfield OMEGA Project Report.

Gatland, D., Hayward, L. and Rooks, S. (2002). Validation of Helicopter Flow Predictions Using Wind Tunnel LDA Measurements. In: *13th Ground Target Modeling and Validation Conference*, Michigan, 5-8 August.

Gazzah, M. H., Boughattas, N., Belmabrouk, H. and Said, R. (2010) The dynamic field in turbulent round jet discharging into a co-flowing stream. *Natural Science*, 2(6), pp. 635-640.

Georgiadis, N. J., Yoder, D. A. and Engblom, W. A. (2006) Evaluation of Modified Two-Equation Turbulence Models for Jet Flow Predictions. *AIAA Journal,* 44(12), pp. 3107-3114.

Gursoy, Z. E. (2009) *A numerical investigation of helicopter flow fields including thermal effects of exhaust hot gases*. MSc thesis, Middle East Technical University, Turkey.

Hamer, A. J. and Roby, R. J. (1997) CFD Modelling of a gas turbine combustor using reduced chemical kinetic mechanism. In: *33rd AIAA/ASME/SAE/ASEE Join Propulsion Conference and Exhibit*, Seattle, July 6-9, AIAA 97-3242.

Hanson, R. K. and Salimian, S. (1984) Survey of Rate Constants in H/N/O Systems. In: Gardiner, W. C. (ed.) *Combustion Chemistry*, New York: Springer-Verlag, pp. 361-421.

Hawkes, E. R. and Cant, R. S. (2000) A flame surface density approach to large-eddy simulation of premixed turbulent combustion. *Proceedings of the Combustion Institute,* 28(1), pp. 51-58.

Heiser, W. H. and Pratt, D. T. (1994) *Hypersonic Airbreathing Propulsion*, Washington, D.C.: AIAA Education.

International Air Transport Association (IATA). (2013) *Responsibly Addressing Climate Change.* IATA.

International Civil Aviation Organisation (ICAO) (1993) International standards and recommended practices. In: *Environmental protection. Annex 16 to the Convention on International Civil Aviation*, 2nd ed., Vol. II, Aircraft Engine Emissions. Montreal: ICAO.

Intergovernmental Panel on Climate Change (IPCC). (1990) *Climate Change - the IPCC Scientific Assessment.* UK: Cambridge University Press.

Intergovernmental Panel on Climate Change (IPCC). (2007) *Climate Change 2007 Synthesis Report - Appendix Glossary*. IPCC.

Janardan, B. A., Hoff, G. E., Barter, J. W., Martens, S., Gliebe, P. R., Mengle, V. and Dalton, W. N. (2000) *AST Critical Propulsion and Noise Reduction Technologies for Future Commercial Subsonic Engines*. NASA, NASA/CR-2000-210039.

Janic, M. (1999) Aviation and externalities: the accomplishments and problems. *Transportation Research Part D: Transport and Environment*, 4(3), pp. 159–180.

Johnson, M. (2013) *Aero gas turbine emission measurements – state-of-the-art review*. Fibre-Laser Imaging of Gas Turbine Exhaust Species (FLITES), Institution of Engineering and Technology, Savoy Place, 22 March.

Karcher, B., Hirschberg, M. M. and Fabian, P. (1996) Small-scale chemical evolution of aircraft exhaust species at cruising altitudes. *Journal of Geophysical Research*, 101(D10), pp. 15169-15190.

Kerstein, A. R. (1992) Linear-eddy modelling of turbulent transport. Part7. Finite-rate chemistry and multi-stream mixing. *Journal of Fluid Mecha*nics, 240, pp. 289-313.

Kikumoto, H. and Ooka, R. (2012) A study on air pollutant dispersion with bimolecular reactions in urban street canyons using large-eddy simulations. *Journal of Wind Engineering and Industrial Aerodynamics*, 104-106, pp. 516-522.

Kim, S. J. and Shin, H. D. (1994) A visual study of the structure of turbulent nonpremixed flames near jet exit. *Combustion Science and Technology,* 99(1-3), pp. 37-49.

Kirkpatrick, M. P., Armfield, S. W. and Kent J. H. (2003a) A representation of curved boundaries for the solution of the Navier-Stokes equations on a staggered three-dimensional Cartesian grid. *Journal of Computational Physics,* 184, pp. 1-36.

Kirkpatrick, M. P., Armfield, S. W., Masri, A. R. and Ibrahim, S. S. (2003b) Large eddy simulation of a propagating turbulent premixed flame. *Flow, Turbulence and Combustion*, 70(1), pp. 1-19.

Klimenko, A. Y. and Bilger, R. W. (1999) Conditional moment closure for turbulent combustion. *Progress in Energy and Combustion Science*, 25(6), pp. 595-687.

Kolbe, W. and Kollmann, W. (1980) Prediction of turbulent diffusion flames with a four-equation turbulence model. *Acta Astronautica*, 7, pp. 91-104.

Kurose, R. (2001) Large eddy simulation of a non-premixed turbulent reacting mixing layer: Effects of heat release and spanwise fluid shear. *Combustion and Flame,* 127(3), pp. 2157-2163.

Langford, J. A. and Moser, R. D. (1999) Optimal LES formulations for isotropic turbulence. *Journal of Fluid Mechanics*, 398, pp. 321-346.

Lee, C. E., Oh, C. B. and Kim, J. H. (2004) Numerical and experimental investigations of the NO, emission characteristics of CH_4-air coflow jet flames. *Fuel,* 83(17-18), pp. 2323-2334.

Lefebvre, A. H. and Ballal, D. R. (2010) *Gas Turbine Combustion Alternative Fuels and Emissions*, 3rd ed., Boca Raton: CRC Press.

Leonard, A. (1974) Energy Cascade in Large-eddy Simulations of Turbulent Fluid Flows*. Advances in Geophysics*, 18A, pp. 237-248.

Li, Y. G., Marinai, L., Gatto, E. L., Pachidis, V. and Pilidis, P. (2009) Multiple-Point Adaptive Performance Simulation Tuned to Aeroengine Test-Bed Data. *Journal of Propulsion and Power*, 25(3), pp. 635–641.

Libby, P. A. and Williams, F. A. (1980) Fundamental aspects. ,In: Libby, P. A. and Willians, F. A. (eds.) *Topics in Applied Physics*, New York: Springer-Verlag, pp. 1-43.

Magnussen, B. F. (1981) On the Structure of Turbulence and a Generalized Eddy Dissipation Concept for Chemical Reaction in Turbulent Flow. In: *19th AIAA Meeting*, St. Louis, 12-15 January.

Magnussen, B. F. and Hjertager, B. H. (1977) On mathematical modeling of turbulent combustion with special emphasis on soot formation and combustion. *Symposium (International) on Combustion*, 16(1), pp. 719-729.

Mahesh, K., Constantinescu, G., Apte, S., Iaccarino, G. and Moin P. (2001) *Large-eddy simulation of gas-turbine combustors*. Stanford: Center for Turbulence Research, Annual Research Briefs, NASA Ames, pp. 3-17.

Mahesh, K., Constantinescu, G. and Moin, P. (2004) A numerical method for large-eddy simulation in complex geometries. *Journal of Computational Physics*, 197, pp. 215-240.

Mahesh, K., Constantinescu, G., Apte, S., Iaccarino, G., Ham, F. and Moin, P. (2006) Large-eddy simulation of reacting turbulent flows in complex geometries. *Journal of Applied Mechanics*, 73, pp. 374-381.

Mallard, W. G., Westley, F., Herron, J. T., Hampson, R. F. and Fizzell, D. H. (1994) *NIST Chemical Kinetics Database: Version 6.0*. Gaithersburg: National Institute of Standards and Technology.

Mazlan, N. M. (2012) *Assessing/Optimising Bio-Fuel Combustion Technologies for Reducing Civil Aircraft Emissions*. PhD thesis, Cranfield University, UK.

Menon, S. and Wu, J. (1998) Effects of micro- and macroscale turbulent mixing on the chemical processes in engine exhaust plumes. *Journal of Applied Meteorology*, 37(6), pp. 639–654.

Miake-Lye, R. C., Martinez-Sanchez, M., Brown, R. C. and Kolb C. E. (1993) Plume and wake dynamics, mixing, and chemistry behind a high speed civil transport aircraft. *Journal of Aircraft*, 30(4), pp. 467-479.

Mineck, R. E. and Gorton, S. A. (2000) *Steady and periodic pressure measurements on a genetic helicopter fuselage model in the presence of a rotor*. NASA, TM-2000-210286

Möller, S. I., Lundgren, E. and Fureby, C. (1996) Large eddy simulation of unsteady combustion. *Symposium (International) on Combustion*, 26(1), pp. 241-248.

Moore, J., Stanitski, C. and Jurs, P. (2008) *Chemistry: The Molecular Science*, 3rd ed., Canada: David Harris, Chapter 10.

Nam, H. J., Park, Y. M. and Kwon, O. J. (2006) Simulation of Unsteady Rotor-Fuselage Aerodynamic Interaction Using Unstructured Adaptive Meshes. *Journal of the American Helicopter Society*, 51(2), pp. 141-149.

O'Brien, E. E. (1980) The probability density function (pdf) approach to reacting turbulent flows. In: Libby, P. A. and Willians, F. A. (eds.) *Topics in Applied Physics*, New York: Springer-Verlag, pp. 185-218.

O'Brien, D., Calvert, M. and Butler, S. (2008) An Examination of Engine Effects on Helicopter Aeromechanics. In: *AHS Specialist's Conference on Aeromechanics*, San Francisco, CA, 23-25 January.

Oates, G.C. (1997) *Aerothermodynamics of Gas Turbine and Rocket Propulsion*. 3rd ed., Reston: AIAA Education.

Ouimette, P. and Seers, P. (2009) NO_x emission characteristics of partially premixed laminar flames of H_2/CO/CO_2 mixtures. *International Journal of Hydrogen Energy,* 34(23), pp. 9603-9610.

Owen, F. K., Spadaccini, L. J. and Bowman, C. T. (1976) Pollutant formation and energy release in confined turbulent diffusion flames. *Proceedings of the Combustion Institute*, 16, pp. 105-117.

Ozel, A. and Edis, F. O. (2006) Computational Analysis of Multi-Stream Turboshaft Engine Exhaust. In: *4th WSEAS International Conference on Fluid Mechanics and Aerodynamics,* Elounda, 21-23 August, pp. 204-208.

Pachidis, V., Pilidis, P., Marinai, L. and Templalexis, I. (2007) Towards a Full Two Dimensional Gas Turbine Performance Simulator. *Aeronautical Journal*,111(1121), pp. 433–442.

Penner, J. E., Lister, D. H., Griggs, D. J., Dokken, D. J. and McFarland, M. (eds.) (1999) *Aviation and the Global Atmosphere : a special report of IPCC Working Groups I and III*. New York: Cambridge University Press, pp. 27–64.

Peters, N. (1983) Local quenching due to flame stretch and non-premixed turbulent combustion. *Combustion Science and Technology*, 30, pp. 1-17.

Peters, N. (1984) Laminar diffusion flamelet models in non-premixed turbulent combustion. *Progress in Energy and Combustion Science*, 10(3), pp. 319-339.

Peters, N. (2000) *Turbulent Combustion*. UK: Cambridge University Press, Chapter 3.

Pham, V. V., Tang, J., Alam, S., Lokan, C. and Abbass, H. A. (2010) Aviation emission inventory development and analysis. *Environmental Modelling & Software,* 25(12), pp. 1738-1753.

Pierce, C. D. and Moin, P. (1998) A dynamic model for subgrid-scale variance and dissipation rate of a conserved scalar. *Physics of Fluids,* 10(12), pp. 3041-3044.

Pierce, C. D. and Moin, P. (2004) Progress-variable approach for large-eddy simulation of non-premixed turbulent combustion. *Journal of Fluid Mechanics*, 504, pp. 73-97.

Pison, I. and Menut, L. (2004) Quantification of the impact of aircraft traffic emissions on tropospheric ozone over Paris area. *Atmospheric Environment,* 38(7), pp. 971-983.

Pitsch, H. and Ihme, M. (2005) An Unsteady/Flamelet Progress Variable Method for LES of Nonpremixed Turbulent Combustion. In: *43rd AIAA Aerospace Sciences Meeting and Exhibit*, Nevada, 10-13 January, AIAA Paper 2004-557.

Pitsch, H. and Steiner, H. (2000) Large-eddy simulation of a turbulent piloted methane/air diffusion flame (Sandia flame D). *Physics of Fluids*, 12(10), pp. 2541-2554.

Pitsch, H. (2006) Large-eddy simulation of turbulent combustion. *Annual Review of Fluid Mechanics*, 38, pp. 453-482.

Poll, D. I. A., Garry, K. P. and Savill, A. M. (2009) *Dispersion of aircraft efflux in proximity to airports.* Cranfield: OMEGA Project Report.

Pope, S. B. (1985) Pdf method for turbulent reacting flows. *Progress in Energy and Combustion Science*, 11(2), pp. 119-195.

Pope, S. B. (2000) *Turbulent Flows*. New York: Cambridge University Press, Chapter 13.

Ranga-Dinesh, K. K. J. (2007) *Large eddy simulation of turbulent swirling flames*. PhD thesis, Loughborough University, UK.

Ranga-Dinesh, K. K. J., Savill, A. M., Jenkins, K. W. and Kirkpatrick, M. P. (2010a) LES of intermittency in a turbulent round jet with different inlet conditions. *Computers & Fluids,* 39(9), pp. 1685-1695.

Ranga-Dinesh, K. K. J., Savill, A. M., Jenkins, K. W. and Kirkpatrick, M. P. (2010b) A study of mixing and intermittency in a coaxial turbulent jet. *Fluid Dynamics Research,* 42, pp. 1-20.

Rhodes, R. P., Harsha, P. T. and Peters, C. E. (1974) Turbulent kinetic energy analyses of hydrogen-air diffusion flames. *Acta Astronautica*, 1, pp. 443-470.

Roux, S., Lartigue, G., Poinsot, T., Meier, U. and Berat, C. (2005) Studies of mean and unsteady flow in a swirled combustor using experiments, acoustic analysis, and large eddy simulations. *Combustion and Flame*, 141, pp. 40-54.

Sagaut, P. (2001) *Large Eddy Simulation for Incompressible Flows*. Berlin: Springer.

Saito, T. and Sato, J. (1994) Studies on $NO_{(x)}$ emission characteristics of premixed type gas turbine combustors. In: *32nd AIAA Aerospace Sciences Meeting and Exhibit*, Reno, Nevada, 10-13 January.

Sattelmayer, T., Felchlin, M. P., Haumann, J., Hellat, J. and Styner, D. (1992) Second-generation low-emission combustors for ABB gas turbines: burner development and tests at atmospheric pressure. *Journal of Engineering for Gas Turbines and Power,* 114(1), pp. 118-125.

Sausen, R.; Isaksen, I.; Grewe, V.; Hauglustaine, D.; Lee, D. S.; Myhre, G.; Köhler, M. O.; Pitari, G.; Schumann, U.; Stordal, F. and Zerefos, C. (2005) Aviation radiative forcing in 2000: An update on IPCC (1999). *Meteorologische Zeitschrift*, 14(4), pp. 555-561.

Schefer, R. W., Namazian, M., Filtopoulos, E. E. J. and Kelly, J. (1994) Temporal evolution of turbulence/chemistry interactions in lifted, turbulent-jet flames. *Symposium (International) on Combustion*, 25(1), pp. 1223-1231.

Seitzman, J., Ungut, A., Paul, P. and Hanson, R. (1990) Imaging and characterization of OH structures in a turbulent nonpremixed flame. *Symposium (International) on Combustion*, 23, pp. 637-644.

Selle, L., Lartigue, G., Poinsot, T., Koch, R., Schildmacher, K. U., Krebs, W., Prade, B., Kaufmann, P. and Veynante, D. (2004) Compressible large eddy simulation of turbulent combustion in complex geometry on unstructured meshes. *Combustion and Flame*, 137, pp. 489-505.

Selle, L., Benoit, L., Poinsot, T., Nicoud, F. and Krebs, W. (2006) Joint use of compressible large-eddy simulation and Helmholtz solvers for the analysis of rotating modes in an industrial swirled burner. *Combustion and Flame*, 145, pp. 194-205.

Shakariyants, S. A. (2006) A multidisciplinary aero-engine exhaust emission study. In: *ASME Turbo Expo 2006: Power for Land, Sea and Air*, Barcelona, Spain, 8-11 May, GT2006-90749.

Shea, J. R. (1976) *A chemical reaction in a turbulent jet*. PhD thesis, California Institute of Technology, USA.

Shea, J. R. (1977) A chemical reaction in a turbulent jet. *Journal of Fluid Mechanics*, 81(2), pp. 317-333.

Sivathanu, Y. R. and Faeth, G. M. (1990) Generalized state relationships for scalar properties in non-premixed hydrocarbon/air flames. *Combustion and Flame*, 82, pp. 211-230.

Smagorinsky, J. (1963) General circulation experiments with the primitive equations: I. The basic experiment. *Monthly Weather Review*, 91(3), pp. 99-164.

Snyder, T. S., Rosfjord, T. J., McVey, J. B. and Chiappetta, L. M. (1994) Comparison of liquid fuel/air mixing and NO_x emissions for a tangential entry nozzle. In: *ASME International Gas Turbine and Aeroengine Congress and Exposition*, Netherlands, 13-16 June, ASME Paper 94-GT-283.

Spalding, D. B. (1971) Mixing and chemical reaction in steady confined turbulent flames. *Symposium (International) on Combustion*, 13(1), pp. 649-657.

Staffelbach, G., Gicquel, L. Y. M., Boudier, G. and Poinsot, T. (2009) Large Eddy Simulation of self excited azimuthal modes in annular combustors. *Proceedings of the Combustion Institute*, 32(2), pp. 2909-2916.

Steijl, R. and Barakos, G. (2008) Sliding mesh algorithm for CFD analysis of helicopter rotor-fuselage aerodynamics. *International Journal for Numerical Methods in Fluids,* 58(5), pp. 527-549.

Steijl, R. and Barakos, G. N. (2012) CFD analysis of complete helicopter configurations - lessons learnt from the GOAHEAD project. *Aerospace Science and Technology,* 19(1), pp. 58-71.

Suto, H., Matsubara, K., Kobayashi, M. and Kaneko, Y. (2004) Large eddy simulation of flow and scalar transport in a round jet. *Heat Transfer-Asian Research,* 33(3), pp. 175-188.

Tilton, B. E. (1989) Health effects of tropospheric ozone. *Environmental Science and Technology,* 23, pp. 257-263.

Tkatchenko, I., Kornev, N., Jahnke, S., Steffen, G. and Hassel, E. (2007) Performances of LES and RANS Models for Simulation of Complex Flows in a Coaxial Jet Mixer. *Flow, Turbulence and Combustion,* 78(2), pp. 111-127.

Turns, S. R. (1995) Understanding NO_x formation in nonpremixed flames: Experiments and modeling. *Progress in Energy and Combustion Science,* 21(5), pp. 361-385.

Turns, S. R. (2000) *An Introduction to Combustion: Concepts and Applications*. 2nd ed., USA: McGraw-Hill.

Turns, S. R. and Lovett, J. A. (1989) Measurements of oxides of nitrogen emissions from turbulent propane jet diffusion flames. *Combustion Science and Technology*, 66(4-6), pp. 233-249.

Turns, S. R. and Myhr, F. H. (1991) Oxides of nitrogen emissions from turbulent jet flames: Part I—Fuel effects and flame radiation. *Combustion and Flame,* 87(3-4), pp. 319-335.

United States Army Aviation Laboratories. (1970) *1500 HP demonstrator engine program (U)*. U.S. AVLABS TR-70-62, 1.

United States Environmental Protection Agency (USEPA). (1977) *Compilation of air pollutant emission factors*. Office of Air Quality Planning and Standards, publication no. AP-42.

United States Environmental Protection Agency (USEPA). (1999) *Evaluation of Air Pollutant Emissions from Subsonic Commercial Jet Aircraft*. US Environmental Protection Agency, Michigan, EPA420-R-99-013.

Wang, Z. and Chen, J. Y. (1997) Modeling of microscale turbulence and chemistry interaction in near-field aircraft plumes. *Journal of Geophysical Research*, 102(D11), pp. 12871-12883.

Wang, K., Yang, Z. and McGuirk, J. J. (2007) Large eddy simulation of turbulent diffusion flame combustion using a conserved scalar methodology. *Journal of Aerospace Power*, 22(7), pp. 1106-1117.

Warnatz, J. (2001) *NO_x Formation in High Temperature Processes*. University of Stuttgart, Germany.

Wayne, R. P. (1991) *Chemistry of Atmosphere*. 2nd ed., Oxford: Clarendon Press.

Wegner, B., Maltsev, A., Schneider, C., Sadiki, A., Dreizler, A. and Janika, J. (2004) Assessment of unsteady RANS in predicting swirl flow instability based on LES and experiments. *International Journal of Heat and Fluid Flow*, 25(3), pp. 528-536.

Weller, H. G., Tabor, G., Gosman, A. D. and Fureby, C. (1998) Application of a flame-wrinkling les combustion model to a turbulent mixing layer. *Symposium (International) on Combustion*, 27(1), pp. 899-907.

Wilcox, D. C. (1993) *Turbulence modeling for CFD.* CA: DCW Industries, Inc.

Wolf, P., Staffelbach, G., Roux, A., Gicquel, L. Y. M., Poinsot, T. and Moureau, V. (2009) Massively parallel LES of azimuthal thermo-acoustic instabilities in annular gas turbines. *Comptes Rendus Mecanique*, 337, pp. 385-394.

Wolf, P., Balakrishnan, R., Staffelbach, G., Gicquel, L. Y. M. and Poinsot, T. (2012) Using les to study reacting flows and instabilities in annular combustion chambers. *Flow, Turbulence and Combustion*, 88(1-2), pp. 191-206.

Wu, X., Tristanto, I. H., Page, G. J. and McGuirk, J. J. (2005) Influence of Nozzle Modelling in LES of Turbulent Free Jets. In: *11th AIAA/CEAS Aeroacoustics Conference (26th AIAA Aeroacoustics Conference)*, Monterey, California, 23-25 May.

Wulff, A. and Hourmouziadis, J. (1997) Technology review of aeroengine pollutant emissions. *Aerospace Science and Technology,* 1(8), pp. 557-572.

Xie, M. (2011) *Effects of Rotor-Fuselage-Engine Aerodynamic Interaction on Helicopter Engine Performance*. MSc thesis, Cranfield University, UK.

Yule, A. J. (1978) Large-scale structure in the mixing layer of a round jet. *Journal of Fluid Mechanics,* 89(3), pp. 413.

Zhang, X. and Stanescu, D. (2010) Large eddy simulations of round jet with spectral element method. *Computers & Fluids,* 39(2), pp. 251-259.

APPENDICES

Appendix A Journal Abstracts

A.1 Numerical analysis and sensitivity study of non-premixed combustion using LES

Abstract—Non-premixed turbulent combustion Computational Fluid Dynamics (CFD) has been carried out in a simplified methane-fuelled coaxial jet combustor employing Large Eddy Simulation (LES). The objective of this study is to evaluate the performance of LES in modelling non-premixed combustion using a commercial software, FLUENT, and investigate the effects of the grid density and chemistry models employed on the accuracy of the simulation results. A comparison has also been made between LES and Reynolds Averaged Navier-Stokes (RANS) predictions. For LES grid sensitivity test, 2.3 and 6.2 million cell grids are employed with the equilibrium model. The chemistry model sensitivity analysis is achieved by comparing the simulation results from the equilibrium chemistry and steady flamelet models. The predictions of the mixture fraction, axial velocity, species mass fraction and temperature by LES are in good agreement with the experimental data. The LES results are similar for the two chemistry models but influenced considerably by the grid resolution in the inner flame and near-wall regions.

A.2 Prediction of NO_x Emissions from a Helicopter Combustor Using Large Eddy Simulation

Abstract—This paper presents a numerical study of Jet A/air reaction in a simplified helicopter combustor employing Large Eddy Simulation (LES) and the non-premixed combustion model. The study aims to assess the performance of LES, at minimal resolution and computational resource requirements, in modelling combustion and predicting NO_x emissions to allow the possibility of future optimisation investigations. The simulations have been carried out on three computational grids consisting of approximately 0.2, 1.8 and 5.0 million tetrahedral elements. The LES predictions in terms of the temperature distributions, maximum flame temperature, mean exit temperature and $EINO_x$ agree generally well with the combustor design, analytical solutions and test measurements. Consequently, the LES code has been employed to model the reaction in a generic combustor. The comparison of results from LES and a one-dimensional emission model highlights the potential of current LES for the calibration of simpler helicopter performance and emission models.

Appendix B Posters

B.1 Combustion large eddy simulation of Jet-A fuel in a helicopter combustor

Combustion Large Eddy Simulation of Jet-A Fuel in a Helicopter Combustor

Cranfield UNIVERSITY

Janthanee Dumrongsak

Supervisor : Professor Mark Savill

Introduction

Due to increasing environmental concerns regarding aviation emissions and stringent regulations, engineers are faced with the challenge of designing more environmental friendly whilst, highly efficient and reliable gas turbine combustors. Computational Fluid Dynamics (CFD) has greatly contributed to the understanding of complex phenomena of combustion systems in recent years. This study employs Large Eddy Simulation (LES), a CFD advanced turbulence modelling approach, to numerically investigate the combustion of Jet-A fuel and air in a simplified helicopter combustor with the aim of assessing the potential of LES as a numerical tool employed to validate other simpler modelling approaches.

Figure 1: An annular combustor with a vaporiser and its location in Bell AH-1Z helicopter.
(Source: Bell Helicopter Textron Inc. and Rolls-Royce Plc.)

Approach To Problem

A general annular combustor configuration and its location in a real helicopter is illustrated in Figure 1. The flow geometry employed in this study, as shown in Figure 2, is a 30° section of the simplified annular combustor with the shape and dimensions resembling those of the helicopter combustor in the design analysis of Curtiss-Wright Corporation (Ref. 1). The computational grid consists of 1.2 million tetrahedral elements. Simulations have been performed in FLUENT employing LES with a standard Smagorinsky-Lilly subgrid scale treatment. The reaction between vaporised Jet-A fuel and air is modelled using the non-premixed combustion approach with equilibrium chemistry. This LES code has already been successfully implemented and validated for a methane-fuelled coaxial jet combustor by Dumrongsak and Savill (Ref. 2).

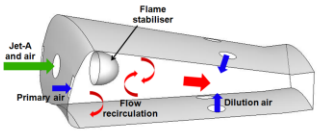

Figure 2: A section of the simplified helicopter combustor and its general flow pattern.

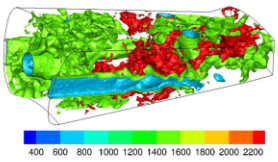

Figure 3: Instantaneous temperature iso-surfaces.

Summary of Results

Instantaneous temperature iso-surfaces in Figure 3 demonstrate the capability of LES in capturing the realistic unsteady behaviours and temperature distributions of the gases inside the combustor. The flame, as indicated by the high temperature contours on the mid planes exhibited in Figure 4, is restrained in the primary zone, the region where flow recirculation takes place. This is consistent with the combustor qualitative design analysis. The LES predictions of the mean temperature and EINOx at the combustor outlet also agree with the analytical solutions reasonably well.

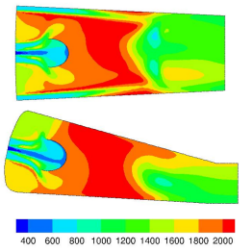

Figure 4: Mean temperature contours on the mid horizontal (top) and axial (bottom) planes.

Conclusions

With a simple chemistry model and moderate level of grid refinement, LES is able to predict Jet-A fuel combustion flow properties with a level of fidelity which is sufficient for environmental and energy optimisation purposes, as well as the use to calibrate simpler performance and emissions models for Techno-economic Environmental Risk Assessment (TERA).

References:
[1] Curtiss-Wright Corporation, *NASA/CR-169486*, (1974).
[2] Dumrongsak and Savill, *33rd ICFMHTT*, (2012).

November 2012

CLEANSKY

B.2 Large eddy simulation of helicopter combustor and exhaust emissions

Large Eddy Simulation of Helicopter Combustor and Exhaust Emissions

Cranfield UNIVERSITY

Janthanee Dumrongsak

Supervisor : Professor Mark Savill

Introduction

The aim of this project is to numerically investigate the reaction and complex flow phenomena in a helicopter combustor and exhaust with the focus on NOx emissions employing Large Eddy Simulation (LES) which is an advance turbulence modelling approach in Computational Fluid Dynamics (CFD). The outcomes will be significantly beneficial to the combustor design optimisation or the calibration of simpler performance and emission models for Techno-economic Environmental Risk Assessment (TERA), leading to the development of more environmental friendly, highly efficient helicopter engines in the future.

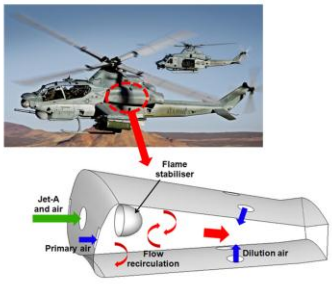

Figure 1: A simplified helicopter combustor section and its location in Bell AH-1Z helicopter.
(Helicopter picture from Bell Helicopter Textron Inc.)

Approach To Problem

The reference helicopter combustor employed in this project is obtained from the design analysis of Curtiss-Wright Corporation (Ref. 1). A section of the simplified helicopter combustor is modelled and its general flow pattern is illustrated in Figure 1. Simulations have been performed in FLUENT employing LES with the standard Smagorinsky-Lilly subgrid scale treatment. The reaction between vaporised Jet-A fuel and air is modelled using the non-premixed combustion approach with the equilibrium chemistry. This LES code has already been successfully implemented and validated for a methane-fuelled coaxial jet combustor by Dumrongsak and Savill (Ref. 2).

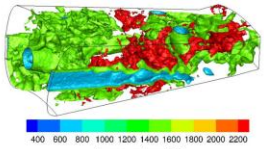

Figure 2: Instantaneous temperature iso-surfaces of the helicopter combustor.

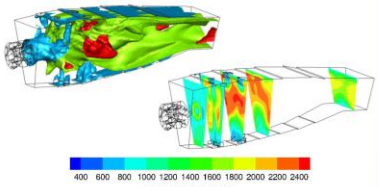

Figure 3: Instantaneous temperature iso-surfaces (left) and mean temperature contours (right) of the generic gas turbine combustor.

Summary of Results

The capability of LES in capturing realistic unsteady flow behaviours has been demonstrated. The flame structure and temperature distributions shown in Figure 2 are consistent with the combustor qualitative design analysis. The predicted mean temperature and EINOx of 2.88 g/kg at the combustor outlet also agree with the designed values (≤5 g/kg for EINOx). The same LES has been applied to a generic gas turbine combustor, as illustrated in Figure 3, in order to calibrate and refine simpler combustor performance modelling. The mean exit temperature and EINOx obtained with an in-house 1D code, HEPHAESTUS, are in reasonable agreement with LES (1476 K and 3.7 g/kg compared to 1512 K and 10 g/kg) especially when a partially stirred reactor model is adopted. A non-combusting chemical reacting jet test case has also been simulated and the results are compared with Ref. 3 and Ref. 4 in Figure 4.

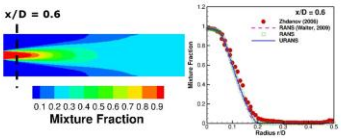

Figure 4: Mixture fraction distributions of the non-combusting chemical reacting jet.

Conclusions or Future Work

With a simple chemistry model and moderate level of grid refinement, LES is able to predict flow properties with a level of fidelity which is sufficient for environmental and energy optimisation purposes, as well as the use to calibrate simpler performance and emissions models. The next stage of the research will be the modelling of the reaction between the engine jet exhaust and ambient air.

References:
[1] Curtiss-Wright Corporation, *NASA/CR-169486*, (1974).
[2] Dumrongsak and Savill, *33rd ICFMHTT*, vol.72, pp.55-66 (2012).
[3] Zhdanov *et al.*, Int. J. Heat Mass Transfer, (2006).
[4] Walter *et al.*, Turbulence Heat and Mass Transfer 6, (2009).

February 2013

CLEANSKY